



MONASH University

**Crane Payload Localisation:
Mid-Air Alignment of Curtain Wall Modules**

Brandon Johns

B.Eng. (Mechanical)

A Thesis Submitted for the Degree of Doctor of Philosophy at

Monash University in 2023

Department of Mechanical and Aerospace Engineering

Faculty of Engineering

Copyright notice

© Brandon Johns (2023).

I certify that I have made all reasonable efforts to secure copyright permissions for third-party content included in this thesis and have not knowingly added copyright content to my work without the owner's permission.

To my dearest friends, Tina and Andrew

Even though we're separated
Even though our time together was cut short
And though our paths now diverge
As we carry on

"Thank you"
This is where you and I met
This is where our paths coincided
An unforgettable encounter
Imbued in my mind

We share an unbreakable bond
That I will treasure forever

I miss you

Abstract

Building construction uses prefabrication to shift manufacturing off the construction site, and into factories. Off-site construction facilitates high efficiency, strict quality control, and the integration of high precision and complex features into the construction element. Increasing the size of prefabricated elements reduces on-site activities, but presents new challenges to the on-site installation task.

This thesis pertains to the on-site mid-air-alignment task, in which a construction element is crane lifted up towards its installation location, aligned to attachment fixtures, and affixed to the building. The alignment tolerance is approximately 1mm and 2deg. However, it is difficult to precisely locate the large and heavy element while it is suspended high in the air.

This thesis contributes to developing the core processes and technologies that are required to make automated localisation of the crane borne unitised curtain wall module (CWM) viable. The research methodologies include process flow modelling, dynamical systems modelling, and localisation through computer vision.

Chapter 1 introduces the motivations and objectives of the thesis.

Chapter 2 identifies the barriers and opportunities. A key opportunity is to strengthen the communication between the crane operator and dogman by providing them with rich localisation information.

Chapter 3 develops a guideline for system designers to choose the optimal dynamical models to represent boom tower cranes. Use of an accurate model facilitates precise control and state estimation. A key finding is that mechanically locking the CWM and crane hook together can make the system easier to precisely control.

Chapter 4 develops an algorithm to measure the pose of a crane borne CWM, as relative to its installation location on the side face of a high-rise building. Also developed, is a practical framework for incorporating the advancements presented in this thesis into the conventional direct CWM installation methodologies.

Chapter 5 concludes the thesis and recommends directions for future research.

Publications during enrolment

Journal Publications

- Brandon Johns, Elahe Abdi and Mehrdad Arashpour. 'Dynamical modelling of boom tower crane rigging systems: model selection for construction'. In: *Archives of Civil and Mechanical Engineering* 23.3 (2023), p. 162. DOI: [10.1007/s43452-023-00702-x](https://doi.org/10.1007/s43452-023-00702-x)
- Brandon Johns, Elahe Abdi and Mehrdad Arashpour. 'Crane payload localisation for curtain wall installation: A markerless computer vision approach'. In: *Measurement* (2023). (In press), p. 113459. DOI: [10.1016/j.measurement.2023.113459](https://doi.org/10.1016/j.measurement.2023.113459)

Conference Publications

- Brandon Johns, Mehrdad Arashpour and Elahe Abdi. 'Curtain Wall Installation for High-Rise Buildings: Critical Review of Current Automation Solutions and Opportunities'. In: *Proceedings of the 37th International Symposium on Automation and Robotics in Construction (ISARC)*. 2020, pp. 393–400. DOI: [10.22260/ISARC2020/0056](https://doi.org/10.22260/ISARC2020/0056)
- Kerry He, Brandon Johns, Elahe Abdi and Mehrdad Arashpour. 'Camera View from Crane Payload: Video Stabilization'. In: *Australasian Conference on Robotics and Automation, ACRA*. 2021. URL: https://ssl.linklings.net/conferences/acra/acra2021_proceedings/views/includes/files/pap104s2-file1.pdf

Research Data

- Brandon Johns, Elahe Abdi and Mehrdad Arashpour. *Glass Curtain Wall Installation Dataset*. 2023. DOI: [10.26180/23538198](https://doi.org/10.26180/23538198)

Free & Open Source Code

- <https://github.com/Brandon-Johns/crane-dynamics-simulator>
- <https://github.com/Brandon-Johns/Vicon-DataStream-SDK-examples>
- <https://github.com/Brandon-Johns/OptiTrack-NatNet-SDK-examples>
- https://github.com/Brandon-Johns/ur_rtde-examples

In the event that any of these links stop working, then I will upload it to another host. If you can't find it, then feel free to contact me.

Thesis including published works declaration

I hereby declare that this thesis contains no material which has been accepted for the award of any other degree or diploma at any university or equivalent institution and that, to the best of my knowledge and belief, this thesis contains no material previously published or written by another person, except where due reference is made in the text of the thesis.

This thesis includes 2 original papers published in peer reviewed journals. The core theme of the thesis is crane payload localisation in the context of curtain wall installation. The ideas, development and writing up of all the papers in the thesis were the principal responsibility of myself, the student, working within the Department of Mechanical and Aerospace Engineering under the supervision of Dr. Elahe Abdi and Dr. Mehrdad Arashpour.

The inclusion of co-authors reflects the fact that the work came from active collaboration between researchers and acknowledges input into team-based research.

In the case of Chapters 3 and 4, my contribution to the work involved the following:

Thesis Chapter	Publication Title	Status	Nature and % Student Contribution	Co-author name(s) Nature and % of Co-author's contribution	Co-author(s), Monash student
3	Dynamical modelling of boom tower crane rigging systems: model selection for construction	Published	Everything (80%)	Elahe Abdi: supervision, writing–review and editing (10%)	No
				Mehrdad Arashpour: supervision, writing–review and editing (10%)	No
4	Crane payload localisation for curtain wall installation: A markerless computer vision approach	In-Press	Everything (80%)	Elahe Abdi: supervision, writing–review and editing (10%)	No
				Mehrdad Arashpour: supervision, writing–review and editing (10%)	No

I have not renumbered sections of submitted or published papers in order to generate a consistent presentation within the thesis.

Student name: Brandon Johns

Student signature: *(redacted for publication)*

I hereby certify that the above declaration correctly reflects the nature and extent of the student's and co-authors' contributions to this work. In instances where I am not the responsible author I have consulted with the responsible author to agree on the respective contributions of the authors.

Main Supervisor name: Elahe Abdi

Main Supervisor signature: *(redacted for publication)*

Acknowledgements

Thank you to everyone who has supported me¹ during my candidature.

Elahe Abdi² — My main supervisor. Elahe has supported me since my undergraduate honours project, during which, Elahe dedicated time and effort beyond the norm to teach me research and research communication. My fate then changed one day, when Elahe invited me to start this PhD under her supervision. I hadn't even considered the possibility! Elahe has been the best mentor. Elahe has encouraged me to pursue the research directions that I discovered, to publish my results, to engage with my peers, to teach, to supervise, and to improve my writing. Elahe has trusted me with editing course content, supervising, and even delivering a lecture. Thanks Elahe!

Mehrdad Arashpour³ — My 2nd supervisor. Mehrdad has supported me throughout my candidature by helping to direct me in choosing my research topic, by encouraging me to get hands on with the robots, and in writing and publishing. Mehrdad has supported the novelty of my work and encouraged me to keep on keeping on. Thanks Mehrdad!

Monash Robotics and the HRI Lab — Everyone in the lab has been great! Wesley Chan: a great lab manager who helped me with getting started on the robots and the motion capture system. Tin: both a great friend and who gave me great advice as I learnt linux, python, and C++. Tina, Rachel, Aimee, Yanjun, Tianjie, Radhik: Great friends who also gave me emotional support and encouragement. And so many others in the lab who were great to work alongside of as we supported and learnt from each other.

Monash M+AE Workshop — The mechanical workshop have supported me since my undergraduate honours project. Big thanks especially to Chris Pierson, who holds a wealth of knowledge in mechanical design. Chris generously sat with me a few times to explain how to choose base materials, how to interface components with shafts, the limits of the workshop's available manufacturing methods, and how to refine and realise my designs.

¹Brandon Johns  <https://orcid.org/0000-0002-8761-5432>

²Elahe Abdi  <https://orcid.org/0000-0003-3748-0442>

³Mehrdad Arashpour  <https://orcid.org/0000-0003-4148-3160>

Building 4.0 CRC⁴ — This research is supported by Building 4.0 CRC. The support of the Commonwealth of Australia through the Cooperative Research Centre Programme is acknowledged. The CRC encouraged me to get involved with industry and gave me the opportunities to do so. Learning about the Industry 4.0 broadened my perspective and helped me towards my goal of developing practical and useful research outputs. The stakeholder interviews too, were made possible because of the CRC.

Australia — This research was supported by an Australian Government Research Training Program (RTP) Scholarship. Australians paid for this research, and so, I shall not let the results be restricted or paywalled. All of the results are open and freely available for the benefit of all.

My family — For their support and encouragement.

And to many others who have supported me, but let's keep this from getting any longer. Sorry for leaving out your names.

Finally, and perhaps unconventionally, I also thank a few others who have kept me sane during my candidature. Special mentions to Pomu Rainpuff, Inugami Korone, and the related communities. Also, the music groups: Kalafina, Fiction Junction, Linked Horizon, Sound Horizon, LiSA, Roselia (Bandori!), Poppin'Party (Bandori!), Afterglow (Bandori!), RAISE A SUILEN (Bandori!), Morfonica (Bandori!), Ave Mujica (Bandori!), RONDO (D4DJ), Starlight Kukugumi, Sakabe Gou, sweet ARMS, Konomi Suzuki, Ado, supercell, Hoshimachi Suisei, Tsunomaki Watame, Tokoyami Towa, Pmaru-sama, μ 's, Aqours, Iron Maiden, Rhapsody of Fire, Sabaton, MCR, Demetori, Kokyo Active NEETs, Release hallucination, Yousei Teikoku, DenKare, Unlucky Morpheus, Draw the Emotional, Foreground Eclipse, X Japan, ... just to name a few. Music really means a lot to me.

Anyways, on with the thesis!

⁴Building 4.0 CRC, Caulfield East, Victoria, Australia

Contents

Dedication	i
Abstract	ii
Publications during enrolment	iii
Thesis including published works declaration	iv
Acknowledgements	vi
Contents	viii
Abbreviations	x
1 Introduction	1
1.1 Motivations	1
1.2 Aims and Objectives	2
1.3 Summary of Thesis Contributions.	3
1.4 Thesis Outline	3
2 Background and Literature Review	4
2.1 Unitised Curtain Walls	4
2.2 UCW Installation Process	6
2.2.1 Staging Methods.	8
2.2.2 Conventional Direct Method.	9
2.2.3 Emerging Direct Methods	11
2.3 Technologies Relevant to Mid-Air Crane Payload Alignment	12
2.3.1 Mechanical System.	13
2.3.2 Localisation	14
2.4 Perspectives of Industry Stakeholders.	17
2.4.1 Perspectives of an Equipment Manufacturer.	18
2.4.2 Perspectives of a TAFE Trainer.	20
2.4.3 Discussion of Interview Results	21
2.5 Summary & Research Directions	22
3 Dynamical Model Selection	25
3.1 Dynamical modelling of boom tower crane rigging systems: model selection for construction	25
3.2 Outlook	43

4	Crane Payload Localisation Relative to the Side Face of a Building	44
4.1	Crane Payload Localisation for Curtain Wall Installation: A Markerless Computer Vision Approach	44
4.2	Outlook	68
5	Conclusions and Outlook	69
	Bibliography	71

Abbreviations

BIM	Building Information Modelling
BTHLD	Below the Hook Lifting Device
CAD	Computer Aided Design
CWM	Curtain Wall Module
DAE	Differential Algebraic Equation
DOF	Degrees of Freedom
IMU	Inertial Measurement Unit
LiDAR	Light Detection and Ranging
NIR	Near Infrared
ODE	Ordinary Differential Equation
ROI	Return on Investment
UCW	Unitised Curtain Wall

1 Introduction

This thesis pertains to the field of high-rise building construction, and specifically, the on-site procedures to install the exterior wall, where the wall type is a unitised curtain wall. The installation procedures are analysed, and solutions to prominent challenges are developed. The described challenges and solutions are additionally applicable to any crane operation in which a crane borne payload must be precisely aligned whilst it is suspended high in the air.

The research uses robotics engineering methodologies. Specifically used techniques include process flow modelling, dynamical modelling, and localisation through computer vision.

1.1 Motivations

The unitised curtain wall (UCW) is a type of exterior wall for high-rise buildings which is comprised of prefabricated modules [6]. Building with prefabricated modular components is a path towards the industrialisation of construction [7]. However, the large size and weight of prefabricated modules presents challenges to the on-site installation task [8, 9, 10].

To install the UCW, each prefabricated module is installed sequentially: each curtain wall module (CWM) is individually lifted, aligned to the side face of the building, and fastened in place [8, 11, 12, 13]. This task is difficult because the CWM must be held suspended in mid-air, outside of the open edge of the building, whilst being aligned and fastened (Figure 1.1).

The current approaches to this task support the weight of the CWM either from outside of the building with a crane (e.g. tower crane, mobile crane, spider crane), or from inside of the building with a mobile manipulator (e.g. telescopic handler, forklift) [8, 10, 11, 12, 13]. Lifting with a crane allows direct CWM transport from the ground to the installation location, eliminating inefficient double-handling of the CWM [8, 10]. However, this method can be dangerous. In the conventional direct CWM installation procedure, workers have to stand at the open edge of the partially constructed high-rise building and reach outwards to take hold of the free-swinging crane-borne CWM so that they can manipulate it into alignment [3]. The workers risk being struck, crushed,

or falling from a height [14, 15]. Risk is increased further in the ‘blind lift’ scenario where the crane operator does not have sight of the payload that they are transporting. Some methodologies have been developed to improve safety and efficiency of this procedure, but they are limited in scope of application [10, 16]. Hence, the unsafe methodologies are still commonly used [3].

The safety and efficiency of the conventional direct CWM installation procedure can be improved with a system to align the crane borne CWM before workers have to physically interact with it [17]. However, the location and orientation of the crane payload is difficult to monitor and control [1, 18, 19]. Improved crane payload localisation is required to make mechanised and automated mid-air alignment viable [3].

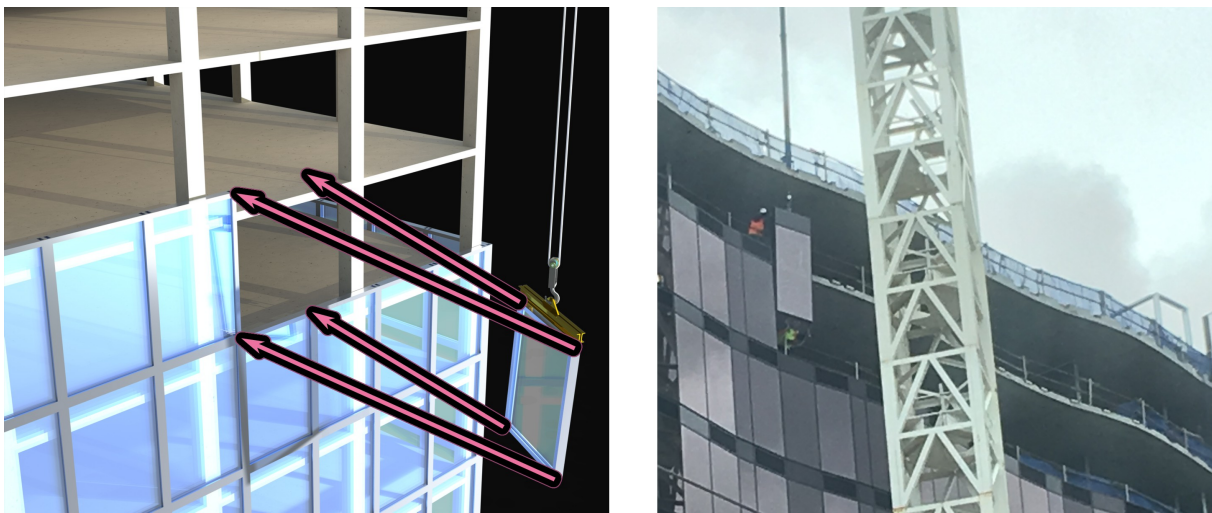


Figure 1.1: The mid-air alignment task in the conventional direct CWM installation procedure (photo by author, 2019)

1.2 Aims and Objectives

This thesis aims to improve the conventional direct CWM installation procedure by making automated localisation of the crane borne CWM viable.

The key objectives are:

- To identify the barriers and opportunities to realising automated mid-air CWM alignment.
- To determine which dynamical model should optimally be used to represent a boom tower crane. Use of the optimal dynamical model facilitates the development of accurate localisation systems.
- To develop a practicable solution to automated CWM localisation.

1.3 Summary of Thesis Contributions

Overall, this thesis contributes to developing the core processes and technologies that are required to make automated localisation of the crane borne CWM viable.

The key contributions of this thesis are:

- Identification of the barriers and opportunities to increasing the level of automation in CWM installation.
- A guideline for system designers to choose the optimal dynamical models to represent the boom tower cranes that are commonly deployed on construction sites.
- An algorithm and methodology to measure the pose of a crane borne CWM, as relative to its installation location on the side face of a high-rise building.

1.4 Thesis Outline

Chapter 2 introduces the background, related literature, and an analysis of the barriers and opportunities to realising automated CWM installation.

Chapter 3 explores the dynamical models used to represent boom tower cranes. The trade-offs between model complexity and accuracy in representation of the real-world system are evaluated. A decision tree to choose the optimal model is introduced.

Chapter 4 introduces a markerless computer vision algorithm and a practical implementation to measure the relative pose between a crane borne CWM and its installation location.

Chapter 5 concludes the thesis and discusses directions for future research.

2 Background and Literature Review

This chapter contains content from my publication [3].

The discussions with industry stakeholders were undertaken with approval from the Monash University Human Research Ethics Committee (MUHREC) – project ID 37652.

This chapter introduces the background and related literature. An analysis of the barriers and opportunities to realising automated CWM installation is used to recommend research directions.

Section 2.1 introduces the unitised curtain wall.

Section 2.2 introduces the on-site installation procedure as a generalised process and evaluates the current and emerging methods.

Section 2.3 discusses potentials to streamline the conventional direct method.

Section 2.4 presents and analyses the perspectives of industry stakeholders on the current methods and the barriers to automated CWM installation.

Section 2.5 summarises the chapter and recommends research directions.

2.1 Unitised Curtain Walls

The core purpose of the exterior wall of a building is to protect the building interior from the outside environment [20]. It may optionally also provide support for the building (a structural wall), security, and aesthetics.

For non-structural walls, the wall is supported by the buildings structure. For high-rise buildings, the load-bearing structure is often made of timber, steel beams, or reinforced concrete. Use of a non-structural wall permits more choice in wall design and materials [6].

A curtain wall is a lightweight non-structural wall that hangs from the side of the building (hence the name ‘curtain’). For concrete floored buildings, the wall is attached to the concrete floor slabs [11]. Otherwise, it is attached to the frame of the building

[6]. Curtain walls are often realised as large glass panels framed in aluminium: a form of structural glazing. e.g. Figure 2.2.

Curtain wall types are often categorised as either stick or unitised [6, 11, 20]. In the stick curtain wall system, additional framing members (mullions and transoms) are affixed to the building before the infill panels (e.g. the glass panels) are affixed to the framing [6, 20]. These operations are completed on-site. To insert the infill panels, it is advantageous to approach from outside of the building (exterior glazing) to avoid any obstructions that may reside inside of the building, and due to problems with air infiltration when interior glazing is used [20]. However, exterior glazing in high-rise construction is a high-risk activity that often has workers manipulate the panel while abseiling down the outer face of the building.

By contrast, the unitised curtain wall (UCW) system is comprised of prefabricated modules that hang from the building on brackets [6, 11]. Each curtain wall module (CWM) consists of both frame and infill panel. CWM assembly and glazing is completed in a factory environment. The required on-site operations are to first position and affix mounting brackets to the building, and then to align and fasten the CWMs to these brackets [11].

Building with prefabricated modular components is considered as a path towards the industrialisation of construction [7]. CWM construction in factory environments affords strict quality control and facilitates the integration of high precision and complex features such as double and triple glazing. Each CWM is typically¹ one storey high (2400–4500mm), 1000–2700mm wide, 50–300mm deep, and 100–1600kg in mass. The maximum CWM size and weight are restricted by the capacity of the public roads between the factory and construction site.

Design requirements of the curtain wall are to bear wind, seismic, pressure, thermal, and blast loading [20]. It must be aesthetic, pressure tight, watertight, thermally insulative, and compliant to structural deformations of the building. Combined, these requirements restrict the possible CWM designs. Therefore, the installation methodologies should conform to the existing CWM designs rather than imposing additional requirements on the design. For example, instead of using a computer vision algorithm that requires markers to be placed on the CWM, the algorithm can detect the CWM by the visual properties of the existing thermally insulative coatings on the glass.

¹Based on product specifications from [Capral Limited](#) and [Reynaers Aluminium](#). Retrieved 2023.

The next section examines the UCW installation process as a generalised process. The current and emerging installation processes are then introduced and evaluated against the generalised process.

2.2 UCW Installation Process

The UCW installation process is described in [11, 12, 13]. The process comprises of designing the wall, manufacturing CWMs, delivery to the construction site, vertical transportation to the installation location, alignment with the attachment location, and attachment of CWMs to the building. Within this process, the attachment interface on the building side can be prepared before, or at the time of, CWM attachment [11].

This thesis focuses on the tasks of CWM vertical transportation and alignment with the attachment location. These tasks are particularly dangerous in the conventional procedure, and there is potential to significantly improve safety and economic efficiency through mechanisation and automation [8, 9, 10, 18, 21].

Figure 2.1 introduces the generalised solution to CWM vertical transportation and precision alignment. The desired state of the system has the CWM aligned to the attachment location. To achieve this, the decision-maker commands the hardware controller, which actuates the mechanical system toward the desired state. The state of the system is sensed, and the sensed information is pre-processed by the analysis unit before being fed back to the decision-maker. Information may also be sent directly from the sensors or analysis unit to the controller, creating an inner feedback loop to stabilise the system state and suppress deviations from the command signal.

The mechanical requirements of this task are CWM load bearing, large distance vertical transportation, and precise position and orientation control with 1mm tolerance [16, 22]. A safe and efficient solution requires performance of each subsystem, as well as unison in communication between the subsystems. A solution should also consider how it affects the rest of the installation process, and the impact on other construction tasks. For example, potential for construction delays is increased with reliance on shared workspace [8, 9, 10] and equipment [8, 10, 21].

The subprocesses in Figure 2.1 are defined in a generic sense. For example, consider the scenario of a single human worker installing a CWM by manual handling. In this scenario, the mechanical system is the combination of the worker and the CWM. Sensing of the system and the environment is achieved by the worker's vision, hearing,

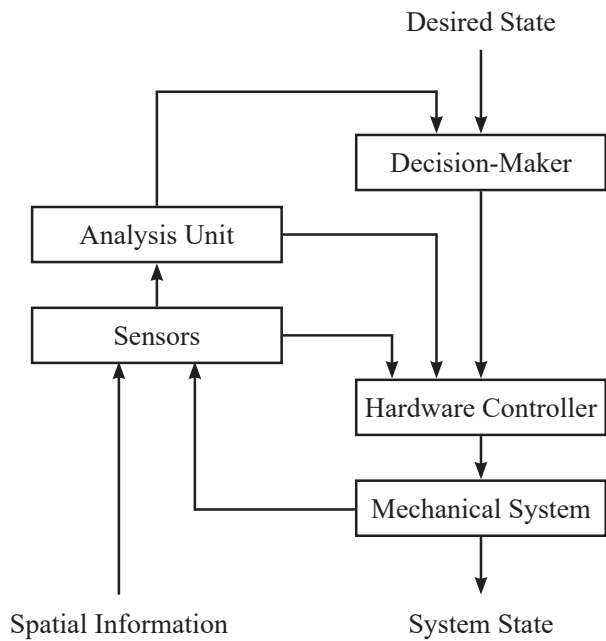


Figure 2.1: Generalised solution to the CWM vertical transportation and alignment tasks in UCW installation.



Figure 2.2: Conventional direct UCW installation method: Transitioning from the vertical transport task to the alignment task (photo by author, 2019).

and tactition. Their mind performs analysis and decision making. Hardware control is achieved by their motor skills.

This manual solution performs with ideal synergy between the subsystems. However, the performance of the mechanical system is limiting: the worker is not strong enough to carry a CWM, nor can they quickly travel from the ground to the installation location. Hence, the conventional methodologies employ lifting equipment to overcome these limitations.

There are two predominant strategies to UCW installation, from which all the current methodologies are derived. In the direct methodologies, CWMs are lifted directly from the ground to the attachment location, as depicted in Figure 2.2. In the staged methodologies, CWMs are bulk transported from the ground to the working floor (the storey at which the CWMs are to be installed), before being individually lifted and installed [8, 9, 11, 13]. Variations of the staged conventional method are depicted in [8, 12, 13], and a more recent staged method is depicted in Figure 2.3.

The direct and staging methodologies are described and discussed in the following subsections.

2.2.1 Staging Methods

The conventional staging methods are described in [8, 9, 11, 13]. In the first stage, CWM vertical transportation from the ground to the working floor is performed in bulk, and the CWMs are placed near the installation location. A material lift (construction hoist, buck hoist, industrial elevator) may be used, if available. Otherwise, a bundle of CWMs may be crane lifted from the ground to a loading platform (outrigger platform). Loading platforms are temporary platforms that extend out the side of the building to allow crane bundles to be landed.

The vertical transportation task requires the use a lift or crane, and the use of additional floor space on which to stage the CWMs. These resources are often shared between multiple contractors. Hence, the procedure can significantly impact or be impacted by the logistics of other construction operations [8, 10].

In the second stage, each staged CWM is then individually lifted and aligned to the attachment location before being fastened in place. A spider crane on a floor above, or the roof, is commonly used to bear the weight of the CWM. In this method, the pose of the CWM is controlled by a combination of the current length of the crane's hoist, and the manual handling of workers on the working floor [8, 12, 13]. As the hoist is raised, the CWM needs to be pushed over the edge of the building to orient it from lying flat to hanging vertically. This process can be very physically demanding of the workers [13]. Sometimes, jigs with sliding mechanisms are used to reduce physical demand [12].

Alternatively, a mobile manipulator (e.g. telescopic handler, forklift) located on the working floor may pick up the CWM with suction cups and carry it to the aligned pose. This is depicted in Figure 2.3. Advanced robotic manipulators have been developed to enable human-robot cooperative manipulation in this task. In [13, 23], the end-effector, which supports the weight of the CWM, can be effortlessly moved by a worker applying force to it. Therefore, the worker can manual-handle CWMs into alignment without having to support their weight.

The alignment task requires heavy machinery and jigs to be located on, or above, the working floor. The building must accommodate the size and mass of this machinery. The space used by the machinery may interfere with other operations. The transportation of the machinery to, from, between, and around floors may also be logistically difficult. For example, by installing the last CWM, the mobile manipulator may be trapping itself inside of the building. Depending on the building's design, or in the case of building renovation, access may not be possible.

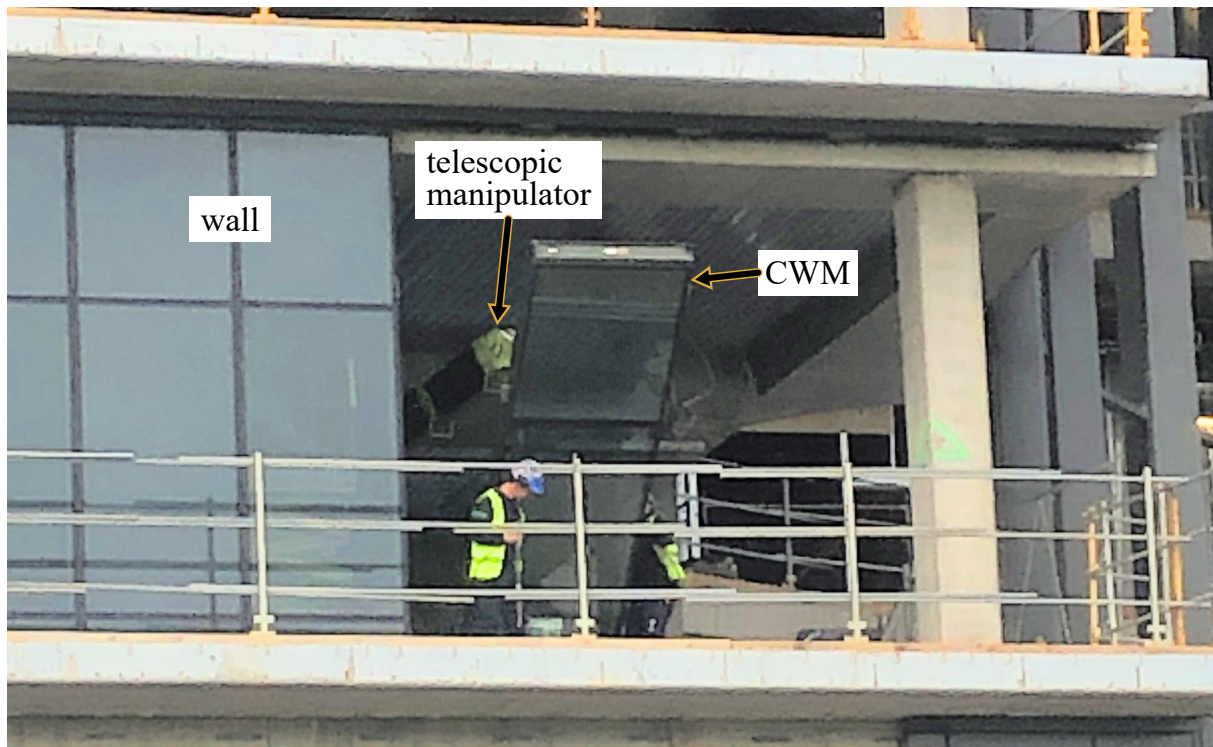


Figure 2.3: Staged UCW installation method using a telescopic manipulator: Performing the alignment task (photo by author, 2021).

In terms of the generalised solution, the synergy between the subsystems is high if a mobile manipulator is used, but low if a spider crane is used. Using a spider crane places multiple hardware controllers on different building floors: the crane operator on the floor above, and the workers on the working floor. Error or delay in communication with the decision maker could result in an accident.

Overall, the staging methodologies can be safe and efficient, but they are not applicable to every CWM installation scenario.

2.2.2 Conventional Direct Method

In the direct approach, each CWM is individually lifted directly from the ground to the attachment location with a crane or hoist. It is then aligned, fastened, and detached from the hoist. The hoist is then lowered, and the process repeats.

The direct methods are most appropriate for large and heavy CWMs. It is faster to install UCWs that are comprised of larger modules [9, 10, 24]. Additionally, by not requiring on-floor staging, the impact on other construction operations can be reduced [8, 10].

In the conventional direct solution, each CWM is individually crane lifted from the ground below the installation location, up towards the installation location. While the CWM is still supported by the crane, workers at the installation location reach out past the open edge of the building to take hold of the free-swinging CWM [3]. They then physically manipulate the CWM into alignment before fastening it to the brackets (Figure 2.2). The CWM is detached from the crane, and the process is repeated.

Cranes are imprecise and can not control load orientation. Therefore, the workers intercepting the CWM are required to stop its swinging and rotate it before it can be brought close enough to the building for them to take hold of it. The workers risk being struck, crushed, or falling from a height [14, 15].

In crane operations, the dogman performs sensing, analysis, and decision-making. The dogman is a designated worker whose job is to direct the crane operator in the movement of the load [25]. The standard modes of communication between the crane operator and the dogman are two-way radio, arm gesture signalling by the dogman, and whistle signalling by the dogman [25]. In case of loss of communication, the crane operator should halt the crane.

The dogman is usually situated at the installation point so that they can precisely determine the pose of the payload during alignment. However, communication of this information is limited by the standard modes of communication. The communication is slow and low in detail e.g. there is no arm signal to communicate distance or speed. The standard sensors on-board a crane do not measure spatial information. Therefore, in the case of a 'blind lift' (where the crane operator cannot see the CWM directly), the operator can not verify their correct interpretation of the dogman's instructions. Overall, the communication speed and information detail are key limiting factors to installation speed and safety [18, 26].

The flow of information and control in the process is mangled. This indicates that safety and efficiency be improved through automation of the work conventionally performed by the dogman and the alignment crew. This requires automation of sensing and analysis, and mechanisation of precision crane payload pose control.

2.2.3 Emerging Direct Methods

A key challenge in implementing a direct method is to achieve precise control of the CWM during alignment. The conventional solution leaves the pose uncontrolled throughout vertical transport. Then when CWM approaches the installation location, it is captured and controlled into alignment. However, safely capturing and manipulating the CWM is difficult if it approaches while swinging or orientated the wrong way around. Therefore, it would be better to control the CWM throughout the vertical transport.

The most appropriate class of robot for high-rise UCW installation without on-floor staging is the hanging robot [27]. Yet, precise control of all the degrees of freedom (DOF) of a hanging system is difficult. The crane system with a single hoist cable is highly underactuated and susceptible to wind induced oscillations [19], hence the need for the dogman and alignment crew to perform fine position and orientation control.

Two approaches to control a hanging system are to either suppress oscillations with control systems or to introduce additional kinematic constraints. A common kinematic constraint for crane operations is a tag line; a rope that is attached to the payload and held by a worker [25]. This solution has been used for mid-rise CWM installation, where two workers positioned on the ground each have a rope to pull the CWM in opposite directions. For high-rise construction, a tag line may be attached to the payload before it is lifted. Then, the workers at the installation location use a shepherd's crook to recover the tag line.

This methodology was developed into a robotic solution in [11, 16, 27, 28, 29, 30]. The redundantly cable-driven parallel robot uses tensioned cables to connect the robot to the corners of the building face. This over-constrains the robot, allowing it to float without swaying. This design can not achieve 1mm precision, hence, a secondary robot arm is attached to the cable suspended base through a passive damper [16, 28]. The high number of DOF is not ideal for cost or maintenance. Another limitation of the design is that for flat faced buildings, the constraint cables will be closely in-plane, which leaves the design sensitive to out-of-plane disturbances [31]. Additionally, the cable tension must increase as the angle of the cable from vertical increases [31]. Very large cable tension would then be required to install the top row of CWMs, a load which the building may not be designed to withstand. However, there are no other practical cable attachment points other than the building that is under construction [27].

Two methods which have been commercialised use guide cables [9] or guide rails [8, 10] for kinematic constraint. Again, the building is used to support the constraining fixtures. As risk of damage by collision with the building is eliminated, the lift path can stay close to the building for the entire lift. This allows for performing the lift with a hoist that is mounted on the building, thus eliminating dependence on the expensive tower crane. However, these solutions are limited in application to geometrically prismatic buildings. Furthermore, the guide rails themselves must be installed without the aid of guide rails, requiring dangerous manual labour.

The prior solutions which introduce additional kinematic constraints are limited to specific or custom designs of building and CWM. Complying with these limitations is not always possible e.g. for the custom design in [32]. Hence, there is still need to use the conventional direct method. The next section investigates opportunities to improve the conventional direct method without limiting its utility.

2.3 Technologies Relevant to Mid-Air Crane Payload Alignment

The conventional direct CWM installation method is inefficient and unsafe [8]. Yet, the current automation solutions are limited in scope of application [10, 16], or in addressing only a small part of the installation procedure [13]. Hence, the conventional method is still needed, and should be improved.

In a review of automation in high-rise construction, it was suggested to review the advancement of basic technologies that can be utilised in high-rise construction [33]. Direct CWM installation was explored in [27], however, the scope of research did not include informational tasks.

This section explores opportunities for improvement in conventional direct CWM installation, with the objective to streamline the flow of information and control in CWM vertical transportation and precision alignment. This involves mechanising precision alignment and improving the quality of the information the crane operator receives.

The literature search used the search keywords identified in [33]. The most relevant were 'curtain wall', 'facade', 'installation', 'assembly', 'automation', and 'robot'. Other keywords were identified through relation to the mechanisms and processes used in UCW installation. For example, 'crane' was combined with 'vision', 'mapping', 'localisation', 'skew control', and 'operator assistance'. The review broadly surveys the applicable technologies rather than focus on specific implementation details. It

is assumed that an operator is required, hence fully autonomous path planning and logistics are not explored.

2.3.1 Mechanical System

Tower cranes, mobile cranes, and spider cranes are all applicable to CWM load bearing and vertical transportation. The lack of other types of support body in high-rise construction indicates that no other independent support structure is practical. This conclusion is supported by the analysis [27]. Using a crane, any geometry of CWM can be lifted to any attachment location that is not below overhanging building geometry. Hence, cranes are applicable to almost any CWM installation scenario. The requirement to situate a tower crane on-site is typically satisfied due to the requirements of other on-site construction operations, and the crane can be shared amongst these operations [8].

To achieve the positional accuracy required for UCW installation, all vibrational modes of the crane borne CWM should be suppressed. There are 6 DOF for a crane borne load: sway (pendulum swinging of the hook with 2 DOF), roll (payload tilting about the hook with 2 DOF), skew (rotation about the cable axis with 1 DOF), and heave (linear oscillation along the cable axis with 1 DOF) [34]. Based on a 2017 review of crane control systems [19], most research considers only the sway modes with a few considering the roll modes. Very little research considers skew [35] or heave [19].

Heave, roll, and sway oscillations can be controlled with regular tower crane motions; however, control is underactuated. Furthermore, the rotational motion of the jib about the tower (slewing), has highly coupled non-linear dynamics, making control of the payload very difficult [19]. Hence, to achieve the positional accuracy needed to install a CWM, an additional mechanism is required.

Below-the-hook-lifting-devices (BTHLDs) are devices that attach between the crane hook and the crane payload. BTHLDs can provide mechanical interfaces for payload attachment, orient payloads, and perform task specific functions. The use of spreader bars, a type of BTHLD, is already common in CWM installation. A BTHLD can be fit to any crane, and the connection/disconnection procedure is fast and simple. They are versatile and compatible with existing cranes.

BTHLDs can be used to adjust roll orientation by small angles by translating the centre of mass of the payload about the hook [36]. This can be an active device, or the roll orientation can be manually set to the aligned orientation before the lift operation.

Active skew control is necessary to perform alignment with complex building geometry or when using slewing cranes [37]. Several BTHLDs have been developed which exert skew torque with fans or through conservation of angular momentum with heavy flywheels [17, 38, 39]. Using these, less manipulation work is required, improving both the safety and speed [17, 38, 40]. Commercial instances of these devices include the EVEREST series, HALO, Roborigger, and the Vita Load Navigator².

Another method of skew control is seen on harbor cranes. For slewing harbor cranes, skew control is achieved with an active rotary crane hook (rotator, power swivel) [35, 37, 41, 42]. For system stability, at least two separated cables must connect the trolley and hook block. Full scale outdoor experiments show that very small skew error is achievable [37], likely to a degree that is sufficient for UCW installation.

To aid in vibration suppression when the CWM is near the building, the building and the previously installed CWMs can act as reactionaries. A robotic manipulator can take hold of the building and drive the CWM into position by using the sway degrees of freedom [43] or an extendable hook attachment [44]. For the gripper type, inspiration can be taken from harbor crane operations, where the spreader is mechanically aligned to the target container with ‘flippers’. The flippers are driven closed onto the edges of the container from all directions, mechanically forcing the parts into alignment. To prevent damage to the building or CWM, a pre-acting control strategy can be used to dampen the impulsive load of the manipulator coming into contact with the reactionary [43].

2.3.2 Localisation

To perform vertical transportation and precision alignment requires localisation of the crane borne CWM with respect to the attachment location and nearby hazards. In the current methodology, the dogman performs localisation and decision-making. However, the standard modes of communication between the crane operator and the dogman are slow and low in detail. Thus, there is risk of miscommunication and low response time in emergency situations. Safety and efficiency can be improved by providing the crane operator with high quality localisation information [18, 26].

Providing the crane operator with too much information or poorly organised information increases the cognitive workload to perform analysis [45], which increases their reaction time. Camera views provided to the operator should be 2D top and side views rather

²Respectively from: [Verton Australia](#), [Torquer Lifting Solutions](#), [Tensa Equipment](#), [Vita Inclinata](#).

than a 3D view [45]. Pre-processing and analysis of camera feed to draw attention to the relevant information is commonly researched. A map can be generated by piecing together images captured by an overhead camera at different crane orientations [46], and the heights of obstacles can be highlighted by thresholding rangefinder data [47]. Video feed can also be generated in a game engine by fusing sensor data with the CAD model of the construction site [45, 48]. However, trials of an operator feedback system indicated that a raw camera view should still be provided to increase operator trust in the system [45]. A raw camera view can also provide a fallback in case of poor operating conditions for automated analysis [49].

The display's controls should be simple, require minimal user interaction, and preferably be hands free [48]. Disruptive feedback (e.g. audio feedback) may be interpreted as either helpful or distracting, depending on the operator's perception of a task's difficulty [18]. Therefore, the types of feedback should depend on the current task. For CWM installation, it may be appropriate to use separate interfaces for vertical transport and precision alignment. Since these tasks are completed separately, the interface can switch as the CWM approaches the installation location.

To produce high-quality visualisations of the localisation and perform automated actions requires obtaining numeric measurements of the localisation. Two measurement tasks are to monitor the distance between the CWM and the side face of the building, and to measure the relative displacement between the CWM and the target aligned pose. Likewise to the display interface, the requirements of the measurement systems are also task dependent. Vertical transport requires a broad view, but does not require high precision. The alignment task has opposite requirements. Hence it may be practical to use different measurement systems for each task.

The global localisation strategy is to individually measure the locations of the crane payload, attachment location, and any hazards, with respect to a global map. Then, any relative measurement can be obtained from the map. The digital building plan can be used as a map, if available [45, 50]. However, this does not provide realtime information on hazards or deviance from the plan. Additionally, this technique is not useful to precision alignment because the state of the art in global crane-payload-pose-measurement achieves error in the order of metres [48, 51, 52, 53], and most systems do not consider payload orientation [19, 54]. The barriers to achieving millimetre accurate crane pose measurement are numerous: a solution would need to consider the highly-coupled non-linear pendulum dynamics of the

payload [19], deflections of the tower, boom, jib, and hoist-rope, the effects of wind and the effects of frictional damping [55, 56, 57, 58, 59].

To circumvent the limitations of global localisation, a proximity sensor or computer vision system can directly measure the relative pose between the payload and fiducial features of the target. Possible locations for camera placement are on the building, the crane, or equipment. If the camera is not attached to the payload or the target, then it should have a view of both, and this view should not be easily obscured. The view should also have sufficiently high resolution (either through zoom or near placement), and because the UCW is very large, this requires the view to continuously follow the target. Requiring workers to position and/or aim the camera would introduce potential for poor camera positioning. A downward-facing camera attached to the top of the crane hoist or spreader can measure the pose of the payload [48, 52] and ground-based objects [60, 61]. High accuracy measurements can be obtained from a camera attached to the spreader [61]. In [38] and [4], a sideways-facing camera mounted on a crane spreader localises itself with respect to artificial markers attached to the target. This system has a very close view, hence achieving high accuracy. However, the markers must be in view of the camera, requiring the system to already be near alignment before the measurement system can function. This could be improved with markerless object recognition.

In case of low certainty in automated object recognition, the operator can provide input. For example, the operator can select locations of interest from a camera feed to provide a region of convergence to the feature detection algorithm [49]. After the alignment target has been identified, the controller can then perform path planning and complete the alignment semi-autonomously. This requires abstracting the operator input into higher level actions and programming the controller to decompose these into actuator inputs [62]. This separates the operator's decision from the actions that are generated by internal feedback-control systems. This separation is beneficial, as absence of separation creates conflict between the operator and the control system [63].

The next section investigates the perspectives of industry stakeholders on the utility of, and barriers to, the potential application of some of these methods and technologies.

2.4 Perspectives of Industry Stakeholders

Two discussions with industry stakeholders were held on the topic of curtain wall installation and applicable technologies. The discussion format was one-on-one interviews between the researcher and the industry stakeholder, with duration of roughly 1 hour.

The researcher first introduced the discussion topic and scope. The discussion that followed was separated into two parts.

The first part focused on the curtain wall installation and mid-air alignment methods that the participant is aware of, where the methods are applied, and why they are or are not used. Slides were displayed to prompt discussion topics. The first slide displayed a partially installed UCW (Figure 2.4) and the text “Stages: Design, Plan, Transport, Align, Secure, Reset, Dismantle”. The second slide displayed the same image, but the text was changed to “Barriers to entry: required training, upfront cost. Application specific barriers: wall design, equipment availability, access requirements, planning effort, speed, no. task repetitions, running cost”.

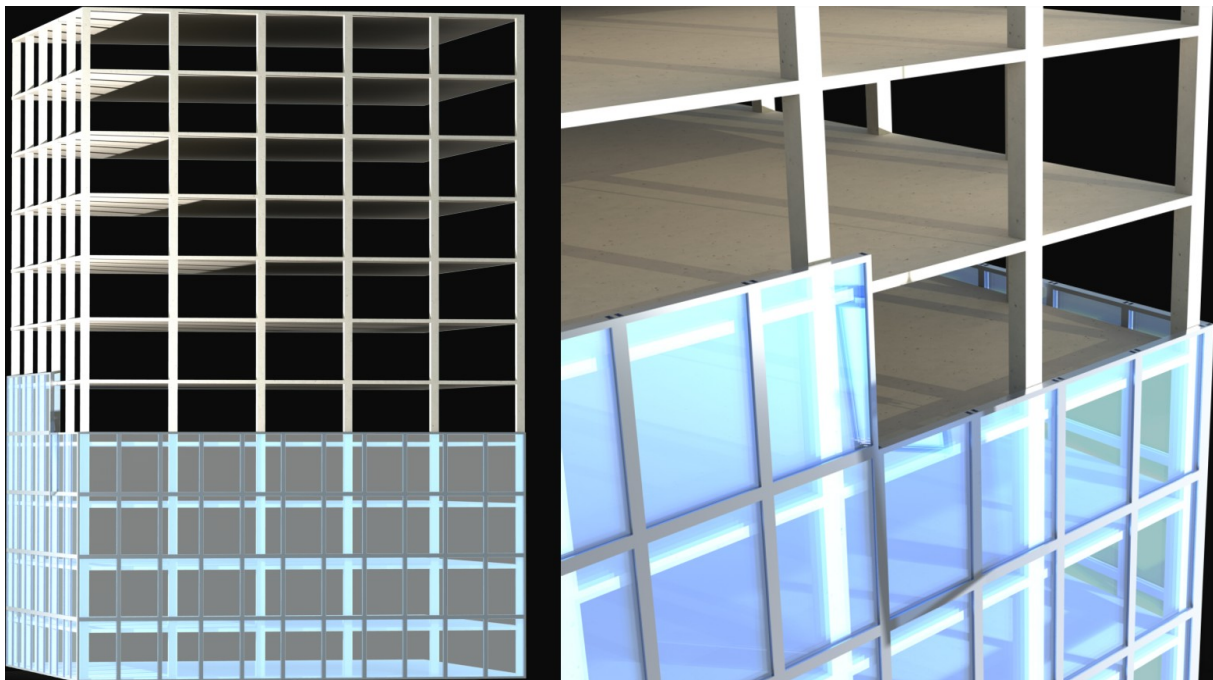


Figure 2.4: Render of a partially installed UCW. Displayed in the first half of the interview.

In the second part of the interview, the researcher introduced all the methods from Section 2.2, the active rotary crane hook, and the concept of placing cameras on the crane. Slides without text were used to depict these, as well as a blind lift scenario.

The discussions in the second part were unstructured, allowing the participant to lead the discussion based on what they saw in the slides.

2.4.1 Perspectives of an Equipment Manufacturer

In this section, the participant is referred to by the pseudonym P.

Discussion was held with a mechanical engineer who holds a leadership position at Verton Australia³. Verton's core business is the design, manufacture, and sale of remote-controlled BTHLDs for rotating crane payloads about the skew axis. These devices rotate the payload by exerting torque through conservation of angular momentum with heavy flywheels. Verton were invited for discussion because their products were identified as potentially applicable to the mechanisation of CWM installation (Section 2.3).

In the first part of the interview, P identified the CWM installation methods involving lifting with telescopic handlers, crane lifting with tag lines, crane lifting where the tag line is released and then later recovered with a shepherd's crook, and crane lifting with a counter balanced BTHLD that holds the CWM with suction cups. P also emphasised that a lifting device should not interfere with how the lifted element engages into its final position.

P described a method of using a load rotating device as turning the payload into the wind for the duration of the lift, to reduce swinging, and then turning the payload into alignment as it nears the installation location. P discussed that the time savings of this methodology are especially significant on windy coastal sites, where a few minutes can be saved on each lift.

The key barrier to the adoption of Verton's devices was described as the disruption caused to the commonly known logistics processes. The introduction of a new device disrupts the risk assessment, requires approvals, and requires planning for storage and charging. P perceived that the leadership are generally not motivated to take on this additional organisational effort. By contrast, requirement of user training was not considered to be a significant barrier. Uncertainty of return on investment (ROI) was considered as a barrier for new usage scenarios only. Requirement of the crane to bear the extra mass of the BTHLD was not considered to commonly cause any issue.

³<https://www.verted.com.au/>

In the second part of the interview, P discussed considerations of moving towards remote or semi-autonomous operation. The discussion focused on asymmetry of information and assignment of authority/responsibility. The current methodologies assign responsibility for payload movement to the dogman, and the crane operator is responsible to ensure that the crane's load-moment-capacity is never exceeded. In the event of conflict, the crane operator has the authority to halt the crane and communicate that they can not perform the requested action.

P discussed that for some simple and repetitive operations, their product has been combined with a semi-automated grabber to eliminate the need for a dogman. Lights and cameras were placed on the BTHLD, and all personnel were cleared from the area. The crane operator was then given full responsibility and authority over the lift. However, because CWM installation is more complex, significantly more information would be required to ensure safety. P perceived the key hazards as collision with obstacles outside of the camera's field of view, and limited ability to assure that the CWM is properly installed before it is released from the crane. Yet, presenting enough information to the operator would significantly increase the cognitive load.

On the topic of information asymmetry and communication efficiency, P discussed that hand signalling is very limiting in complex scenarios, and that 2-way radio communication works better. The researcher then prompted P to discuss the idea of giving more information to the crane operator (including a sideways camera view), without shifting authority away from the dogman. To this, P stated:

“There's no problem with giving [the crane operator] more information. And, in fact, the sideways view, I think it would be very good, because some of the footage I've seen from block cameras looking straight down - very difficult to really orient yourself. ... If you're looking directly down the hoist rope, trying to understand what angle you're looking at it. And the other thing is because of the height, very difficult to go to where you are. But if you had a sideways looking camera, yeah, that that would make a lot of sense.”

2.4.2 Perspectives of a TAFE Trainer

In this section, the participant is referred to by the pseudonym T.

Discussion was held with an Australian TAFE teacher who teaches in the field of OH&S in construction and has worked as a dogman. T was invited for discussion because of their experience in teaching students who perform high-altitude glazing, and because their teaching work is relevant to the theme of increasing safety in UCW installation.

In the first part of the interview, T identified the CWM installation methods involving lifting with telescopic handlers, and crane lifting with tag lines. T was familiar the stick curtain wall system, but not UCWs. T identified that for the stick system, it is common to crane lift the panel toward the building while two workers abseil down the building to meet it. The workers then catch the panel and manipulate it into alignment. T discussed that tag lines can be very lightweight, allowing them to span multiple building storeys, and that when there is no fixture on the panel to which a tag line may be attached, then a hand-pump vacuum cup is sometimes placed on the panel to provide a fixture.

T discussed that lifting crews commonly receive panels that are damaged or incorrectly dimensioned, treated, or finished. If the difference is subtle, then the lifting crew may not realise until mid-lift, during the alignment stage.

In the second part of the interview, T discussed the continued use of unsafe methods. For every construction project, the method is chosen through an individualised risk assessment. The risk assessment involves consultation with experts, workers with experience, who would typically suggest the same method that they have always used. T discussed that it is not the job of the lifting crew to be creative. Hence, the continued use of the conventional procedure is due to the culture of 'this is how it's always been done'. To change the procedure would require the leadership or site engineer to be assertive.

On the topic of asymmetry of information and assignment of authority/responsibility, T discussed the procedure developed during the risk assessment defines the authority and responsibility. When a dogman is used, the crane operator must try to follow the dogman's instructions exactly (or otherwise halt the crane). They do not have authority to perform even millimetre adjustments. Thus, T emphasised that good communication is key to the procedure.

T further discussed that it is reasonable to delegate information collection and processing. For example, a second dogman may provide information to the lead dogman. The responsibilities and chain of authority would need to be carefully defined in the procedure.

2.4.3 Discussion of Interview Results

Both participants discussed that culture is a key barrier to introducing new CWM installation procedures. The culture favours repeating the previously known procedure, with variation only to satisfy the risk assessment of the project.

Regarding the assignment of authority and responsibility, both participants discussed the assignment may be changed, but that there should not be any overlap. The crane operator should halt the crane in event of loss of communication or receiving an instruction that conflicts with their responsibilities. Both participants emphasised the importance of communication. The restrictive nature of the current modes of communication was also recognised.

Between the participants, the discussion indicates that a dogman will be required for any scenario that does not achieve a high level of automation. Monitoring should include the location of all parts of the crane, panel alignment, and the fit of the panel. Hence, it was suggested to provide processed information to the dogman as well as the crane operator.

Based on these results, a successful solution to improve the conventional direct CWM installation procedure should strengthen the communication between the crane operator and the dogman while minimally changing the assignment of authority/responsibility, the chosen method, or the logistics. Hence, the solution would be to provide technologies that can replace aspects of the current methodologies in isolation. This allows the workers to still choose the variant that they are familiar with, while using the provided technologies to enhance their work. Additionally, this solution should ideally require minimal managerial effort to implement.

2.5 Summary & Research Directions

A unitised curtain wall is a type of exterior wall for high-rise buildings which is comprised of prefabricated modules that hang from the side of the building on brackets. Each CWM consists of both frame and infill panel. CWM assembly and glazing is completed in a factory. The required on-site operations are to first position and affix the mounting brackets to the building, and then to align and fasten the prefabricated modules to the brackets.

This thesis focuses on the tasks of CWM vertical transportation, and CWM alignment with the attachment location. The methodologies can be classed as direct or staged. In the direct methodologies, CWMs are lifted directly from the ground to the attachment location. In the staged methodologies, CWMs are bulk transported from the ground to the working floor, before being individually lifted and installed.

The staged methodologies can achieve high synergy between the subsystems (Figure 2.1) if a mobile manipulator is used. However, the access requirements are not always satisfied. Additionally, staged methodologies are not suitable for large CWMs.

The direct methodologies are more streamlined and can be applied in most scenarios. However, a key challenge in implementation is to achieve precise control of the CWM's pose during alignment. Prior works introduce additional kinematic constraints to solve this challenge. However, these solutions are limited in scope of application, or in addressing only a small part of the installation procedure. Hence, there is still need to use the conventional direct methodologies.

In the conventional direct methodologies, each CWM is individually crane lifted from the ground to the installation location. While the CWM is still supported by the crane, workers at the installation location reach out past the open edge of the building to take hold of the free-swinging CWM. They then physically manipulate the CWM into alignment before fastening it to the brackets. The workers risk being struck, crushed, or falling from a height. In this method, the dogman is responsible for all movement of the crane borne CWM. The crane operator must follow the dogman's instructions exactly, and if they lose communication or receive an instruction that conflicts with their responsibilities, then they should halt the crane. The alignment task and its key limitations are depicted in Figure 2.5.



Figure 2.5: Render of the alignment task in the conventional direct UCW installation methodology, depicting the key limitations.

Key directions to improve the conventional direct methodologies are:

- To research construction crane dynamics to determine what dynamical models provide an accurate representation. There are many different models, but it is not clear which models are most appropriate to use. Use of an accurate model facilitates precise control and state estimation.
- To develop automated systems to obtain and process localisation information that is relevant to mid-air alignment, and present this to the dogman and crane operator. Providing both workers with this information provides a common basis for forming and interpreting instructions.
- To develop a practical framework for incorporating these advancements and the relevant technologies identified in Section 2.3 into the conventional direct methodologies, whilst respecting the considerations identified in Section 2.4.

The perspectives of two industry stakeholders support strengthening the communication between the crane operator and dogman by providing them with rich information. The assignment of authority and responsibility may be changed, but there should not be any overlap. In practice, the culture inhibits changing the chosen procedure. Therefore, to increase the chance of uptake, any proposed changes should minimally impact the logistics.

The remainder of this thesis investigates these research directions. Chapter 3 evaluates the optimal dynamical models that should be used to represent boom tower cranes. Chapter 4 introduces a markerless computer vision measurement algorithm to measure the relative pose between a crane borne CWM and its installation location. A practical

implementation is proposed which incorporates the measurement algorithm to obtain a localisation, a BTHLD for control, and a system to present the localisation.

3 Dynamical Model Selection

This chapter embeds a copy of my publication [1], which is distributed under the [Creative Commons CC BY 4.0 license](#).

Boom tower cranes are commonly used in conventional direct CWM installation to perform vertical transport, and to support the mass of the CWM during alignment. Safety and efficiency in this task can be improved with more accurate payload monitoring and control.

In mid-air alignment operations, all 6 DOF of the payload's pose must be controlled. This differs from the more common crane operation to land a payload on the ground, where roll and heave can reasonably be ignored because the payload rights itself as it lands, and where manual handling can be used to correct location error, oscillation, and payload skew. In mid-air alignment, the use of manual handling and tag lines is less efficient because the payload is difficult to reach. Hence, there is need for precise 6 DOF payload pose monitoring and control.

A dynamical model is the representation of a real-world system to its monitoring and control systems. Use of an accurate model facilitates precise control and state estimation. Many different models have been developed; however, it is not clear which model is most appropriate to use for any given scenario. Therefore, this chapter determines which dynamical models are most appropriate to use to represent boom tower cranes for different task requirements.

3.1 Dynamical modelling of boom tower crane rigging systems: model selection for construction

List of Amendments to [1]

- Equation 6 contains a typographical error, in which ${}^O\mathbf{p}_i$ should be ${}^O\dot{\mathbf{p}}_i$



Dynamical modelling of boom tower crane rigging systems: model selection for construction

Brandon Johns¹ · Elahe Abdi¹ · Mehrdad Arashpour²

Received: 9 February 2023 / Revised: 18 May 2023 / Accepted: 20 May 2023
© The Author(s) 2023

Abstract

Accurate dynamical models are imperative to the development of accurate monitoring and control systems, which are foundational to safety in construction and infrastructure projects. However, the highly coupled non-linear dynamics of crane systems requires the application of many simplifying assumptions to the dynamical crane model. To achieve accurate control, simplifications should yield minimal error in modelled behaviour for maximal reduction in model complexity. However, limited information is available on the situational suitability of different combinations of simplifications to construction tower crane models. This paper informs designers of the optimal dynamical models to represent boom tower cranes, with respect to the crane characteristics and selection criteria. The optimal models are determined through the comparison of ten 2D and 3D dynamical models in representation of three variations of boom tower crane that are commonly deployed on construction sites. The comparison includes analysis of over 100 simulations and experimentation. The value of the presented optimal model selection framework is in facilitating systems designers to develop accurate crane monitoring and control systems.

Keywords Boom crane · Construction · Dynamics · Modelling · Tower crane

1 Introduction

A dynamical model is the representation of a real-world system to its monitoring and control systems. The state estimator predicts the state of the system by evaluating the dynamical model, and the control system is developed to control the dynamical model. If the dynamical model inaccurately represents the dynamics of the real-world system, then the performance of the monitoring and control system is reduced upon application to the real-world system [1].

Boom tower cranes (Fig. 1) are deployed in construction operations to lift large and heavy payloads. Current tower

crane control systems are insufficiently accurate in the task of payload alignment to the target [2]. Hence, human workers must physically manipulate the suspended payload into alignment. For steel beam erection [3] and curtain wall installation [4] this task is near to a fall-from-height hazard. This methodology is not safe; the most common types of construction accident include workers falling from a height [5] or being struck by a crane payload [6]. Safety in construction can be improved with more accurate automated crane monitoring [7] and control systems [4].

The development of monitoring and control systems for boom tower cranes is particularly difficult. Many limitations in current tower crane modelling and control literature were identified in [8]. Boom tower cranes are under-actuated and exhibit highly coupled nonlinear dynamics during luffing and slewing motions [9]. Hence, many approximations and simplifications are applied during modelling [1]. While simplifications to the dynamical model are a necessity, there is flexibility for the designer to choose which simplifications to apply. An optimal set of simplifications should yield minimal error in modelled behaviour for maximal reduction in model complexity.

The most common lumped parameter models approximate the system as a single or double pendulum. Control of

✉ Brandon Johns
brandon.johns@monash.edu

Elahe Abdi
elahe.abdi@monash.edu

Mehrdad Arashpour
mehrdad.arashpour@monash.edu

¹ Department of Mechanical and Aerospace Engineering, Monash University, 14 Alliance Lane, Clayton, VIC 3800, Australia

² Department of Civil Engineering, Monash University, 14 Alliance Lane, Clayton, VIC 3800, Australia

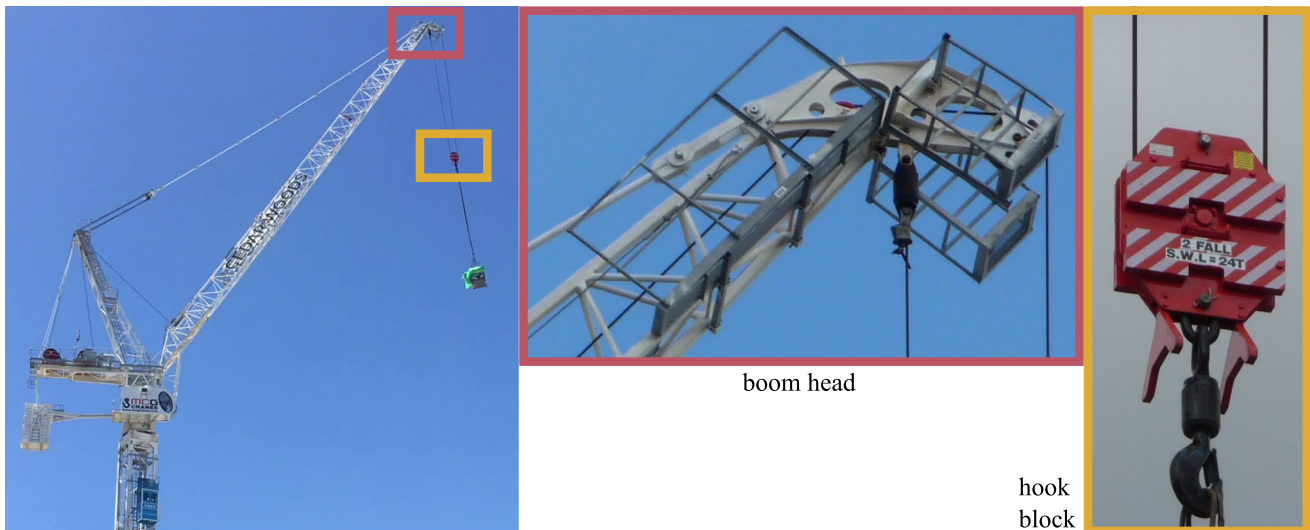


Fig. 1 Boom tower crane with a returning hoist rope (Photos by authors, 2020)

these systems was comprehensively reviewed most recently in [9]. In the double pendulum model, the hook block and payload (Fig. 3) are separate point or lumped masses, while in the single pendulum model they are combined [9]. The truss structures (tower, boom, jib) of the crane are usually assumed to be inelastic [10], thus, the position of the boom head is a function of only the actuator positions. The actuator dynamics and limits are also often ignored [8], thus, the position of the boom head is effectively assumed to be precisely position controllable by an independent servomechanism. The hoisting rope is almost always considered straight, inelastic, and massless [9]. The degrees of freedom (DOF) of this double pendulum model are sway (hook block swinging about the top of the hoist with two DOF) and roll (payload tilting about the hook block with two DOF).

Evaluation of the double pendulum model in 2D found that the single pendulum model is insufficient when the sway and roll eigenfrequencies differ [11]. The payload point-mass assumption neglects the payload orientation. However, for long or flat payloads, the payload orientation is coupled with the sway dynamics. This was demonstrated for the 2D bridge crane [12], 3D bridge crane [13], 3D single pendulum jib tower crane [14], and the 3D double pendulum jib tower crane [15].

The approximation of inelastic truss structures neglects the complex dynamical coupling between the tower, boom, jib and the active load [10]. The approximation of inelastic rope neglects the heave vibrational mode (linear oscillation along the rope axis with one DOF). Consideration of heave is important in scenarios requiring high positional accuracy if the payload is heavy and the hoisting rope is long [16]. Transverse vibration in the rope has also been considered, however this significantly complicates the model, reducing

the viability of modelling other features [17]. Likewise, consideration of wind force and frictional damping significantly complicates the model [18], especially where the payload shape [19] or transverse rope vibration [17] is considered.

Moreover, many rigging configurations of boom tower crane use multiple hoisting ropes. The sufficiency of the pendulum model to represent the dynamics of multi-rope systems is dependent on the specific rigging configuration, crane design, and operational requirements. For example, the four-nonparallel-rope rigging systems for gantry container cranes exhibit highly complex dynamics dependent on the hoisting rope angle and elasticity [20]. Conversely, in the modelling of a four-parallel-rope robotic crane, the pendulum model simplification is justified and supported with experimental validation showing high accuracy during feedback control [21]. Consideration of model complexities can allow creative control strategies. In [22], a novel two-rope system utilises the complexities of the model to change the sway dynamics based on luffing angle, moving the system away from resonance. In [23] auxiliary ropes are used to control external disturbances. In [24], the multi-rope model complexities are used to estimate the payload mass. In [25], the stick-slip behaviour of rope over pulleys is modelled with consideration to the resultant form of the dynamical equations, however, the work is limited by simplifying the system geometry. Assumptions to simplify multi-rope geometry [26] and pulley geometry [21] can significantly affect the modelled skew behaviour (twisting of the hook block about the hoist rope with one DOF).

Specifically for rotary boom cranes, control research is mostly focused on operations to transport shipping containers (container cranes) [9]. However, construction cranes and container cranes differ in rigging configuration.

Rotary container cranes typically use multiple separate hoist ropes, each terminating at the hook block, whereas construction cranes typically have only a single hoist rope that passes through sheaves on the hook block before returning to terminate at the top of the hoist (Fig. 1). This specific rigging configuration has been modelled in [27], where numerous vaguely justified simplifying assumptions effectively reduced the system to a single-pendulum model, and in [11], where similar assumptions were used in the 3D study.

The existing research does not evaluate which simplifications are appropriate to apply in the modelling of construction boom tower cranes. Therefore, this paper evaluates the question “*What are the optimal dynamical models to represent the boom tower cranes that are commonly deployed on construction sites?*”.

Answering this question raises the prerequisite question of how the established simplified models from literature relate to these cranes in a geometric sense. For example, when attempting to apply a pendulum model to a crane with a returning hoist rope, where on the real crane (Fig. 1) should be designated as the top of the pendulum? Most literature does not clearly define this relation [1]. Possible locations are where the hoist rope leaves the boom head sheave (although this is variable with the luffing angle and angle of sway), where the hoist rope returns to terminate, or somewhere between.

Having a rigorous geometric description dually reveals the whole family of cranes that share the same optimal dynamical model. This answers the auxiliary question “*Should a controller that was designed for a particular crane system be deployed on a similar crane with a different rigging configuration?*”.

The methods of this research represent the variations of boom tower crane with either a returning hoist rope or a non-returning hoist rope rigging configuration (Figs. 1 and 3). The hook block is optionally rotationally joined-to or separate-from the payload. Five 3D and five corresponding 2D dynamical models are derived in representation of these cranes. The models rigorously related to the geometry of the real-world crane and are derived to be comparable to each other through a common ancestor model.

The dynamical equations are programmatically generated and simulated to evaluate differences in hook block and payload trajectory, for each model, with respect to variation in model parameters (e.g. mass values, hoist rope length, boom length). The trials are made independent from the specifics of any monitoring or control system by not implementing any control system. Instead, the inputs are position controlled on pre-defined trajectories. The results are additionally verified through experimentation on a lab-scale model.

Model accuracy is evaluated against complexity. This reveals which dynamical models are optimal with respect to

the crane and payload characteristics, rigging configuration, and operational requirements.

The main contributions of this paper are:

- A methodology to directly compare a series of crane models to each other. The methodology considers separating the comparison from any control or monitoring system, rigorously establishing commonality between models, and permitting various rigging configurations of the real-world crane.
- A programmatic method to derive dynamical equations from geometric descriptions, while allowing for a holonomic algebraic constraint. The system of differential algebraic equations (DAEs) is generated by applying the Euler-Lagrange formulation with Lagrange multipliers and the decomposition of the rotation matrix derivative. The DAEs are then reformed into ordinary differential equations (ODEs) by solving for the Lagrange multiplier. This reduces numerical error in simulation by six orders of magnitude.
- Precise description of models that represent three variations of boom tower crane that are commonly deployed on construction sites. The most complex model accounts for rope interaction with the pulley sheaves, while the most simplified model is a single pendulum. Each model is fully defined in how it relates to the geometry of the real crane.
- A decision tree, Fig. 10, which guides system designers to choose the optimal dynamical models to represent the boom tower cranes that are commonly deployed on construction sites. The optimal model is dependent on the crane and payload characteristics, rigging configuration, and operational requirements. Understanding these dependencies both enables choice of the optimal model during systems development, and guides application of the developed system to the whole family of cranes which share the same optimal model.

Section 2 describes a method to programmatically formulate and simulate dynamical models from given geometric descriptions. Section 3 describes the models being compared. Section 4 discusses considerations of simulating high-complexity dynamical models. Section 5 compares the models through scaled simulation and experimentation for common construction scenarios. A decision tree to choose the optimal model is presented in Fig. 10. Section 6 concludes the paper and identifies opportunities for future research.

2 Method of dynamical model formulation

Crane systems can be mathematically represented by systems of differential equations, where the solution to the equations describes the motion of the system [9]. The chosen

crane systems are of high complexity, thus manual formulation of the equations of motion is infeasible.

The equations were generated programmatically with the MATLAB Symbolic Math Toolbox. The input to the equation generator was the geometric description of the system. This was realised through symbolic homogeneous coordinate transformation matrices, symbolic constraint equations, and specification to distinguish between the symbols that represent generalised coordinates or constants.

The output of the generator was the system equations, formulated and rearranged for input to the ordinary differential equation (ODE) solver. Following limitations of MATLAB to solve the more complex ODEs generated by the 3D models, the generator was made to cross-generate C++ code for solving with the SUNDIALS CVODE solver [28]. This solver was chosen based on the comparison of many ODE solvers in [29]. The SUNDIALS CVODE is a variable-step, variable-order (VSVO) explicit ODE solver of orders from 1 to 5 [28]. The solver was configured for solving stiff ODEs by using the Backward Differentiation Formulas.

To improve performance in both generation and solving, as much as possible of the equation formulation was delayed to occur numerically during solving. This required the generator to output the matrix coefficients of the semi-formulated system equations. The coefficients could then be evaluated at runtime, and solving completed through applying linear algebra on the numeric equations. To perform linear algebra at runtime in C++, the Armadillo C++ library [30] was used.

The following subsections describe the model specification (geometric description) which is input to the automated generator and solver; the method of equation generation; and the verification of the methodology.

2.1 Notation

The notation in this paper writes scalars in non-bold, vectors in bold-lowercase, and matrices in bold-uppercase. Right-superscripts are used only for powers or the matrix transpose. Right-subscripts of i or j denote the index to a parent vector, matrix, or set. Unless specified otherwise, other right-subscripts and left-scripts are used to distinguish between variables.

Centred dots above variables denote the single, \dot{a} , and double, \ddot{a} , time derivatives. The Euclidean norm is denoted $\|a\|$.

Square brackets notate matrix concatenation. Where otherwise ambiguous, parentheses notate function arguments. Hence, $a \cdot b$ contextually represents either scalar multiplication or dot product. In unambiguous cases, ab is also used to represent scalar multiplication.

Position vectors are notated as ${}^A\mathbf{p}_B$ to specify the vector from the origin of frame A pointing to the origin of frame B ,

as measured in the coordinates of frame A . The inertial frame is designated the letter O . Rotation matrices are notated as \mathbf{R} to satisfy ${}^A\mathbf{p}_C = {}^A\mathbf{R} \cdot {}^B\mathbf{p}_C$.

2.2 Formulation of geometric description

For each model, the geometric description was formed by approximating the system as a kinematic linkage and assigning a set of linearly independent generalised coordinates.

$$\mathbf{q} = \begin{bmatrix} \mathbf{q}_{\text{free}} \\ \mathbf{q}_{\text{input}} \end{bmatrix}, \tag{1}$$

where \mathbf{q}_{free} is the vector of n number of unactuated DOF, and $\mathbf{q}_{\text{input}}$ is the vector of m number of externally position controllable DOF, as given by Eqs. (2) and (3) respectively.

$$\mathbf{q}_{\text{free}} = [q_1 \dots q_n]^T, \tag{2}$$

$$\mathbf{q}_{\text{input}} = [q_{n+1} \dots q_{n+m}]^T. \tag{3}$$

The kinematic linkage was then described with a set of homogeneous coordinate transformation matrices. To maintain linear independence for the closed chain linkages, additional dependent coordinates were temporarily assigned and then solved for in terms of the independent generalised coordinates by means of inverse kinematics. The solution was found by equating the transformation from one node of the closed chain to another in a clockwise direction, to the transformation in the anti-clockwise direction. Equating these transformations, the matrix elements were simultaneously solved to isolate the dependent coordinates.

The transformations from the centre of mass frames to the inertial frame were obtained, then decomposed into position and orientation transformations, ${}^O\mathbf{p}_i(\mathbf{q})$ and ${}^O\mathbf{R}_i(\mathbf{q})$.

Directly solving all the system constraints proved difficult for the system models which describe the pulley behaviour. In this case, one more generalised coordinate than degrees of freedom was used, accompanied by a holonomic constraint equation of the form $\mathcal{C}(\mathbf{q}) = 0$. The following formulation allows either zero or one constraint equations, as is sufficient to describe the system.

2.3 Formulation of system equations

The system equations were obtained through the Euler-Lagrange formulation with Lagrange multipliers

$$\frac{d}{dt} \frac{\partial \mathcal{L}}{\partial \dot{q}_i} - \frac{\partial \mathcal{L}}{\partial q_i} + \lambda \frac{\partial \mathcal{C}}{\partial q_i} = Q_i, \quad i \in [1, n], \tag{4}$$

where $\mathcal{L}(\mathbf{q}, \dot{\mathbf{q}})$ is the Lagrangian, $Q_i(\mathbf{q}, \dot{\mathbf{q}})$ is the generalised force, $\mathcal{C}(\mathbf{q})$ is the left-hand side of the constraint equation,

and λ is the Lagrange multiplier. The Lagrangian is formed as

$$\mathcal{L} = K - V, \tag{5}$$

where the kinetic and potential energies, K and V , are found through

$$K = \sum_{i=1}^{\text{masses}} \frac{1}{2} m_i \cdot \left\| {}^O \mathbf{p}_i \right\|^2 + \frac{1}{2} \boldsymbol{\omega}_i^T \cdot \mathbf{I}_i \cdot \boldsymbol{\omega}_i, \tag{6}$$

$$V = \sum_{i=1}^{\text{masses}} -m_i \cdot \mathbf{g}^T \cdot {}^O \mathbf{p}_i, \tag{7}$$

where ${}^O \mathbf{p}_i$ is the position of the centre of mass frame i , with respect to the inertial frame. This is obtained from the geometric description. m_i is the corresponding mass, and \mathbf{I}_i is the corresponding moment of inertia tensor, measured in frame i . \mathbf{g} defines the gravity vector in the inertial frame. $\boldsymbol{\omega}_i$ is the angular velocity of frame i with respect to the inertial frame, as measured in the coordinates of frame i . It is calculated by decomposing the angular velocity tensor, $\boldsymbol{\Omega}_i$, as

$$\boldsymbol{\omega}_i = \left[\boldsymbol{\Omega}_i(3, 2) \quad \boldsymbol{\Omega}_i(1, 3) \quad \boldsymbol{\Omega}_i(2, 1) \right]^T, \tag{8}$$

where $\boldsymbol{\Omega}_i(\text{row}, \text{column})$ is the matrix element (*row*, *column*) of $\boldsymbol{\Omega}_i$, which is obtained from the well-known rotation matrix derivative [31]

$$\boldsymbol{\Omega}_i = {}^O \dot{\mathbf{R}} \cdot {}^O \mathbf{R}^T, \tag{9}$$

where ${}^O \mathbf{R}$ is the orientation of frame i , as measured in the inertial frame. This is obtained from the geometric description.

The generalised forces are obtained by remapping the external forces, \mathbf{F}_j , with

$$Q_i = \sum_{j=1}^{\text{forces}} \mathbf{F}_j \cdot \frac{\partial {}^O \mathbf{p}_j}{\partial q_i}, \tag{10}$$

where ${}^O \mathbf{p}_j$ is the position where \mathbf{F}_j acts.

2.4 Reforming of system equations for solving

Computing the derivatives in (4) and moving all terms to the same side of the equation results in the form

$$0 = {}^a \mathbf{f}_i(\mathbf{q}, \dot{\mathbf{q}}, \ddot{\mathbf{q}}) + \lambda \cdot {}^b f_i(\mathbf{q}), \quad i \in [1, n]. \tag{11}$$

Of the MATLAB ODE and DAE solvers, only ode15i is compatible with system equations of the form $0 = \mathbf{f}(t, \mathbf{x}, \dot{\mathbf{x}})$. However, ode15i is an inefficient and low accuracy solver. Hence, the system equations resulting from the Euler-Lagrange formulation were reformed for compatibility with the higher accuracy solvers.

The common methodology is to reform (11) into matrix equations and isolate $\ddot{\mathbf{q}}$. However, due to the constraint, the resulting equations would still be index-1 DAEs. DAE solvers are low accuracy and inefficient in general. Hence, we developed the general solution to reform (11) into a system of ODEs by algebraically solving the constraint equation.

Starting from (11), for each i , ${}^a f_i$ can be decomposed into

$${}^a \mathbf{f}_i(\mathbf{q}, \dot{\mathbf{q}}, \ddot{\mathbf{q}}) = \sum_{j=1}^n M_{ij}(\mathbf{q}) \cdot \ddot{q}_j + {}^c \mathbf{f}_i(\mathbf{q}, \dot{\mathbf{q}}, \ddot{\mathbf{q}}_{\text{input}}). \tag{12}$$

Hence, (11) can be reformed into (13) and then rearranged into (14)

$$\mathbf{0} = \mathbf{M}(\mathbf{q}) \cdot \ddot{\mathbf{q}}_{\text{free}} + {}^c \mathbf{f}(\mathbf{q}, \dot{\mathbf{q}}, \ddot{\mathbf{q}}_{\text{input}}) + \lambda \cdot {}^b \mathbf{f}(\mathbf{q}), \tag{13}$$

$$\begin{aligned} \ddot{\mathbf{q}}_{\text{free}} = & -\mathbf{M}^{-1}(\mathbf{q}) \cdot {}^c \mathbf{f}(\mathbf{q}, \dot{\mathbf{q}}, \ddot{\mathbf{q}}_{\text{input}}) \\ & - \lambda \cdot \mathbf{M}^{-1}(\mathbf{q}) \cdot {}^b \mathbf{f}(\mathbf{q}). \end{aligned} \tag{14}$$

To solve for λ , the constraint equation is first double differentiated and then reformed into a matrix equation

$$\begin{aligned} 0 = & \frac{d^2 \mathcal{C}(\mathbf{q})}{dt^2} \\ = & \ddot{\mathcal{C}}(\mathbf{q}, \dot{\mathbf{q}}, \ddot{\mathbf{q}}) \\ = & \sum_{j=1}^n {}^d f_j(\mathbf{q}) \cdot q_j + {}^e f(\mathbf{q}, \dot{\mathbf{q}}, \ddot{\mathbf{q}}_{\text{input}}) \\ = & {}^d \mathbf{f}^T(\mathbf{q}) \cdot \ddot{\mathbf{q}}_{\text{free}} + {}^e f(\mathbf{q}, \dot{\mathbf{q}}, \ddot{\mathbf{q}}_{\text{input}}). \end{aligned} \tag{15}$$

Substituting (14) into (15) and solving for λ gives

$$\lambda = \frac{{}^e f(\mathbf{q}, \dot{\mathbf{q}}, \ddot{\mathbf{q}}_{\text{input}}) - {}^d \mathbf{f}^T(\mathbf{q}) \cdot \mathbf{M}^{-1}(\mathbf{q}) \cdot {}^c \mathbf{f}(\mathbf{q}, \dot{\mathbf{q}}, \ddot{\mathbf{q}}_{\text{input}})}{{}^d \mathbf{f}^T(\mathbf{q}) \cdot \mathbf{M}^{-1}(\mathbf{q}) \cdot {}^b \mathbf{f}(\mathbf{q})}. \tag{16}$$

Substituting (16) into (14) gives the system equations in the form

$$\ddot{\mathbf{q}}_{\text{free}} = {}^f \mathbf{f}(\mathbf{q}, \dot{\mathbf{q}}, \ddot{\mathbf{q}}_{\text{input}}). \tag{17}$$

The differential order of the system must be reduced for solving. The vector of the inputs, \mathbf{u} , is defined to comprise the externally controlled generalised coordinates and their derivatives (18). The state vector, \mathbf{x} , is defined to comprise the free generalised coordinates and their first order derivatives (19).

$$\mathbf{u} = \begin{bmatrix} \mathbf{q}_{\text{input}} \\ \dot{\mathbf{q}}_{\text{input}} \\ \ddot{\mathbf{q}}_{\text{input}} \end{bmatrix}, \tag{18}$$

$$\mathbf{x} = \begin{bmatrix} \dot{\mathbf{q}}_{\text{free}} \\ \mathbf{q}_{\text{free}} \end{bmatrix}. \tag{19}$$

Appending the order reducing relation $\dot{\mathbf{q}}_{\text{free}} = \dot{\mathbf{q}}_{\text{free}}$ to (17) gives rise to

$$\frac{d}{dt} \begin{bmatrix} \dot{\mathbf{q}}_{\text{free}} \\ \mathbf{q}_{\text{free}} \end{bmatrix} = \begin{bmatrix} \mathbf{f}(\mathbf{q}, \dot{\mathbf{q}}, \ddot{\mathbf{q}}_{\text{input}}) \\ \dot{\mathbf{q}}_{\text{free}} \end{bmatrix}. \tag{20}$$

Substituting the generalised coordinates, \mathbf{x} and \mathbf{u} , into (20) results in the nonlinear state equation

$$\dot{\mathbf{x}} = \mathbf{g}(\mathbf{x}, \mathbf{u}). \tag{21}$$

To enable the ODE solvers to solve with time varying input, (21) was aliased with

$$\mathbf{h}(\mathbf{x}, t) = \mathbf{g}(\mathbf{x}, \mathbf{u}(t, \mathbf{x})), \tag{22}$$

where $\mathbf{u}(t, \mathbf{x})$ is the function that calculates \mathbf{u} at the solution time t . This function can implement state feedback control; or open loop control if $\mathbf{u}(t, \mathbf{x}) = \mathbf{u}(t)$. To implement this function alias, a wrapper function with inputs \mathbf{x} and t is defined to first evaluate the input vector, and then evaluate (21).

Finally, this results in the time and state dependent state equation

$$\dot{\mathbf{x}} = \mathbf{h}(\mathbf{x}, t). \tag{23}$$

This form of the system equations is compatible with ODE solvers, for example the MATLAB ode45 and SUNDIALS CVODE solvers.

2.5 Algorithm performance and verification

Two tests were conducted to verify the performance and correct functioning of the dynamical equation generator and simulator.

All of the applicable matlab ODE and DAE solvers were tested. The ode23 and ode45 are low-to-medium accuracy explicit ODE solvers that respectively implement Bogacki and Shampine’s Runge–Kutta (2,3) pair, and Dormand and Prince’s Runge–Kutta (4,5) pair [32]. The ode78 and ode89 are high accuracy explicit ODE solvers that respectively implement Verner’s “most efficient” Runge–Kutta (7,8) pair, and Verner’s “most robust” Runge–Kutta (8,9) pair [33]. The ode113 is a variable-step, variable-order (VSVO) Adams–Bashforth–Moulton explicit ODE solver of orders from 1 to 13 [32]. The ode15s is a VSVO explicit ODE and semi-explicit index-1 DAE solver of orders from 1 to 5 [32]. The ode23t is a variation of ode23 that can solve explicit ODEs and semi-explicit index-1 DAEs [34]. The ode15i is a VSVO fully implicit index-1 DAE solver of orders from 1 to 5 [35]. The ode23s, ode23t, and ode23tb solvers were not tested

because they require that the mass matrix is constant, which is not generally true for this problem.

The first test modelled a 4-parallel-bar linkage to be equivalent to the point mass pendulum (Fig. 2). The linkage was modelled as an open kinematic chain $A-B-C$ combined with the algebraic constraint equation, to realise (15), as

$$0 = \ddot{L}_{CD} = \frac{d^2}{dt^2} \left\| \mathbf{p}_A + \mathbf{p}_B + \mathbf{p}_C \right\|. \tag{24}$$

The resultant DAEs were simulated both as DAEs, and then as reformed into ODEs. The results were compared to the analytic solution of an unforced point mass pendulum [36]. The simulation duration was 20 s, from initial conditions with the pendulum almost inverted ($\theta_0 = 0.9\pi$), and with integration tolerances of 10^{-10} .

The second test modelled a 2D triple pendulum, where the first link was given as a prismatic joint. The constraint equation realise (15) was given as $0 = \ddot{L}_1$, where L_1 was the displacement of the prismatic joint. The same simulation conditions were used. The reference ‘true’ solution was the simulation using ode89 with the MATLABs maximum allowable tolerances.

The results (Table 1) were analysed by the time taken to form and simulate the equations, and by the root-mean-square error to the reference solution. The results for the first test closely follow the analytic solution, near to the integration tolerances, verifying the correct function of the dynamical equation generator and simulator. The reformulation reduced the error by six orders of magnitude. The results for the second test have greater error, as attributed to the greater complexity of the problem. The reformulation allowed for solving the system, where the the original system of DAEs gradually diverged.

3 Dynamical models

Five 3D and five corresponding 2D models were developed to represent three rotary boom construction tower crane systems. The models are full complexity (FC), zero-radius

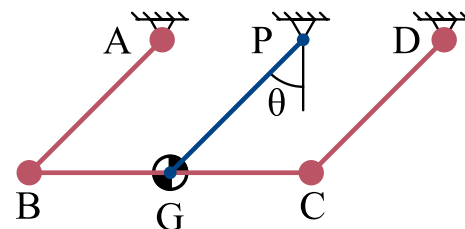


Fig. 2 Kinematic linkage describing the case of equivalence between a 4-parallel-bar linkage ($A-B-C-D-A$) and a point mass pendulum ($P-G$), where each only hold a single point mass at G

Table 1 Results of the algorithm performance verification for a 20 s simulation duration with integration tolerances of 10^{-10}

Equation formulation	MATLAB solver	4-Parallel-bar linkage		Triple pendulum	
		Run time (s)	RMS error	Run time (s)	RMS error
Original DAE	ode15s	2.5	9E-03	Diverged at 65% solved	
	ode23t	158	8E-03	Diverged at 49% solved	
	ode15i	Failed to solve		Failed to solve	
Reformed into ODE	ode45	2	9E-09	5.8	7E-06
	ode23	5.2	3E-08	51	7E-05
	ode113	2.0	2E-08	3.9	5E-05
	ode78	2.1	3E-09	4.5	1E-05
	ode89	2.1	1E-09	4.6	3E-07

The criteria for divergence was when the absolute error in the signal passed $1E-01$. All link lengths were of value 1 m, and all mass values were 1 kg

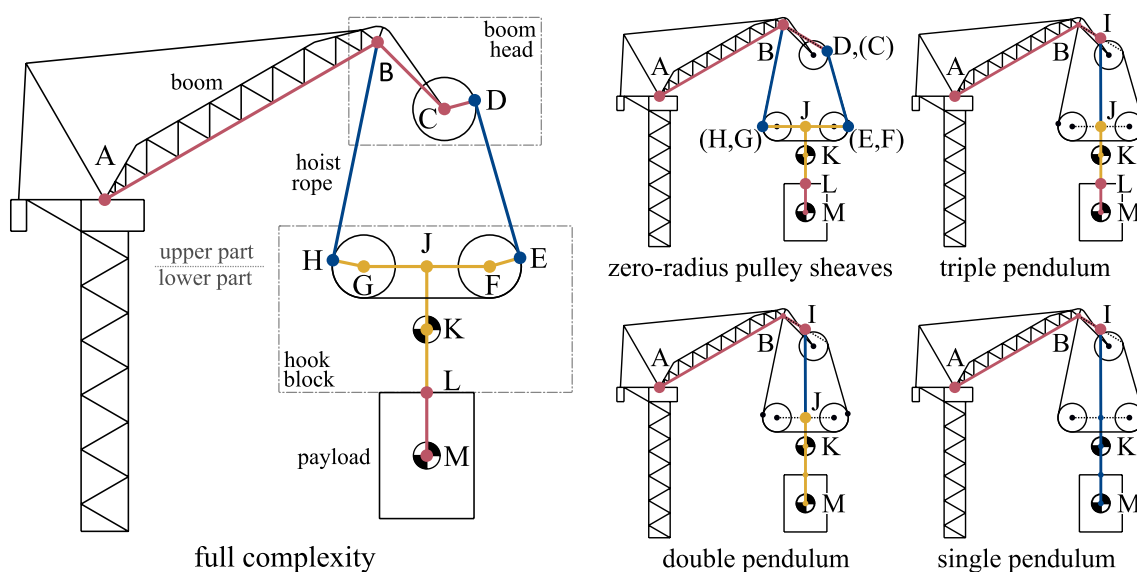


Fig. 3 Kinematic linkages describing a boom tower crane with a pulley mounted hook block and rotator. Figure not in Scale

pulley sheaves (ZS), triple pendulum (3P), double pendulum (2P), and single pendulum (1P), each with a 3D and 2D variant. The models FC, 3P, and 2P all closely relate to different crane rigging configurations, whereas the models ZS and 1P are impossible rigging configurations.

The models are comparable to each other through a common ancestor, the ‘full complexity’ model, from which the remaining models were derived (Fig. 3).

All models assume that the hoist rope is inelastic and massless; the tower and boom are inelastic, transverse vibration in the rope can be ignored; and wind force and frictional damping can be ignored. We justify that these assumptions are required to avoid greatly increasing the complexity of the model. As discussed in the introduction, relaxing any of these assumptions significantly inhibits modelling other features.

3.1 Full complexity model and crane

The full complexity model describes the crane rigging configuration using a returning hoist rope (Fig. 1). Additionally, this model includes an active skew rotary hook block (rotator), per the recommendations of [37] to deploy rotators on construction cranes for increased safety and economic efficiency. The kinematic linkage of this model is shown in Fig. 3. Coordinate frames were attached to this linkage (Figs. 4 and 5). The orientation of each frame is set to make solving the inverse kinematics equations simpler.

The location *A* is the intersection of the luffing and slewing axes; *B* is where the hoist rope returns to attach to the boom; *C* is the centre of the boom head sheave; and *D* is where the hoist rope leaves this sheave. These locations

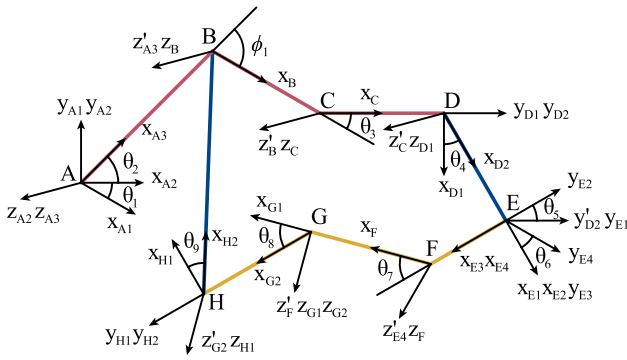


Fig. 4 Coordinate frames, generalised coordinates, and dependent coordinates attached to the full complexity model, Fig. 3. Upper part

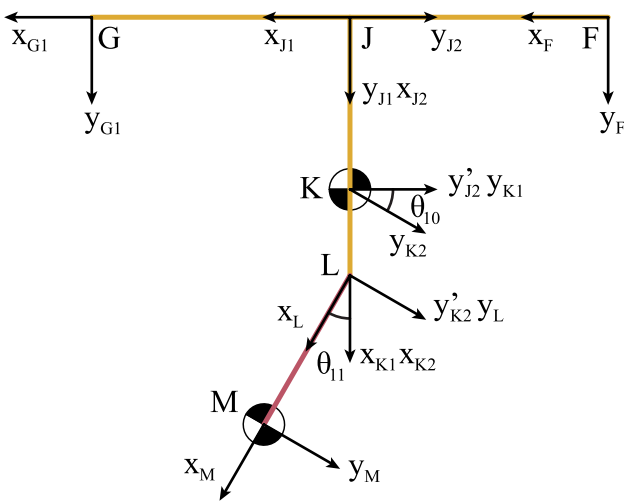


Fig. 5 Coordinate frames, generalised coordinates, and dependent coordinates attached to the full complexity model, Fig. 3. Lower part

all lie in the plane that is perpendicular to the luffing axis, intersecting the slewing axis.

E and *H* are where the hoist rope leaves the hook block sheaves. *F* and *G* are the centres of the hook block sheaves. *J*, *K*, and *L* are in-line, defining the axis in which the skew actuator rotates. This axis is assumed to be perpendicular to the line joining *F* and *G*, with *J* located halfway between *F* and *G*. Thus, the hook block is symmetric.

K is the centre of mass of the hook block. *L* is the point where the hook joins to the payload, which is free to tilt with 1 DOF. *M* is the centre of mass of the payload.

The generalised coordinates are

$$\mathbf{q}_{\text{free}} = [\theta_3 \ \theta_4 \ \theta_5 \ \theta_6 \ \theta_7 \ \theta_{11} \ L_{DE}]^T, \tag{25}$$

$$\mathbf{q}_{\text{input}} = [\theta_1 \ \theta_2 \ \theta_{10} \ L_{\text{rope}}]^T, \tag{26}$$

as defined by Figs. 4 and 5. Note that this definition is over-determined by 1 DOF. Therefore, the constraint Eq. (28) is used to ensure that the coordinates are consistent.

θ_1 is the slewing angle; θ_2 is the luffing angle; and θ_{10} is the skew actuator angle. θ_5 is related to the skew of the hook block. θ_{11} is the angle of payload relative tilt.

The rope leaves each sheave in a direction tangent to the contacting surface at the point of departure, where the points of departure vary with θ_3 , θ_7 , and θ_8 . The tangent relations are described with $\angle CDE = \angle DEF = \angle GHB = \frac{\pi}{2}$. This definition allows the rope to bend out of plane from the sheaves, at the angles designated θ_4 , θ_6 , and θ_9 .

The length from *D* to *E* is designated L_{DE} . L_{DE} and L_{HB} vary with hoisting actuation and rolling of the hook block along the rope. The effective length of the rope, L_{rope} , describes the path length of the rope from partial a turn before it leaves the boom head sheave, to the end of the rope at *B*.

$$L_{\text{rope}} = L_{HB} + L_{GH} \cdot \left(\frac{\pi}{2} - \theta_8\right) + L_{FG} + L_{EF} \cdot \left(\frac{\pi}{2} + \theta_5\right) + L_{DE} + L_{CD} \cdot (\pi - \theta_3). \tag{27}$$

Change in this length is wholly determined by the input rotation of the hoist actuator, hence L_{rope} is used as a control input. Since this length is easily measurable with encoders, it is reasonable to use (27) as the constraint equation. Moving all terms of (27) to the right-hand side of the equation and double differentiating gives the constraint in the form of (15)

$$\ddot{C} = -\ddot{L}_{\text{rope}} + \ddot{L}_{HB} - L_{GH}\ddot{\theta}_8 + L_{EF}\ddot{\theta}_5 + \ddot{L}_{DE} - L_{CD}\ddot{\theta}_3. \tag{28}$$

The dependent coordinates, θ_8 , θ_9 , and L_{HB} , were found in terms of the independent coordinates with inverse kinematics methodology. Using the transformation from *B* to *G* as described in terms of the independent coordinates

$${}^{G1}\mathbf{p}_B = -{}^B_{G1}\mathbf{R}^T \cdot {}^B\mathbf{p}_{G1}. \tag{29}$$

Splitting (29) into its components

$${}^{G1}\mathbf{p}_B = [{}^{G1}x_B \ {}^{G1}y_B \ {}^{G1}z_B]^T, \tag{30}$$

gives the inverse kinematic solution

$$L_{HB} = \sqrt{\|{}^{G1}\mathbf{p}_B\|^2 - L_{GH}^2}, \tag{31}$$

$$\theta_8 = 2 \cdot \arctan \left(\frac{{}^{G1}y_B + \sqrt{{}^{G1}x_B^2 + {}^{G1}y_B^2 - L_{GH}^2}}{{}^{G1}x_B + L_{GH}} \right), \tag{32}$$

$$\theta_9 = \arcsin \left(-\frac{G^1 z_B}{L_{HB}} \right). \tag{33}$$

The constants of the crane geometry which must be known are the lengths $L_{AB}, L_{BC}, L_{CD}, L_{EF}, L_{FG}, L_{GH}, L_{FJ}, L_{JK}, L_{KL}$, and the angle ϕ_1 . L_{LM} , a constant of the payload geometry, must also be known. Additionally, the masses and moment of inertia tensors of the hook block (m_K and \mathbf{I}_{K1}) and payload (m_M and \mathbf{I}_M) must be known.

Thus defines the kinematic linkage of the full complexity model. Section 2 describes the translation of this description into the dynamical system equations. In this, the equation correspondence respectively maps (2), (3), and (15), to (25), (26), and (28). Finally, the transformations from the centre of mass frames to the inertial frame, ${}^{A1}\mathbf{p}_{K1}, {}^{A1}\mathbf{p}_M, {}^{A1}\mathbf{R},$ and ${}^{A1}\mathbf{R}_M$ are obtainable by composition of the transformations from the origin, $A1$, through the locations $A-B-C-D-E-F-J-K-L-M$, to the centre of mass frames $K1$ and M (Fig. 4 and Fig. 5).

3.2 Model with zero-radius pulleys

Using the full complexity model as a starting point, the remaining models were derived by applying geometric simplifications.

An ideal simplification reduces model complexity without introducing error in modelled behaviour. From the Euler-Lagrange formulation, it can be seen that the behaviour of the system masses is central to the modelled behaviour. Therefore, simplifications should minimally alter the manifold of achievable configurations of the masses. Given that crane systems should always be kept near to the equilibrium configuration, then this requirement should be most strictly imposed near to equilibrium. This is analogous to linearising a system about an equilibrium point.

However, the equilibrium configuration varies with the luffing angle. Hence, all our simplifications are based on the requirement to not change the equilibrium configuration of the masses at the luffing angle $\theta_2 = \frac{\pi}{4}$. This angle was chosen for being near to the middle of the operational range, thereby providing the most benefit across all angles of operation.

Starting from the full complexity model, the pulley sheave radii are reduced to zero by means of the simplifications

$$L_{CD}(\text{new}) = L_{EF}(\text{new}) = L_{GH}(\text{new}) = 0, \tag{34}$$

$$L_{FG}(\text{new}) = L_{EF}(\text{old}) + L_{FG}(\text{old}) + L_{GH}(\text{old}), \tag{35}$$

and C and D are moved to where D would be when the rope leaves the main hoist sheave vertically with the luffing angle $\theta_2 = \frac{\pi}{4}$.

This model is not physically viable to implement on a construction crane as cables are rated with a minimum allowable cable bending radius to prevent fatigue failure.

3.3 Triple pendulum model and crane

The triple pendulum model is formed by assuming that a virtual rope joins the locations I and J , where I is exactly midway between B and D (Fig. 3). Thus, the kinematic linkage is the sequence joining $A-I-J-K-L-M$. I is a three DOF spherical joint (sway and hook block skew), and J a two DOF universal joint (roll).

Combined with simplifications to the pulley radius, the virtual rope model is argued to offer great value in simplification for eliminating complexity while minimally impacting the expected position of the mass, by comparison to the large scale of the crane system [21]. However, it is cautioned that this small change in payload height is the dominant term in the restoring force against hook block skew [21].

Starting from the full complexity model, two underlying assumptions are made in this formulation:

- The position of I does not change.
- The virtual rope is of constant length.

For effective control of the system, these parameters should be set so that the model matches the true system at equilibrium. However, the values change between the equilibria of different luffing angles and hoist rope lengths. For an overall close approximation, the equilibrium parameters with the luffing angle of $\theta_2 = \frac{\pi}{4}$ were used to specify the length of the rope and position of I . The hoist rope length was held constant during experimentation.

This model is additionally representative of a crane with a single, non-returning, hoist rope, where the size of the hook block is significant. Hence, bending can occur either at the join of the hoist to the hook block, or at the join of the hook block to the payload.

3.4 Double pendulum model and crane

In the double pendulum model, it is assumed that the payload sways with hook block. This represents systems where the hook block and payload are rigidly joined together, as is seen on container cranes, where the spreader locks to the container.

Starting from the triple pendulum model, the only additional assumption is that $\theta_{11} = 0$. This definition differs from the double pendulum model that is common in crane control literature, in that the hook block mass is not concentrated at the pivot point J [9]. We consider this to be a more accurate representation of the system for no increase in complexity, given that moment of inertia is included in the model.

The common definition of the double pendulum model in literature assumes that the size of the hook block is negligible [9]. This allows for use of the double pendulum model when the hook block and payload are not rigidly joined.

Mechanically, it is not possible for bending to occur at the centre of mass of a typically shaped hook block. Hence, the choice of the pivot point is somewhat arbitrary. If the size of the hook block is significant, then for this case, the triple pendulum model may be more appropriate.

3.5 Single pendulum model

In the single pendulum model, it is assumed that the payload sways with hook block and hoist rope; that I , J , K , L , and M all remain inline. The separation of the hook block and payload masses is equivalent to the typical realisation in which they are lumped together at the total centre of mass.

No construction crane directly relates to the single pendulum model as the joint between the hoist rope and hook block does not sit at the centre of mass of the hook-payload pair. Hence, the system dynamics can induce bending at this joint.

3.6 3D to 2D model simplifications

Each 3D model has a corresponding 2D model. The 3D to 2D simplification enforces

$$\theta_1 = \theta_4 = \theta_5 = \theta_6 = 0, \quad (36)$$

$$\theta_{10} = \frac{\pi}{2}. \quad (37)$$

These are the minimum necessary simplifications required to reduce the 3D model to 2D. The skew actuator angle is set to allow relative tilt between the hook block and the payload (37). An alternative simplification to (37) could be $\theta_{10} = \theta_{11} = 0$, although, this prevents the relative tilt.

4 Considerations in simulation

MATLAB succeeded in the generation and manipulation of the equations, even for the high complexity models. However, it was unable to solve the higher complexity models. Hence, the coefficients of (13) and (15) were exported to C++ and solved with SUNDIALS CVODE. To visualise the size of these equations, a single evaluation of the full complexity system's system equations calls the trigonometric function $\sin()$ 1.7 million times.

A key technique to reduce numerical error and make generation and solving feasible was to delay the required matrix inversion until runtime, where the inversion could be completed numerically. In MATLAB this was achieved by storing the partially formed equations in an object and passing a method to evaluate the equations to the MATLAB's inbuilt ODE solver. In C++, this was achieved by exporting the matrix coefficients of (13) and (15), which were evaluated

for the final formation to be completed numerically with Armadillo.

Another specific code optimisation was found to be necessary to enable compilation of these large C++ source files. Without optimisation, the 3D triple pendulum model took over 3 h to compile. Post optimisation, the same model compiled in under 1 min. The required optimisation was to reduce the number of calls to $\sin()$ and $\cos()$ by substituting repeated calls with variables evaluated before the body of the ODE.

All the 2D and 3D simulations completed in less time than the length of simulation. Hence, real time evaluation of even the highly complex models is feasible.

In numerically solving differential equations, numerical error accumulates with each solve step, eventually causing the solution to diverge. For the crane models, divergence occurred sooner with the increasing ratio of the smallest length in the kinematic chain to the largest link length and increasing model complexity. The closed chain models suffered significantly greater numerical error.

For the closed chain models and the triple pendulum model, the mass matrix is singular when the moment of inertia of the hook block is set to zero. Similarly, if other mass or moment of inertia values are set to zero, the mass matrix can become singular. Hence, if these values are small, the ODEs can become very stiff. To solve this problem, the stiff model can be simplified by setting the related joint in the kinematic chain as fixed, resulting in a non-stiff model. For example, where no payload is attached, the angle of the payload can be set to a constant without reducing the accuracy of the solution.

5 Simulated and experimental comparison

Two set of comparisons were conducted. First, a simulated and experimental comparison of the model trajectories under slewing and luffing input. Second, over 100 simulated trails are compared under luffing input, measuring the maximum angular disturbance for variation in model parameters.

5.1 Model realisations

The model parameters represent a Liebherr 710 HC-L 32/64 crane, described by the manufacturer as a high capacity construction crane (Table 2). This crane is capable of multiple rigging configurations, where the rope either terminates at the hook block (the triple pendulum model), or passes through sheaves on the hook block and returns to terminate at the boom (the full complexity model). The hook block was replaced with an active skew rotary hook block, as discussed in Sect. 3 to increase safety in crane operations.

Two payloads were tested, representing a 1000 kg glass curtain wall module, and a 9000 kg prefabricated concrete wall module. Hence, this crane and payload system is representative of dangerous construction crane operations which have need for greater monitoring and control accuracy. Optionally, the payloads may be mechanically orientation locked to the hook block. In total, this results in three experimental rigging configurations (full complexity, triple pendulum, double pendulum), each with a choice from two payloads (curtain wall module, prefabricated concrete wall module).

All the experiments and simulations were scaled down by a length factor of 25. Dimensional analysis relates the mass and time scaling factors as $mass : length^3$ and $time : \sqrt{length}$. Hence, time scaled 5 times faster and mass was reduced by a factor of 15625. This was verified by comparing that a full-scale simulation and a scaled simulation produce identical scaled results. The following figures and equations use the experimental scale.

The experimental setup used a Universal Robots UR5 robot to emulate the movement of the crane boom, with the end effector holding the head of the boom from which the hook block was hung (Fig. 6). The accuracy of this setup to represent a full-scale crane was limited by imperfect replication of the flexural and torsional rigidity of the crane's structure [38].

The robot was servo controlled to smoothly follow the input trajectories. The motion of the system was captured with 0.1 mm accuracy by a Vicon Bonita motion capture system. The motion capture software Tracker 3 directly returns the global position and orientation of each rigid body in the system, as determined by directly resolving the location of markers attached to the body.

Comparison requires the model parameters, inputs, and configurations to be in some way equivalent between every model. Hence, across all models, we required that the centres of mass have the same initial and equilibrium locations with zero-velocity initial conditions. These requirements were satisfied by initialising every model in static equilibrium. For any other initial configuration, the requirements are non-trivial to satisfy due to the geometric differences of the closed kinematic chain models to the pendulum models.

From these initial conditions, motion was induced by actuating the inputs, (26), within the operational limits of a Liebherr 710 HC-L 32/64 crane. The trajectories of the inputs were pre-defined. This enables comparison between the dynamic responses of each model in a way that is independent of any control system. From preliminary tests, inputs that induced the most variation in trajectory between models were chosen. Hence, the reported results show where the models behave most differently from each other.

The trajectory comparison trials used input to induce oscillation with gradually increasing amplitude, up to the amplitude limit of the experimental workspace. This is realised as

$$\theta_1(t) = \frac{7\pi t}{540} \sin\left(\frac{2\pi t}{5}\right), \quad t \in [0, 15], \quad (38)$$

$$\theta_2(t) = \frac{\pi}{4} + \frac{\pi t}{120} \left(\cos\left(\frac{8\pi t}{15}\right) - 1\right), \quad t \in [0, 15], \quad (39)$$

$$\theta_{10}(t) = \frac{\pi}{2}, \quad t \in [0, 15]. \quad (40)$$

For the 2D trials, the slew and skew inputs were instead held at their initial values.

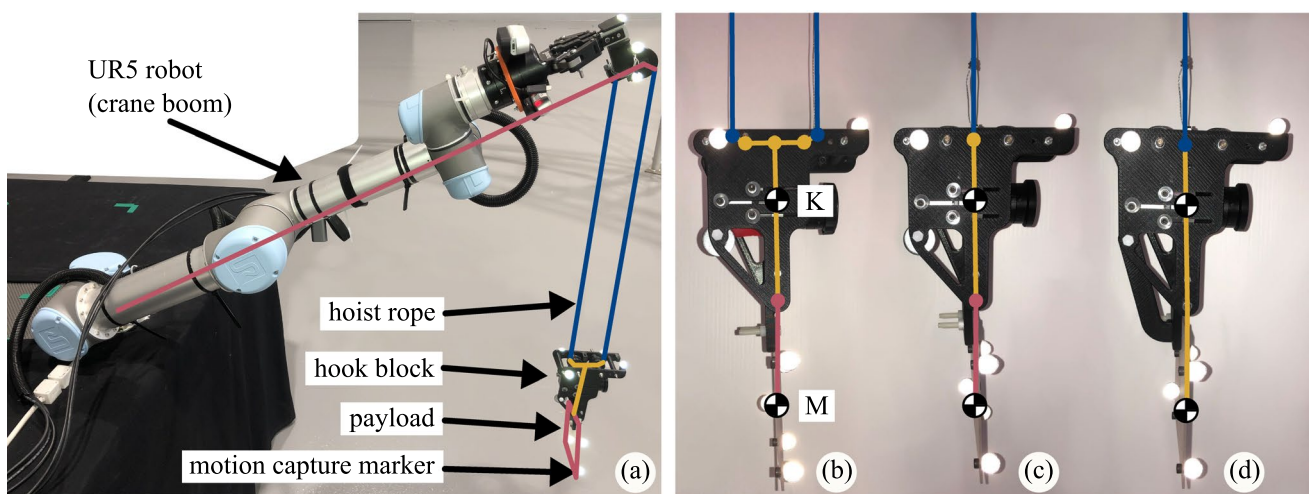


Fig. 6 a Experimental setup. Hook and payload variations for b full complexity, c triple pendulum, and d double pendulum. The double pendulum model uses a bracket to lock the hook block and payload together, while on the other models the hinge is free to rotate

Table 2 Values of system constants and initial conditions used in the trajectory comparison trials, and base values used in the trials with varying system parameters

Parameter	Unit	Value in experimental scale	
		Trajectory comparison	Varying parameters
g	m/s ²	9.8	9.8
m_K	kg	409×10^{-3}	409×10^{-3}
m_M (glass)	kg	71×10^{-3}	Not applicable
m_M (concrete)	kg	586×10^{-3}	586×10^{-3}
\mathbf{I}_{K1}	kg·m ²	diag(422, 560, 719) $\times 10^{-6}$	diag(422, 560, 719) $\times 10^{-6}$
\mathbf{I}_M (glass)	kg·m ²	diag(58, 129, 184) $\times 10^{-6}$	Not applicable
\mathbf{I}_M (concrete)	kg·m ²	diag(681, 768, 1443) $\times 10^{-6}$	diag(681, 768, 1443) $\times 10^{-6}$
ϕ_1	rad	0	$\frac{\pi}{4}$
L_{AB}	m	1.108	1.108
L_{BC}	m	40×10^{-3}	40×10^{-3}
L_{CD}	m	22×10^{-3}	22×10^{-3}
L_{EF}	m	9.5×10^{-3}	9.5×10^{-3}
L_{FG}	m	45×10^{-3}	43×10^{-3}
L_{GH}	m	9.5×10^{-3}	9.5×10^{-3}
$L_{HB}(t)$	m	(31)	(31)
L_{FJ}	m	22.5×10^{-3}	21.5×10^{-3}
L_{JK}	m	36.6×10^{-3}	36.6×10^{-3}
L_{KL}	m	83.4×10^{-3}	83.4×10^{-3}
L_{LM} (glass)	m	57×10^{-3}	Not applicable
L_{LM} (concrete)	m	73×10^{-3}	73×10^{-3}
$\theta_1(t)$	rad	(38)	0
$\theta_2(t)$	rad	(39)	(41)
$\theta_3(t = 0)$	rad	$-\frac{\pi}{4}$	0
$\theta_4(t = 0)$	rad	0	0
$\theta_5(t = 0)$	rad	0	0
$\theta_6(t = 0)$	rad	0	0
$\theta_7(t = 0)$	rad	0	0
$\theta_8(t)$	rad	(32)	(32)
$\theta_9(t)$	rad	(33)	(33)
$\theta_{10}(t)$	rad	(40)	$\frac{\pi}{2}$
$\theta_{11}(t = 0)$	rad	0	0
$L_{DE}(t = 0)$	m	0.6	0.6

The values given by equations are variable with time, and should be continuously evaluated during solving

For the trails with varying system parameters, the input was a smooth upward luffing motion, realised with a cubic spline. The crane was then held still to continue to capture the oscillations after the luffing finished. The trial ended after the largest amplitude oscillation was captured.

$$\theta_2(t) = \begin{cases} \frac{45\pi}{180} + \frac{25\pi}{180} \left(-2\left(\frac{t}{2}\right)^3 + 3\left(\frac{t}{2}\right)^2 \right), & t \in [0, 2] \\ \frac{70\pi}{180}, & t \in (2, 5] \end{cases} \quad (41)$$

5.2 Trajectory comparison

Comparison of the simulated and experimental results for 2D motion is Fig. 7. The comparison uses the inertial frame A1, formed by the triad $(x_{A1} \ y_{A1} \ z_{A1})$ in Fig. 4. The general shape of motion agrees. The larger amplitude in simulation is attributed to the simulator omitting frictional forces and air resistance. This provides strong evidence to the correct functioning of the simulator.

Comparison of 3D experimental and simulated trials for different models and rigging configurations is Fig. 8. All experimental models are plotted. The omitted simulated models diverged during solving for reasons discussed in

Sect. 4. Similarly to in Fig. 7, the simulated results have greater amplitude.

All the pendulum models closely follow the same trajectory in both simulation and experiment, while behaviour of the full complexity model differs more significantly from the pendulum models. This same pattern occurred for both payloads and inputs.

The input prevalently excited the first vibrational mode, which explains the strong similarity between the results of the pendulum models. For this case, the single pendulum model achieves a very accurate and low complexity representation of the single-hoist-rope system. However, for less smooth inputs which excite other vibrational modes, the similarity between the configurations is expected to reduce. This is tested as follows.

5.3 Comparison with varying system parameters

Figure 9 compares the maximum angular disturbance from an upward luffing input for differing system parameters.

Across all combinations of system parameters, all models show similar behaviour. The angle of the payload shows the most variation between the models, particularly for lighter payloads.

In general, the single pendulum model exhibits the smallest hook block and payload angles. This is because these angles are bound to the angle of the hoist. The great length

of the hoist results in a very large moment of inertia about the pivot. The other models can rotate the hook block and payload more freely.

Likewise, the double pendulum model exhibits smaller payload angles than the triple pendulum and pulley models. Mechanically locking the payload and hook block together increases the moment of inertia of the combined mass, attenuating any disturbance that is applied to either component. This is most evident when the payload is much lighter than the hook block, where the large payload oscillations exhibited by the higher complexity models are attenuated.

The triple pendulum and zero radius pulley sheave models exhibit almost identical behaviour. This similarity can be likened to the similarity between a 4-parallel-bar-linkage and a pendulum because the ropes of the pulley model are close to parallel, as is typical of the rigging on construction cranes. It is important to note that the system with significantly nonparallel ropes has already been shown to behave significantly differently from the pendulum model in [22].

The full complexity model is most similar to the triple pendulum and zero radius pulley sheave models, as is most evident when the payload is lightweight.

5.4 Optimal rigging choice and model choice

In choosing the physical rigging configuration, mechanically locking the hook block and payload together has the

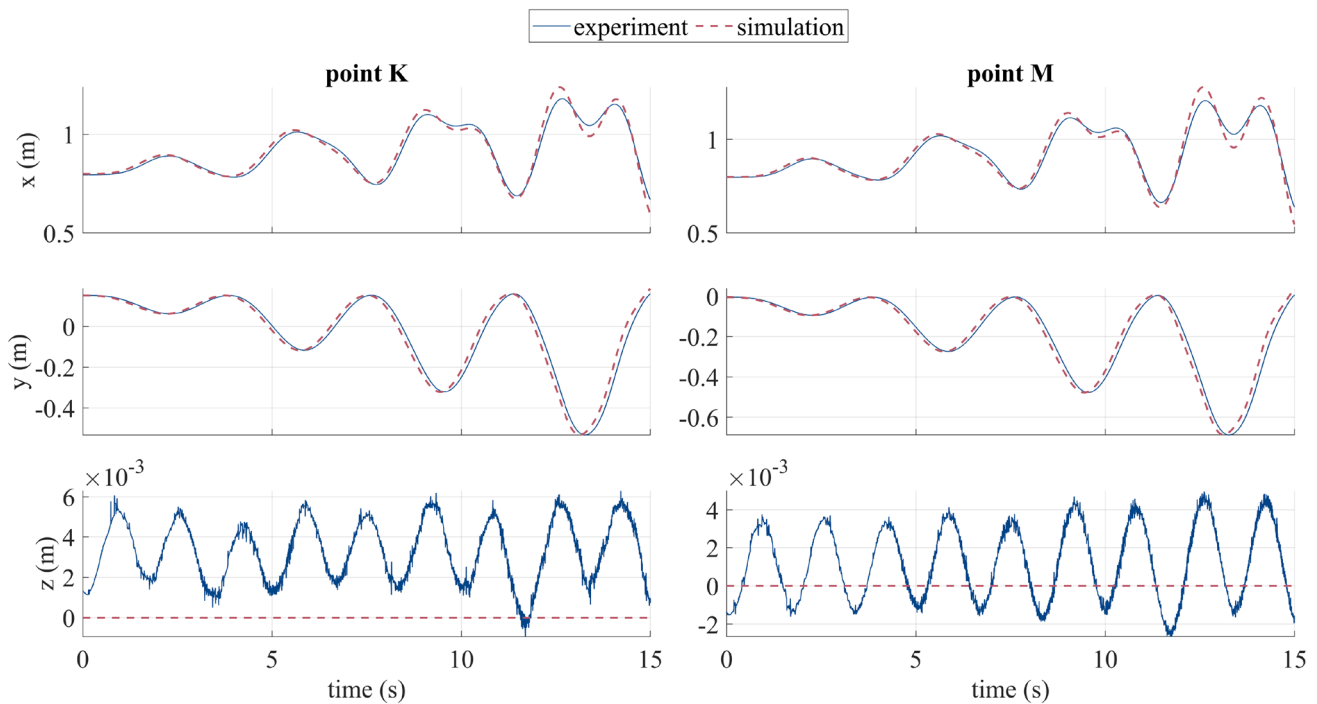


Fig. 7 Trajectory of the prefabricated concrete wall module relative to the inertial frame A1. Comparison of the simulated triple pendulum model to the experimental triple pendulum. The positions K and M coincide with the masses of the hook block and payload respectively

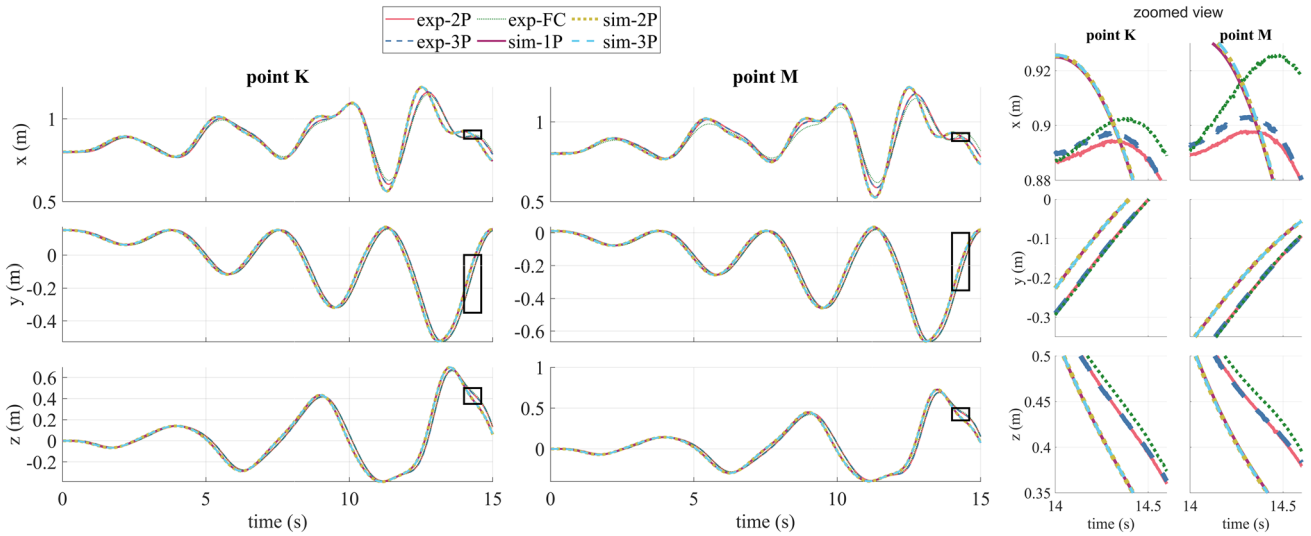


Fig. 8 Trajectory of the prefabricated curtain wall module, relative to the inertial frame A1. As simulated (sim) or experimentally measured (exp). Models: 1P (single pendulum), 2P (double pendulum), 3P (triple pendulum), FC (full complexity). The positions *K* and *M* coincide

with the masses of the hook block and payload respectively. The pendulum plots closely occlude each other. The boxes on the plots correspond to the limits of the zoomed view

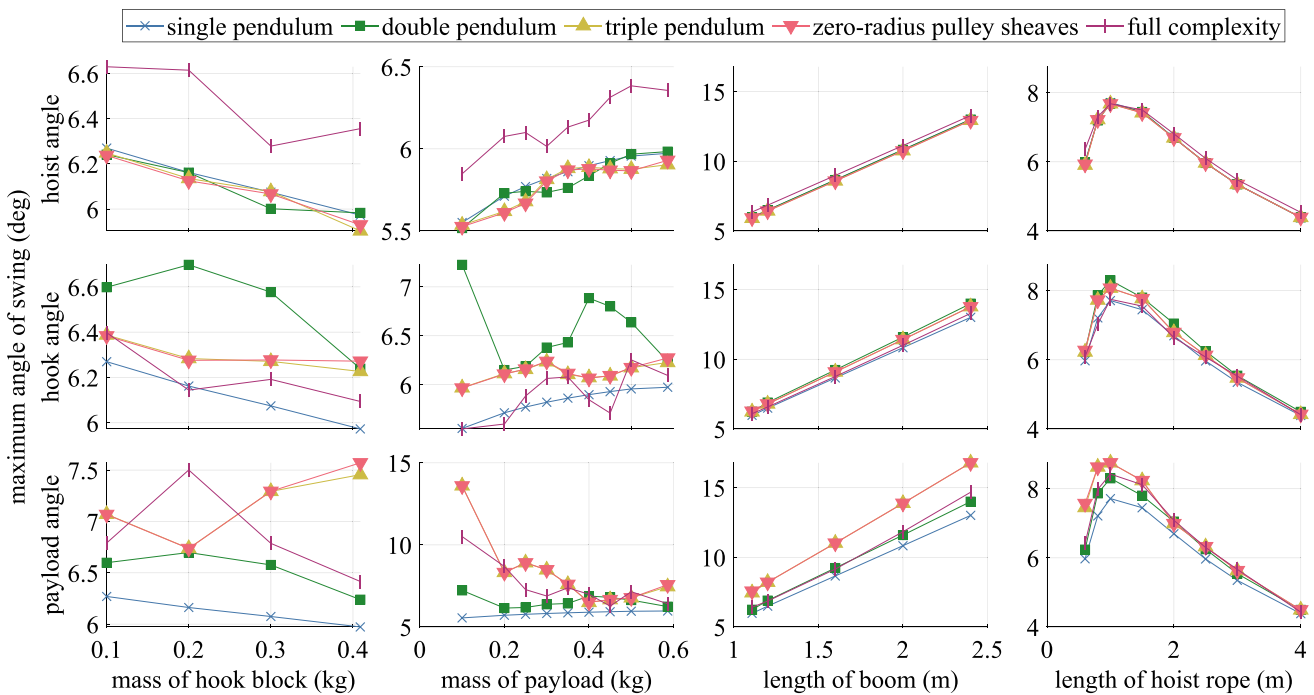


Fig. 9 Simulated maximum angular disturbance for various system parameters, compared between each dynamical model. In each plot, only one parameter is varied, while holding the other values constant as per Table 2

desirable effect of reducing payload swing, particularly where the payload is lightweight. This knowledge can then be used by designers to make the system easier to control. Additionally, this design is highly compatible with the implementation of a robotic hook block which can assist in payload alignment to the target.

In choosing which model should represent a given physical system, we present Fig. 10, a decision tree to choose the optimal model for different requirements. The design of this decision tree is discussed as follows.

For each leaf of the decision tree, the optimisation followed the methodology:

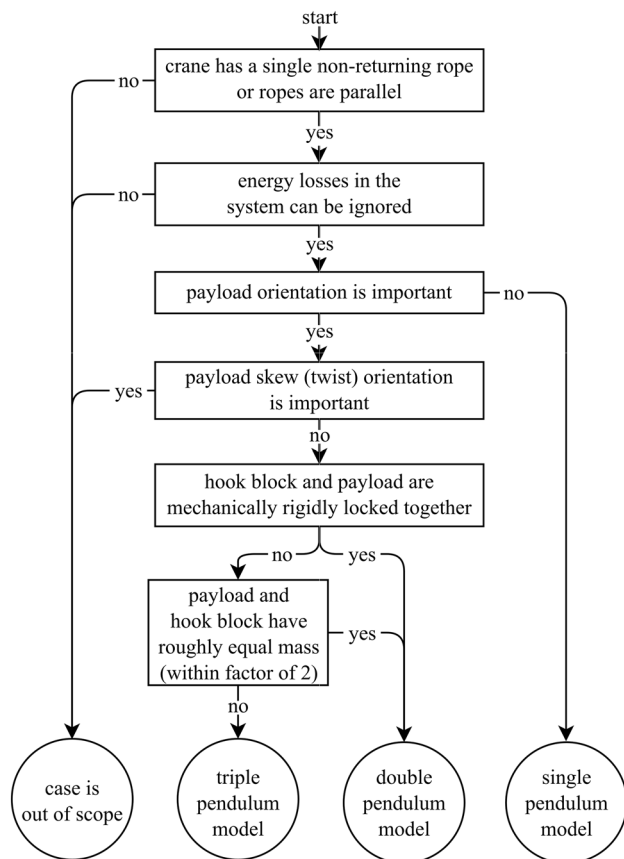


Fig. 10 Decision tree for choosing the optimal model for different requirements

1. The results are interpreted to classify each model's ability to describe system information (payload skew or roll orientation), and classify the compatibility of the geometric features of each model to each variation of real-world crane (parallelism of the hoist ropes, joint between the hook block and payload).
2. Using the model classifications, models that do not satisfy the categorical requirements of the decision tree leaf are discarded. For example, the single pendulum model inadequately describes payload roll, hence, it is discarded for the applications where payload roll is considered important.
3. Of the remaining models, the least complex model is optimal. The order of most-to-least complex model is full complexity, zero-radius pulley sheaves, triple pendulum, double pendulum, and single pendulum.

Following, we discuss the model classifications and decision tree requirements.

Pendulum models have previously been shown to be inappropriate for application to non-parallel-rope systems [22]. Many variations of non-parallel-rope rigging

configurations exist. Hence, choice of the specific closed kinematic chain model is out of scope.

Next, the combined impact of all model simplifications should be considered. Figure 8 demonstrates a case where the magnitude of error in the location of the centre of mass from choosing a pendulum model over a higher complexity model is comparable to the error from omitting frictional forces. The approximation of this system as a pendulum system could hence be considered appropriate in the same circumstances that justify omitting friction from the model. However, for a more accurate representation of the system that includes frictional forces, the impact of representing the system with a pendulum model should be carefully tested for the exact system parameters.

Omitting frictional losses is common practice, for example in closed-loop control systems design, which requires very low model complexity [1]. In this case, the simplification is acceptable. Thus, controllers designed for low-friction parallel-rope systems and pendulum systems should be interchangeable without significant impact on performance.

In contrast, a state estimator may make use of the higher accuracy of a closed kinematic chain model to improve estimation accuracy, or to estimate otherwise unobservable parameters [24]. The choice of model is then dependent on the specific problem requirements.

Furthermore, consider what information is required from the model. If only the location of the centre of mass is important, then large error in the payload angle may be acceptable for the case where the length of the hoist is much greater than the length of the payload. Hence, a double or single pendulum model may be sufficient.

Finally, it should be considered that, for the higher-complexity models, the mass matrix can become singular in special loading cases, inhibiting solving of the system equations. Furthermore, the equations can become very stiff for other combinations of system parameters which may realistically be expected to be encountered during crane operation. For example, when no payload is attached, the model should fix the angle of the payload as a constant.

6 Conclusions and future work

The current practice for construction crane operations is not safe and can be improved with more accurate payload monitoring and control. Crane control systems development requires the application of many simplifying assumptions to the dynamical crane model. The optimal dynamical model should achieve maximal reduction in model complexity, with minimal error in modelled behaviour, while satisfying the application requirements.

For the first time, this research presents the decision tree Fig. 10 which guides systems designers to choose the

optimal dynamical model, and guides the application of these systems to the family of cranes which share the same optimal dynamical model. The models represent three variations of boom tower crane that are commonly deployed on construction sites. We also present a methodology to rigorously evaluate crane models through their relation to the real-world crane, and a complete programmatic method to reform the constrained dynamical equations to reduce numerical error in simulation by six orders of magnitude.

The modelling methodology ignored frictional damping, assumed inelasticity and weightlessness of the hoist rope, and assumed infinite stiffness of the tower and boom. Simultaneous inclusion of all these complexities in a single model results in the model becoming too complex to feasibly solve. The trajectory comparison shows the impact of these assumptions on the simulated trajectory. As a result, this work considers some modelling cases to be out of scope of Fig. 10. Future work is recommended to systematically review the literature that addresses these cases in detail. Further expansion of the investigation to more types of crane is also recommended.

In the derivation of the pendulum models, a virtual rope is assumed to replace the complex pulley system. This requires choosing a single nominal luffing angle where the locations of the masses match the real locations at equilibrium. At other luffing angles there is a constant offset error, which is very small by comparison to the large scale of the crane system. Hence, the error has minimal effect on sway dynamics, irrespective of the choice of nominal luffing angle. However, for use in systems to estimate the location of the payload, it should be recognised that the resultant length of the hoist rope has a small offset error that is dependent on the luffing angle.

In future work, we will apply these results to the development of a robotic crane end effector for assembling prefabricated modules on high-rise buildings. Understanding the effects of rigging configuration on system dynamics enables choice of the optimal rigging configuration. Understanding the family of cranes with similar dynamics enables targeting the system to the whole family of cranes instead of just one crane. Furthermore, the situations in which operation of the device will be safe can be identified. Finally, the perception, monitoring, and control systems onboard the device can deploy the optimal dynamical model to achieve optimal performance.

Acknowledgements This research was supported by an Australian Government Research Training Program (RTP) Scholarship. This research is supported by Building 4.0 CRC.

Author Contributions BJ: conceptualization, data curation, formal analysis, investigation, methodology, project administration, resources, software, validation, visualization, writing—original draft, writing—review and editing. EA: funding acquisition, supervision, writing—review and editing. MA: supervision, writing—review and editing.

Funding Open Access funding enabled and organized by CAUL and its Member Institutions.

Data availability The code and data will be available at <https://github.com/Brandon-Johns/crane-dynamics-simulator>.

Declarations

Conflict of interest The authors declare that they have no known competing financial interests or personal relationships that could have appeared to influence the work reported in this paper.

Ethical standards This work does not contain any studies with human participants or animals performed by any of the authors.

Open Access This article is licensed under a Creative Commons Attribution 4.0 International License, which permits use, sharing, adaptation, distribution and reproduction in any medium or format, as long as you give appropriate credit to the original author(s) and the source, provide a link to the Creative Commons licence, and indicate if changes were made. The images or other third party material in this article are included in the article's Creative Commons licence, unless indicated otherwise in a credit line to the material. If material is not included in the article's Creative Commons licence and your intended use is not permitted by statutory regulation or exceeds the permitted use, you will need to obtain permission directly from the copyright holder. To view a copy of this licence, visit <http://creativecommons.org/licenses/by/4.0/>.

References

- Hong K-S, Shah UH. Dynamics and control of industrial cranes. Berlin: Springer; 2019.
- Iturralde K et al. A cable driven parallel robot with a modular end effector for the installation of curtain wall modules. Proceedings of the 37th International Symposium on Automation and Robotics in Construction (ISARC), 2020.
- Liang C-J, Kang S-C, Lee M-H. Ras: a robotic assembly system for steel structure erection and assembly. *Int J Intell Robot Appl*. 2017;1(4):459–76. <https://doi.org/10.1007/s41315-017-0030-x>.
- Johns B, Arashpour M, Abdi E. Curtain wall installation for high-rise buildings: Critical review of current automation solutions and opportunities. In: Proceedings of the 37th International Symposium on Automation and Robotics in Construction (ISARC). (2020).
- Choi SD, Guo L, Kim J, Xiong S. Comparison of fatal occupational injuries in construction industry in the United States, South Korea, and China. *Int J Ind Ergon*. 2019;71:64–74. <https://doi.org/10.1016/j.ergon.2019.02.011>.
- Gharaie E, Lingard H, Cooke T. Causes of fatal accidents involving cranes in the Australian construction industry. *Constr Econ Build*. 2015;15(2):1–12. <https://doi.org/10.5130/AJCEB.v15i2.4244>.
- Fang Y, Cho YK, Durso F, Seo J. Assessment of operator's situation awareness for smart operation of mobile cranes. *Autom Constr*. 2018;85:65–75. <https://doi.org/10.1016/j.autcon.2017.10.007>.
- Ouyang H, Tian Z, Yu L, Zhang G. Partial enhanced-coupling control approach for trajectory tracking and swing rejection in tower cranes with double-pendulum effect. *Mech Syst Signal Process*. 2021;156: 107613. <https://doi.org/10.1016/j.ymssp.2021.107613>.
- Ramli L, Mohamed Z, Abdullahi AM, Jaafar HI, Lazim IM. Control strategies for crane systems: a comprehensive review. *Mech*

- Syst Signal Process. 2017;95:1–23. <https://doi.org/10.1016/j.ymsp.2017.03.015>.
10. Rauscher F, Sawodny O. Modeling and control of tower cranes with elastic structure. *IEEE Trans Control Syst Technol*. 2021;29(1):64–79. <https://doi.org/10.1109/TCST.2019.2961639>.
 11. Abis C. Kalman Filter approaches on crane swing. Master's thesis, Michigan Technological University (2012).
 12. Wu Q, Wang X, Hua L, Xia M. Modeling and nonlinear sliding mode controls of double pendulum cranes considering distributed mass beams, varying roped length and external disturbances. *Mech Syst Signal Process*. 2021;158: 107756. <https://doi.org/10.1016/j.ymsp.2021.107756>.
 13. Huang J, Xie X, Liang Z. Control of bridge cranes with distributed-mass payload dynamics. *IEEE/ASME Trans Mechatron*. 2015;20(1):481–6. <https://doi.org/10.1109/TMECH.2014.2311825>.
 14. Ye J, Huang J. Analytical analysis and oscillation control of payload twisting dynamics in a tower crane carrying a slender payload. *Mech Syst Signal Process*. 2021;158: 107763. <https://doi.org/10.1016/j.ymsp.2021.107763>.
 15. Peng J, Huang J, Singhose W. Payload twisting dynamics and oscillation suppression of tower cranes during slewing motions. *Nonlinear Dyn*. 2019;98(2):1041–8. <https://doi.org/10.1007/s11071-019-05247-4>.
 16. Yoon J, Nation S, Singhose W, Vaughan JE. Control of crane payloads that bounce during hoisting. *IEEE Trans Control Syst Technol*. 2014;22(3):1233–8. <https://doi.org/10.1109/TCST.2013.2264288>.
 17. Jin L, Liu H, Zheng X, Chen S. Exploring the impact of wind loads on tower crane operation. *Math Prob Eng*. 2020. <https://doi.org/10.1155/2020/2807438>.
 18. Tomczyk J, Cink J, Kosucki A. Dynamics of an overhead crane under a wind disturbance condition. *Autom Constr*. 2014;42:100–11. <https://doi.org/10.1016/j.autcon.2014.02.013>.
 19. Cekus D, Gnatowska R, Kwiatkoń P. Impact of wind on the movement of the load carried by rotary crane. *Appl Sci*. 2019;9(18):3842. <https://doi.org/10.3390/app9183842>.
 20. Arena A, Casalotti A, Lacarbonara W, Cartmell MP. Dynamics of container cranes: three-dimensional modeling, full-scale experiments, and identification. *Int J Mech Sci*. 2015;93:8–21. <https://doi.org/10.1016/j.ijmecsci.2014.11.024>.
 21. Schlott P, Geise A, Grabmair G, Fritzel T, Sawodny O. A crane-based five-axis manipulator for antenna tests. *Control Eng Pract*. 2019;85:149–62. <https://doi.org/10.1016/j.conengprac.2019.01.014>.
 22. Kimiaghalam B, Homaifar A, Bikdash M, Hunt BR. Feedforward control law for a shipboard crane with Maryland rigging system. *J Vib Control*. 2002;8(2):159–88. <https://doi.org/10.1177/107754602023816>.
 23. Lee J-W, Kim D-H, Park K-T. Fuzzy control of sway and skew of a spreader by using four auxiliary cables. In: *Proceedings of International Conference on Control, Automation, and Systems*. (2005).
 24. Sato K, Ohishi K, Miyazaki T. Anti-sway crane control considering wind disturbance and container mass. *Elect Eng Jpn*. 2015;193(1):21–32. <https://doi.org/10.1002/ej.22580>.
 25. Zheng X, et al. Ale formulation for dynamic modeling and simulation of cable-driven mechanisms considering stick-slip frictions. *Mech Syst Signal Process*. 2022;168: 108633. <https://doi.org/10.1016/j.ymsp.2021.108633>.
 26. Ho T, et al. A switched optimal control approach to reduce transferring time, energy consumption, and residual vibration of payload's skew rotation in crane systems. *Control Eng Pract*. 2019;84:247–60. <https://doi.org/10.1016/j.conengprac.2018.11.018>.
 27. Cibicik A, Myhre TA, Egeland O. Modeling and control of a bifilar crane payload. In: *2018 Annual American Control Conference (ACC)*. (2018).
 28. Hindmarsh AC, et al. Sundials: suite of nonlinear and differential/algebraic equation solvers. *ACM Trans Math Softw*. 2005;31(3):363–96. <https://doi.org/10.1145/1089014.1089020>.
 29. Rackauckas C. A comparison between differential equation solver suites in matlab. In: Julia R, Python C, Editors, *Mathematica, Maple, and Fortran*. The Winnower (2018). <https://doi.org/10.15200/winn.153459.98975>.
 30. Sanderson C, Curtin R. Armadillo: a template-based c++ library for linear algebra. *J Open Source Softw*. 2016;1(2):26. <https://doi.org/10.21105/joss.00026>.
 31. Hamano F. Derivative of rotation matrix-direct matrix derivation of well-known formula. In: *Proceedings of the IEEE Green Energy and Systems Conference (IGESC 2013)*. (2013).
 32. Shampine LF, Reichelt MW. The MATLAB ODE suite. *SIAM J Sci Comput*. 1997;18(1):1–22. <https://doi.org/10.1137/S1064827594276424>.
 33. Verner JH. Numerically optimal Runge-Kutta pairs with interpolants. *Num Algor*. 2010;53(2):383–96. <https://doi.org/10.1007/s11075-009-9290-3>.
 34. Shampine LF, Reichelt MW, Kierzenka JA. Solving index-1 DAEs in MATLAB and Simulink. *SIAM Rev*. 1999;41(3):538–52. <https://doi.org/10.1137/S003614459933425X>.
 35. Shampine LF. Solving $0 = F(t, y(t), y'(t))$ in MATLAB. *J Numer Math*. 2002;10(4):291–310. <https://doi.org/10.1515/JNMA.2002.291>.
 36. Beléndez A, Pascual C, Méndez D, Beléndez T, Neipp C. Exact solution for the nonlinear pendulum. *Revista brasileira de ensino de física*. 2007;29(4):645–8.
 37. Lee C, Lee G. Feasibility of beam erection with a motorized hook-block. *Autom Constr*. 2014;41:25–32. <https://doi.org/10.1016/j.autcon.2014.01.003>.
 38. Takahashi H, et al. Sensor-less and time-optimal control for load-sway and boom-twist suppression using boom horizontal motion of large cranes. *Autom Constr*. 2022;134: 104086. <https://doi.org/10.1016/j.autcon.2021.104086>.

Publisher's Note Springer Nature remains neutral with regard to jurisdictional claims in published maps and institutional affiliations.

3.2 Outlook

The outcomes of this work imply several practical directions towards the mechanisation and automation of CWM mid-air alignment.

The work finds that “simultaneous inclusion of [pulley geometry, wind, frictional damping, and elasticity of the hoist rope, tower, and boom] in a single model results in the model becoming too complex to feasibly solve”, yet the impact of each complexity on the simulated trajectory is not negligible if sub-meter accuracy is desired. Towards the objective of eliminating the requirement for manual handling, this result indicates that crane control systems alone can not feasibly satisfy the requirements. Towards the objective of precise payload localisation, the result indicates that evaluation of the model alone is not sufficient. Hence, additional mechanisms are required.

Whilst optimal model choice is not sufficient by itself, it can still contribute to increased precision. Additionally, the decision tree (Figure 10) reveals that the triple pendulum dynamics of the system can be reduced to double pendulum dynamics through changes to the physical system. For mid-air alignment with a BTHLD, mechanically locking the CWM, BTHLD, and crane hook together is sufficient to achieve this. Thus, the system would become easier to precisely control.

The next chapter applies these results to develop a localisation strategy and practical implementation.

4 Crane Payload Localisation Relative to the Side Face of a Building

This chapter embeds a copy of my publication [2], which is distributed under the [Creative Commons CC BY 4.0 license](#).

Chapter 3 finds that additional mechanisms are required to precisely localise a crane borne CWM. Chapter 2 suggests that a proximity sensor or computer vision system can directly measure the relative pose between the payload and fiducial features of the target. Therefore, this chapter introduces a markerless computer vision measurement algorithm to complete this task.

Also introduced, is a practical framework to implement the algorithm in conventional direct CWM installation. The framework incorporates the relevant technologies and considerations identified in Section 2.

4.1 Crane Payload Localisation for Curtain Wall Installation: A Markerless Computer Vision Approach

Crane Payload Localisation for Curtain Wall Installation: A Markerless Computer Vision Approach

Brandon Johns^{a,b,*}, Elahe Abdi^a, Mehrdad Arashpour^c

^a*Department of Mechanical and Aerospace Engineering, Monash University, 14 Alliance Lane, Clayton, 3800, Victoria, Australia*

^b*Building 4.0 CRC, 28 Derby Rd, Caulfield East, 3145, Victoria, Australia*

^c*Department of Civil Engineering, Monash University, 14 Alliance Lane, Clayton, 3800, Victoria, Australia*

1. Author information

1.1. ORCID

Brandon: 0000-0002-8761-5432

Elahe: 0000-0003-3748-0442

Mehrdad: 0000-0003-4148-3160

1.2. CRediT authorship contribution statement

Brandon Johns: Conceptualization, Data curation, Formal analysis, Investigation, Methodology, Project administration, Resources, Software, Validation, Visualization, Writing - original draft, Writing - review & editing. **Elahe Abdi:** Funding acquisition, Supervision, Writing - review & editing. **Mehrdad Arashpour:** Supervision, Writing - review & editing.

2. Acknowledgments

This research was supported by an Australian Government Research Training Program (RTP) Scholarship. This research is supported by Building 4.0 CRC. The support of the Commonwealth of Australia through the Cooperative Research Centre Programme is acknowledged.

3. Ethics declarations

3.1. Conflict of interest

The authors declare that they have no known competing financial interests or personal relationships that could have appeared to influence the work reported in this paper.

3.2. Ethics declarations

This work does not contain any studies with human participants or animals performed by any of the authors.

*Corresponding author

Email addresses: `brandon.johns@monash.edu` (Brandon Johns), `elahe.abdi@monash.edu` (Elahe Abdi), `mehrdad.arashpour@monash.edu` (Mehrdad Arashpour)

4. Data availability statement

The data is available at <https://doi.org/10.26180/23538198> and <https://github.com/Brandon-Johns/glass-curtain-wall-installation-dataset>

5. blinded citations

The blinded citations are marked as

Details omitted for double-anonymized reviewing (a).

Details omitted for double-anonymized reviewing (b).

Details omitted for double-anonymized reviewing (c).

These respectively correspond to

```
@InProceedings{citeKey04,  
  author    = {Johns, Brandon and Arashpour, Mehrdad and Abdi, Elahe},  
  booktitle = {Proceedings of the 37th International Symposium on Automation and  
              Robotics in Construction (ISARC)},  
  title     = {Curtain Wall Installation for High-Rise Buildings: Critical Review  
              of Current Automation Solutions and Opportunities},  
  year      = {2020},  
  pages     = {393--400},  
  doi       = {10.22260/ISARC2020/0056},  
  isbn      = {978-952-94-3634-7},  
}
```

```
@InProceedings{citeKey21,  
  author    = {Kerry He and Brandon Johns and Elahe Abdi and Mehrdad Arashpour},  
  booktitle = {Australasian Conference on Robotics and Automation, ACRA},  
  title     = {Camera View from Crane Payload: Video Stabilization},  
  year      = {2021},  
}
```

```
@Dataset{citeKey44,  
  author = {Johns, Brandon and Abdi, Elahe and Arashpour, Mehrdad},  
  doi    = {10.26180/23538198},  
  title  = {Glass Curtain Wall Installation Dataset},  
  year   = {2023},  
}
```

Crane Payload Localisation for Curtain Wall Installation: A Markerless Computer Vision Approach

Abstract

Automated measurement of the relative pose between a crane borne curtain wall module and its installation location on the side face of a high-rise building can be applied to increase the safety and efficiency of crane operations though informing the action required to achieve alignment. However, the detection and measurement tasks are challenging because the construction site is large, unstructured, and highly dynamic. This article introduces a markerless computer vision measurement algorithm and a practical implementation, which uses a forward-facing infrared camera attached to the crane spreader. The algorithm self-verifies the measurement against known information so that it can fail safely instead of returning a malformed measurement. The algorithm is experimentally validated in challenging lighting conditions. The window frame segmentation achieved $F_\beta = 0.59$. Overall, the algorithm returned 71% successful and 0 malformed measurements.

Keywords: Crane, Construction, Computer Vision, Monocular Vision, Facade Segmentation, Curtain Wall

1. Introduction

Measurement of the relative pose between a crane borne curtain wall module (CWM) and its installation location on the side face of a high-rise building has never before been successfully automated. The strong glare of the sun off the building's glass wall defeats most markerless proximity sensing techniques [1, 2]. In this article, we use the near infrared properties of the thermally insulative coating on the glass to facilitate the measurement task.

A unitised curtain wall is a type of exterior wall for high-rise buildings, which is comprised of prefabricated modules that hang from the building floor slabs. To install the curtain wall, first, mounting brackets are positioned and affixed to the floor slabs [3]. Then the modules are individually aligned and fastened to the brackets.

In the direct CWM installation methodology [4] (Fig. 1), each CWM is individually crane lifted from the ground below the installation location, up towards the installation location. While the CWM is still supported by the crane, workers at the installation location take hold of the CWM and physically manipulate it into alignment before fastening it to the brackets [3, 5, 6]. The CWM is then detached from the crane, and the process is repeated. This methodology has high risk of 'struck by', 'crushed between', and 'fall from height' injury to the workers who must physically

Abbreviations: balanced accuracy (BA), below-the-hook-lifting-device (BTHLD), building information modelling (BIM), curtain wall module (CWM), inertial measurement unit (IMU), light detection and ranging (LiDAR), Matthews correlation coefficient (MCC), near infrared (NIR)

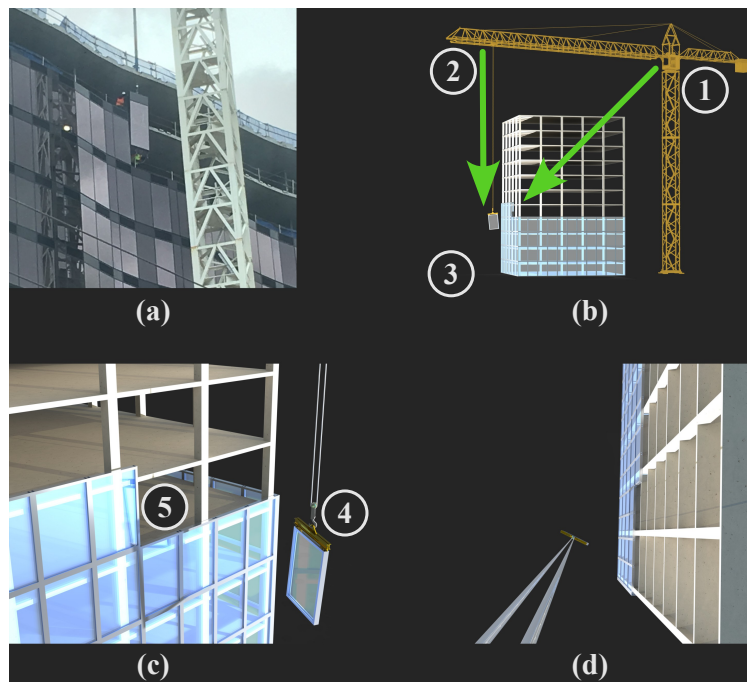


Figure 1: The Direct CWM installation process. Location 1 is crane operator, 2 is the top of the hoist, 3 is the CWM pickup location on the ground, 4 is the crane payload, and 5 is the installation location. a) Two human workers receiving a CWM. b) Depiction of a blind lift scenario. c) Near view of the installation location. d) View from the top of the hoist.

manipulate the CWM into alignment [4]. These are among the most common types of construction accidents [7, 8].

The crane operator does not always have visibility of the crane payload or installation location. Fig. 1b depicts line-of-sight arrows for a blind lift scenario where the building obscures the line of sight of the operator. A common solution to provide the operator with vision is with the video feed from a downward facing camera located at top of the hoist [9]. However, Fig. 1d illustrates that this solution is insufficient for the task of CWM installation. This view provides insufficient depth perception for a mid-air alignment operation [9]. In general, the crane operator must rely on a human worker (known as the ‘dogman’) for direction by means of arm signals, whistle signals, and radio communication [10]. However, this methodology is unsafe, as it is susceptible to communication error or delay [4].

Two safety critical measurement tasks in the CWM installation procedure are to, in real-time, monitor the distance between the CWM and the side face of the building, and to measure the relative displacement between the CWM and the target aligned pose. The quality of this information is safety critical; delay or error could cost a worker’s life. Safety in this task can be improved with an automated system to directly inform the crane operator of these measurements [4, 11]. Therefore, this article introduces a novel automated system for this purpose.

Automated measurement of the relative pose between the crane payload and installation location is a non-trivial task. A common strategy to achieve this measurement is to individually find the locations of the crane payload and the installation location, with respect to a global coordinate frame. Then, the required measurement can be obtained as the difference between these locations.

The measurement of the installation location in the global coordinate frame is often defined by Building Information Modelling (BIM) [12, 13]. However, sole reliance on BIM data risks inaccurate measurement due to deviance of the real building from the plan, and misalignment of the model to the real building [13]. Additionally, the state of the art in global crane-payload-pose-measurement achieves error on the order of metres [14, 15, 16, 17], and most systems do not consider payload orientation [18, 19].

To circumvent the limitations of global localisation, a proximity sensor or computer vision system attached to the crane payload can directly measure the relative pose between the payload and the target. Of the vision systems used in crane operations, many depend on artificial markers [20, 21, 22, 23, 24, 25, 26], or colour contrast [14, 27, 28, 29] to locate the target. However, curtain walls are generally architectural; permanent changes to the visual design are not acceptable. Temporary markers could be used, but the additional required work for marker removal is not desirable. In another approach, sonar beacons are integrated into the facade at 3m intervals [30], however, requirement of hundreds of beacons increases cost and complexity. [31] projects structured light onto the facade to perform inspection, however, outdoor environments or glass facades are not considered. Solar radiation can interfere with structured light sensing. [32] uses an RGB-D camera to detect the window frame, however, outdoor environments are not considered.

Object recognition on a construction site without markers or beacons is challenging because construction sites are large, unstructured, and highly dynamic environments [1]. Additionally, curtain walls are mostly glass, which is difficult to detect by proximity sensing [2, 33, 34, 35, 36]. Active proximity sensors (e.g. structured light, LiDAR) struggle to detect glass at large viewing angles due to the high specular reflectivity of the surface [36]. Sensor fusion of LiDAR with a polarization camera or sonar can be used to infer the class of detection from the missing information of each sensor [33, 35]. However, the cost of LiDAR is prohibitive. Polarising filters are commonly applied to reduce glare in outdoor images. However, when the sun is directly behind the camera which is aimed at perpendicular to the wall, the solar reflection off the wall would not be polarised, hence, the filter would be ineffective [33]. Stereo reconstruction is challenging in the presence of specular reflections and transparency [2]. Visible-spectrum cameras can not see glass due to its transparency. In the domain of machine learning, [37] performs bounding box detection and activity recognition of the crane borne CWM, assuming view from CCTV feed. YOLO-based methods are common [38]. Many machine learning works attempt facade segmentation [39, 40, 41, 42]. However, the training datasets include few curtain walls, are viewed from a large distance, are of fully constructed buildings, and do not include harsh lighting conditions. While machine learning methods are comparable to human coded logic, the dataset creation is cost prohibitive.

The glass used in CWM construction uses thermally insulative or low-emissivity (low-E) coatings to increase the energy efficiency of the building [43]. However, these coatings also change the visual properties of the glass according to the relation $transmittance + reflectance + absorptance = 1$ [43]. In the near infrared (NIR) band, low-E glass reduces transmittance in favour of increasing reflectance, while insulative glass reduces transmittance in favour of increasing absorptance [43]. Any absorbed light is re-emitted, per conservation of energy. In this article, we use the NIR properties of CWMs to facilitate the measurement task.

This article introduces a novel system to measure the relative pose between the crane payload and installation location. Markerless computer vision is applied with a forward-facing infrared camera attached to the crane spreader bar. The boundaries of the previously-installed CWMs are identified by exploiting the properties of aluminium and architectural glass as viewed in infrared.

The measurement is then derived from the correspondence between the detected boundary and the known dimensions of the CWM. The system is designed to be cost effective and practical to implement at scale by requiring very little change to existing components, equipment, or procedures. We additionally ensure that the camera is never poorly positioned, and its view is never occluded.

Experimental validation uses a dataset designed to include the most challenging lighting conditions. Strong glare from the sun reflecting off the curtain wall is present in the images taken just before sunset. The dataset includes motion capture measurements for every image. The camera calibration data is also included. The value of including the camera calibration with the dataset is that the calibration is required for many computer vision operations (perspective-undistortion, extrinsics estimation, aspect ratio estimation). The calibration is necessary to recreate our results. The value of including the motion capture is that it may be used to verify extrinsics estimation. This was used to validate our results. We did not find any public datasets in the domain of facade detection or glass detection that include this information. We release this dataset under the Creative Commons CC BY 4.0 license at [44].

The key contributions of this article are:

- The development of a methodology to measure the pose of a crane borne CWM, as relative to its installation location on the side face of a high-rise building. To the best of our knowledge, this has never before been successfully automated.
- The development of a computer vision algorithm to segment the frame of a glass facade in the presence of strong glare. The state-of-the-art do not consider these harsh lighting conditions.
- The development of a dataset of joint image and motion capture data, depicting a partially constructed curtain wall from the perspective of the crane hook, and measuring the relative pose of the camera with respect to the installation location.

The key findings of this article are that:

- The thermally insulative and low-E coatings on architectural glass can benefit the computer vision systems which use NIR cameras.
- The robustness of glass facade segmentation systems can be significantly improved by verifying the result against the known panel dimensions, with minimal setup effort to input the dimensions into the system.
- The developed segmentation algorithm resulted in 3 times more successful measurements than the state-of-the-art glass segmentation algorithms [45, 46].

Directions for future work are suggested to incorporate the algorithm into a system that retains information between frames. Data fusion with an IMU may also improve estimation accuracy. The algorithm may be extended to function with non-rectangular or non-glass CWMs. The broader implications of this work are to use in the localisation of a crane hook relative to the side face of the building, which may benefit blind lift operations. Inspection drones may also use the algorithm to localise.

Section 2 introduces the measurement algorithm. Section 3 validates the performance of the algorithm as applied to the dataset. Section 4 introduces a practical implementation of the algorithm and discusses the design considerations and expected benefits. Section 5 concludes the article and discusses future work.

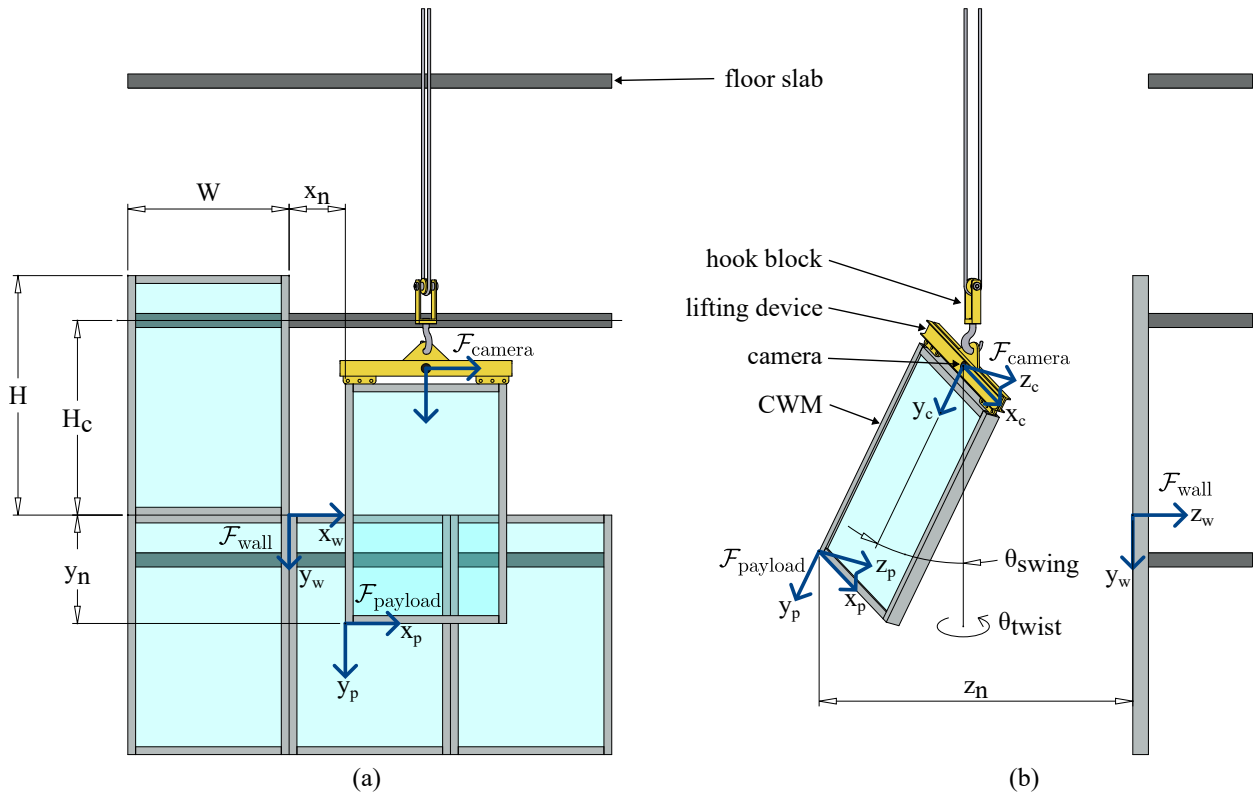


Figure 2: Coordinate frames and dimensions related to the measurement problem. a) front view. b) side view.

2. Measurement Algorithm

The measurement procedure requires a NIR camera to be attached to either the crane hook block, spreader, or payload, and for it to point towards the side face of the building. The measurement algorithm uses an image from this camera to measure the relative pose between the crane borne CWM and its installation location on the side face of the building. Pseudocode of the measurement algorithm is Algorithm A.1.

Additionally to the image, the algorithm requires the camera intrinsic parameters and distortion coefficients. These can be determined by camera calibration. Also required, are the dimensions of the curtain wall, H , W , and H_C , defined by Fig. 2. While not all of these parameters are required to perform the measurement [47], we use them to increase the robustness of the algorithm. The additional required setup effort is small because these parameters are mostly constant for a given curtain wall and camera.

In the first stage of the algorithm (Lines 2–3), the image is undistorted and then downsampled. Downsampling is used to improve speed of the operations to follow.

To then detect the CWM boundaries (Lines 4–6), the thermal radiative properties of the CWM are considered. For low-E glass, the NIR reflectivity is high, and the reflections are specular. Hence, to a NIR camera, low-E glass appears dark for most angles of the sun, and dark with glare when the sun is viewed in the reflection. By contrast, the aluminium frame produces more diffuse reflections. Hence, it appears bright for a greater range of viewing angles. Fig. 3a shows the appearance of the curtain wall for when the sun is behind the camera. In this image, the pixels capturing the

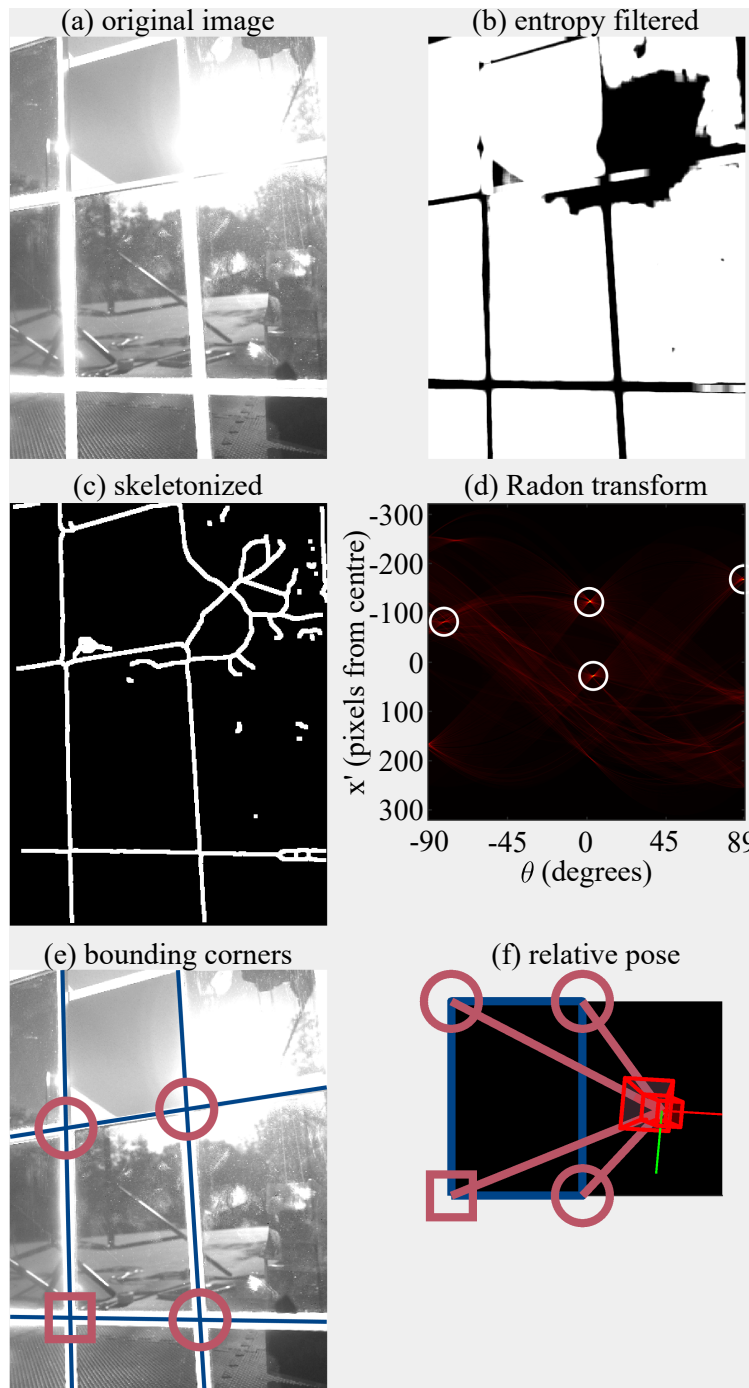


Figure 3: Stages of processing an image with the algorithm.

frame are saturated by the intense sunlight. The light also bleeds beyond the boundary of the aluminium, blurring the edge.

This blurring of the edge by the intense lighting conditions reduces the effectiveness of traditional edge detection techniques. This effect can be somewhat reduced by tuning the camera

sensitivity or exposure time. However, we found in preliminary testing that tuning alone cannot fully remove the bleed. With consideration that lighting conditions can change suddenly, we concluded that a robust algorithm design should function with suboptimal tuning.

Therefore, instead of applying edge detection, we use the saturation of the image to our advantage. The saturated segments of the image have low local entropy. Hence, we apply an entropy filter to the image to segment the window frame from the image (Fig. 3b). Thresholding is applied to the resulting image, followed by morphological skeletonization (Fig. 3c). Because the bleed obscures the edge between adjacent CWMs, both frames appear in a single low entropy blob. Skeletonization produces a line following the centre of the blob, which is also the boundary line dividing the CWMs. At any spots of intense glare over the aluminium, the bleed is symmetric. Hence, the centreline is still the CWM boundary.

The CWM boundary lines are then extracted from the skeleton image by the local maxima of its Radon transform (Lines 7–8). Thresholding by value is applied to filter out noise from glare on the glass. The noise is characterised by low peak values in the radon transform due to short jagged lines in the skeleton image. The thresholding is realised by selecting only the peaks with a value at least half that of the maximum value. Then, further thresholding to suppress noise selects only the strongest peak in each peak’s neighbourhood (Fig. 3d).

From the resulting lines, the two most vertical lines, and the two most horizontal lines are chosen (Lines 9–10). As it would be too dangerous to allow the crane payload to tilt by a large angle, the vertical lines can be reliably assumed to correspond to vertical CWM boundaries, and horizontal lines to the horizontal CWM boundaries. Assuming perfect fitting of lines to the CWM boundaries, the quadrilateral formed by the chosen lines bounds a single CWM because the perspective projection of a set of parallel lines produces a fan shape. Hence, two lines that are next to each other are closer in gradient than two lines separated by another line. In the cases where the lines were poorly fit to the CWM boundaries, this assumption may not hold true. Such cases are rectified in the operations to follow.

The chosen four lines are intersected to find the pixel coordinates of the CWMs corners (Fig. 3e). The coordinates are then upscaled to correspond to the full size image instead of the downsampled image (Lines 11–13).

To verify that the coordinates correspond to the corners bounding a single CWM, the aspect ratio of the perspective-undeformed rectangle is found according to the methodology described in [47]. The calculated aspect ratio is then compared to the true aspect ratio of the CWM. In the case of large error, the aspect ratios of other likely detection scenarios are tested. Common false detection scenarios include the bounding multiple adjacent CWMs, or extending past the top of the CWM to the concrete floor slab. The edge face of the concrete slab also has low entropy (Fig. 3b), hence it is sometimes used as an edge line by the algorithm. If no scenario is matched, the algorithm halts and returns an error.

Other halt conditions are triggered in Lines 9–10 if not enough peaks remain after thresholding. In this way, the algorithm was designed to be conservative in labelling success, so that the system may fail safely instead of returning a malformed measurement. If the algorithm were to return a malformed measurement, this could result in the crane operator taking an unsafe action.

With the detection classified by what it bounds (Lines 14–22), the dimensions of the bounding box in the world coordinate frame are calculated Line 23). The origin of the world coordinate frame is placed at the bottom-left corner of the CWM because for all detection cases, this is a CWM corner. By necessity of the curtain wall being installed row by row, from the bottom floor

to the top floor, the exposed concrete will always be above the CWM, hence, in a false detection, it will always form the top edge.

The 3D pose of the camera is then estimated by correspondence of the detected corners in the image with the corners of the bounding box in the world coordinate frame (Line 24). The MATLAB *extrinsics* and OpenCV *solvePnP* functions can compute this estimation.

The estimated pose is the transformation between the coordinate frames $\mathcal{F}_{\text{wall}}$ and $\mathcal{F}_{\text{camera}}$, as measured with respect to $\mathcal{F}_{\text{wall}}$ (Fig. 2). We represent this with the homogeneous transformation matrix ${}_{\text{camera}}^{\text{wall}}\mathbf{T}$.

The coordinate frame $\mathcal{F}_{\text{payload}}$ is the bottom-left corner of the crane borne CWM (Fig. 2). The value of ${}_{\text{payload}}^{\text{camera}}\mathbf{T}$ is determined by the camera placement. Combining this with the measured value ${}_{\text{camera}}^{\text{wall}}\mathbf{T}$ results in ${}_{\text{payload}}^{\text{wall}}\mathbf{T}$, the relative alignment between the wall and the payload.

$${}_{\text{payload}}^{\text{wall}}\mathbf{T} = {}_{\text{camera}}^{\text{wall}}\mathbf{T} \cdot {}_{\text{payload}}^{\text{camera}}\mathbf{T} \quad (1)$$

Alignment is achieved when ${}_{\text{payload}}^{\text{wall}}\mathbf{T}$ becomes the identity matrix.

3. Experimental Validation

The algorithm was validated against a specifically created dataset of 140 images. The dataset includes challenging lighting conditions, with strong glare from the sun reflecting off the partially constructed wall. Motion capture measurements were taken for every image, to verify the measurement results against. This dataset was created because no relevant existing dataset includes these challenging lighting conditions or captures the scene in infrared.

3.1. Dataset Creation

The dataset was created with a 1 : 25 scale model (Fig. 4), with dimensions $H = 153\text{mm}$, $W = 103\text{mm}$, and $H_C = 129\text{mm}$ (Fig. 2). The model CWMs were comprised of plain float glass in a mill-finish aluminium frame. The side of the glass that faces the building interior was coated with vinyl to emulate a low-E coating. The low-E coating is usually applied on the interior side of the outermost glass pane. Hence, double/triple glazing has minimal effect on the visual properties and was not required for the model. The concrete of the building was modelled with grey painted wood. The paint was found to be more reflective than actual concrete, hence, the algorithm is proved to be more robust for its capability in functioning with this additional challenge.

The camera and crane hook-block were only seen in reflections; hence, their appearance was not as strictly constrained. The hook-block was 3D printed plastic, and the hoist rope was twine. A Basler ace acA2040-55uc camera with a 6mm fixed focal length lens was used to take the images, from which only the red channel was used, because red is closest to infrared. We justify that this produces a close approximation of an NIR image with the visual comparison Fig. B.7. We note that the red and NIR photos in Fig. B.7 are only similar because our experimental model was intentionally prepared so that when observed by the red channel of an RGB camera, it looks similar to a real facade as observed by an NIR camera. In a real-world scenario with low-E coated glass, the red light would transmit, while the NIR light would reflect. The camera focus was set to the median operating distance.

An OptiTrack motion capture system of four FLEX 13 cameras was used to locate 19mm markers attached to the hook-block and the curtain wall. The motion capture system is an active proximity sensing system; it projects an NIR light on the scene and looks for the reflection of this

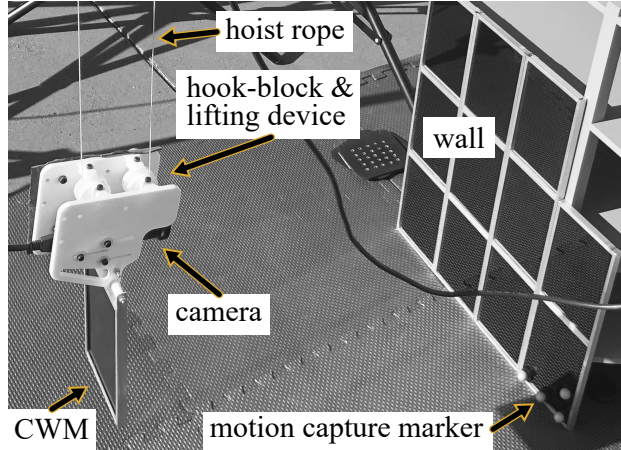


Figure 4: The data collection setup.

light off the markers. Hence, the challenging lighting conditions also reduce the performance of the motion capture. The ground was covered with black EVA foam mats to absorb the NIR light from the cameras and the sun. The area around the markers was also covered with black eva foam. With this, the OptiTrack system self-reported its precision as between 0.2mm and 10mm per object, varying with the severity of the lighting conditions. The majority of captured images were discarded due to momentary failure of the motion capture at the time when the image was taken. This further emphasises the failure of active proximity sensing in these conditions.

The camera calibration was performed indoors, before data collection, by motion capturing the system whilst showing a motion-captured checkerboard pattern to the camera. The camera intrinsic and extrinsic parameters were obtained for these images through the MATLAB Camera Calibrator. The transformation $\mathbf{T}_{\text{payload}}^{\text{camera}}$ was determined through the composition of the measurements from the image coordinate frame, to the checkerboard, to the checkerboard motion capture frame, to the camera motion capture frame, to the payload bottom-left corner. These measurements were performed respectively with the extrinsic data, calipers, motion capture, and calipers. This resulted in one measurement of $\mathbf{T}_{\text{payload}}^{\text{camera}}$ for each image in the calibration dataset.

Each measurement of $\mathbf{T}_{\text{payload}}^{\text{camera}}$ was decomposed into a (x_i, y_i, z_i) translation and a q_i quaternion rotation. The mean translation was then calculated as $(\text{mean}(x_i), \text{mean}(y_i), \text{mean}(z_i))$ and the standard deviation was calculated likewise. The mean rotation was calculated with the MATLAB Sensor Fusion and Tracking Toolbox function `meanrot()`, which implements the algorithm [48]. The standard deviation of the rotation was calculated as

$$\sqrt{\frac{1}{n-1} \sum_{i=1}^n \text{dist}(q_{\text{mean}}, q_i)^2} \quad (2)$$

where n is the number of measurements of $\mathbf{T}_{\text{payload}}^{\text{camera}}$ and the function `dist()` computes the angular distance between the quaternions. While there are multiple interpretations for the mean and standard deviation for a rotation, calculation by angular distance provides a single value result that is independent of any coordinate system. Therefore, the interpretation of the result is unambiguous.

The calibrated value of $\mathbf{T}_{\text{payload}}^{\text{camera}}$ for use in data collection was constructed from the mean

translation and rotation. The standard deviations of the translation and rotation were 1.4mm and 0.3° respectively. In classifying the sources of error in the verification data, the calibration error is a constant offset for the entire dataset, and the motion capture measurement error is distributed.

In data collection, the camera pose, ${}_{\text{camera}}^{\text{wall}}\mathbf{T}$, was varied between 180mm to 400mm in distance and up to 55° in angular distance. The locations of the previously installed CWMs were also varied. As each photo was taken, the motion captured pose ${}_{\text{payload}}^{\text{wall}}\mathbf{T}$ was recorded. Thus, the motion captured measurement can be compared to the measurement by the algorithm.

3.2. Validation Results

The overall measurement accuracy of the algorithm is presented in Table 1 as the difference between the algorithm’s measurement and the motion capture measurement.

$${}_{\text{wall}}^{\text{wall}}\mathbf{T}(\text{error}) = {}_{\text{payload}}^{\text{wall}}\mathbf{T}(\text{algorithm}) \cdot {}_{\text{payload}}^{\text{wall}}\mathbf{T}^{-1}(\text{motion capture}) \quad (3)$$

For each successful measurement, (3) was calculated and decomposed into a translation and a quaternion rotation. The means and standard deviations (Table 1) were then computed with the same methodology as used in the calibration. The magnitude of the measurement error is comparable to the accuracy of the verification data. The error in the measurement was approximately normally distributed across the dataset. Fig. B.8 is a visualisation of these results.

Table 1: Average measurement error over all 99 successful measurements. (x_n, y_n, z_n) are defined by Fig. 2. θ_q is the rotational misalignment as a quaternion angular distance.

Measurement	Unit	Measurement error	
		Mean	Standard deviation
x_n	mm	5.2	8.6
y_n	mm	3.5	3.0
z_n	mm	-6.5	9.1
θ_q	degrees	1.6°	2.9°

From the dataset of 140 images, 99 resulted in a successful measurement. For all 41 cases of boundary detection failure, the algorithm successfully detected that it was unable to perform the measurement and halted with the error Line 22. The algorithm did not return any malformed measurements. This validates the function of the algorithm to fail safely.

The MATLAB implementation of the algorithm computed each measurement in an average of 0.1 seconds on the researcher’s computer (Intel Xeon E3-1231 v3 CPU, DDR3 RAM). It is therefore expected that a C++ implementation could solve the measurement sufficiently fast for real-time use.

The sources of error in the measurement are deduced by inspecting the accuracy of the CWM boundary detection, as presented in Fig. 5. The effectiveness of the entropy filter is evident in that the only reflection to remain after filtering was the direct reflection of the sun, and due to the circularity of this reflection, no reflection was falsely detected as a boundary.

The outer face of the concrete is seen in the entropy image and was sometimes falsely detected as a boundary. This false detection is the main source of error in the boundary detection. However, the error case was always successfully classified by the aspect ratio check (Lines 14–22), hence, the algorithm still successfully deduced the correct measurement. Additionally, the entropy of the experimental model concrete is not true to the entropy of real concrete, hence, the false detection is not expected to occur in a real application.

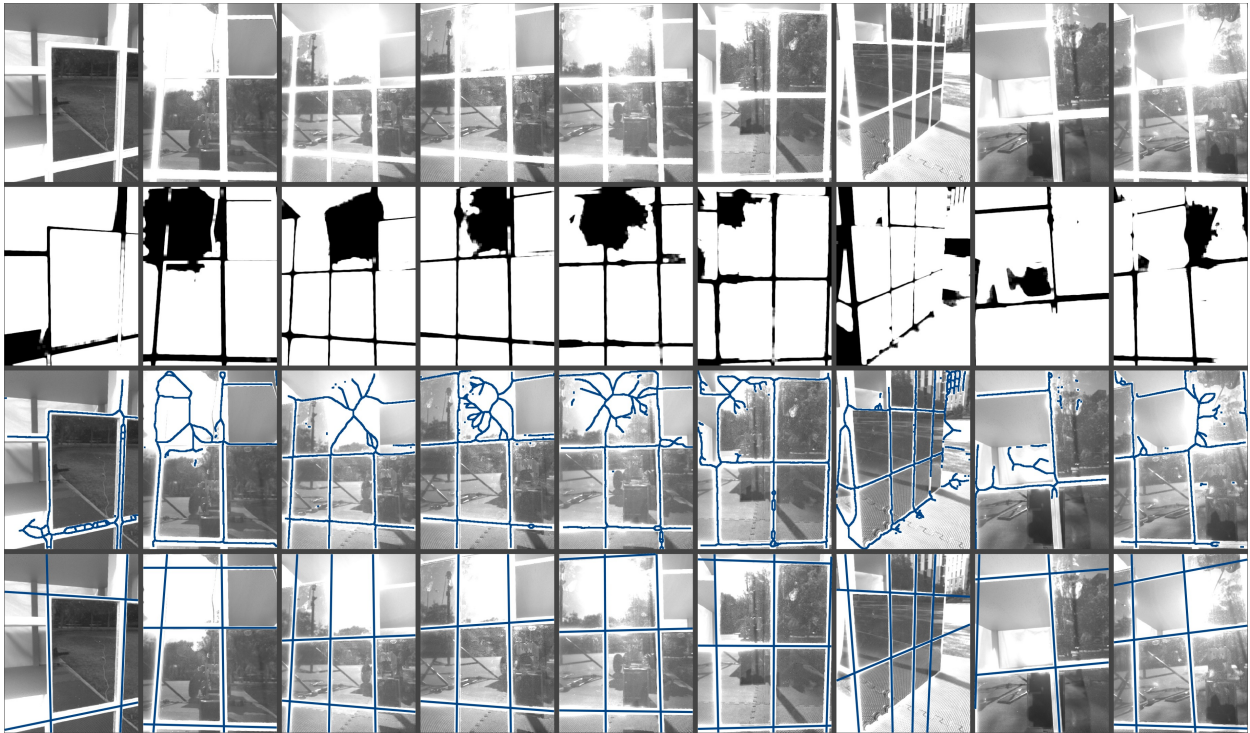


Figure 5: Stages of processing. First row: input image. Second row: entropy filtered. Third row: skeleton image overlaid on the input image. Fourth row: strong lines from the Radon transform overlaid on the input image.

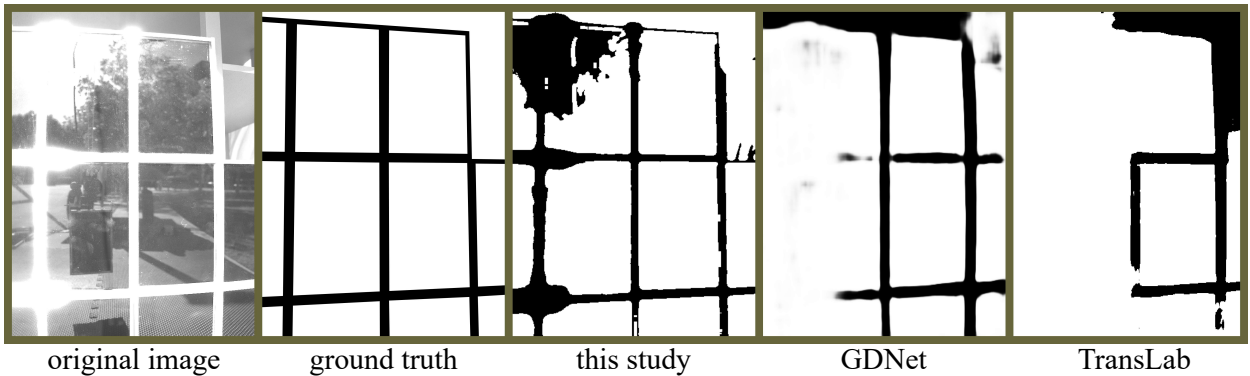


Figure 6: Comparison of the binary images produced by the methodology in this study, by GDNNet [45], and by TransLab [46]. The ideal result should mask only the window frame, as depicted in the ground truth.

3.3. Segmentation Performance

The methodology to compute the binary image (Lines 4–5) was compared to the most recent machine learning approaches to glass detection. The dataset was input to the pre-trained models of GDNNet [45], and TransLab [46], which directly output binary images that classify the glass in images. Thus, the inverse of the output binary image classifies the union of window frame with other non-glass objects. By contrast, the methodology in this study aims to only detect the frame. Hence, for an image that mostly contains glass and frame, the results should be similar. Fig. 6 shows a typical result of each segmentation method.

The methods were also compared through the well-known image segmentation metrics that relate to the confusion matrix. We labelled the ground truth for 60 randomly selected images to create a sub-dataset against which the automatic methods could be compared.

First, we define N_{total} as the number of pixels in a binary image. Then, we define N_P , N_N , and N_{PP} respectively as the number of pixels that are part of the window frame, not part of the frame, and detected to be part of the frame. Finally, we define TP , TN , FP , and FN respectively as the number of pixels that are correctly detected to be part of the frame, correctly detected to be not part of the frame, incorrectly detected to be part of the frame, and incorrectly detected to be not part of the frame.

The *Prevalence* $= N_P/N_{total}$ of the sub-dataset has a mean value of 0.14. This means that only 14% pixels are part of the frame. This skew in the data is considered because the most common metrics of Intersection over Union $IoU = \frac{TP}{TP+FN+FP}$, *precision* $= TP/N_{PP}$, *recall* $= TP/N_P$, and $F_\beta = \frac{(1+\beta^2) \cdot \text{precision} \cdot \text{recall}}{\beta^2 \cdot \text{precision} + \text{recall}}$ are all invariant to the value of TN . Thus, these metrics are not symmetric under the inversion of perspective from a glass detection problem to a frame detection problem, as was applied to the GDNet and TransLab results.

Metrics that are invariant under inversion of perspective are Balanced Accuracy $BA = \frac{1}{2} \cdot (\frac{TP}{N_P} + \frac{TN}{N_N})$, and Matthews Correlation Coefficient (MCC) [49]

$$MCC = \frac{TP \cdot TN - FP \cdot FN}{\sqrt{(TP + FP) \cdot (TP + FN) \cdot (TN + FP) \cdot (TN + FN)}} \quad (4)$$

With consideration to how the binary image is used, we still consider the non-symmetric metrics to be important, in that it is preferable to miss a detection than to obtain a false detection. A missed detection results in failure to calculate a pose, whereas a false detection may result in an incorrect calculation of pose. The former does not yield any information, whereas the latter could result in an unsafe action being taken. Hence, for F_β , we use $\beta^2 = 0.3$, which weighs precision more important than recall. This is the same value used by [45].

Table 2 specifies mean value of each metric. Our method achieves highest results in IoU, precision, F_β , and MCC. The recall of our method is low due to being tuned to be conservative in labelling a pixel as part of the frame, whereas GDNet achieves high recall with low precision due to excessive labelling of pixels near the frame boundary to be part of the frame, as seen in Fig. 6. This behaviour may be related to the inversion of perspective. GDNet is actually being conservative in labelling a pixel as being glass, if that pixel is near the boundary.

The output binary images from GDNet and TransLab were also connected to the remainder of the algorithm (Lines 6–25). From the 140 input images, using GDNet returned 34 measurements, and using TransLab returned 33 measurements. Of these measurements, respectively 7, and 16 measurements were malformed. By contrast, the segmentation methodology of this study produced 99 successful and 0 malformed measurements. This shows the susceptibility of the algorithm to unsafe behaviour when the frame detection precision is low.

4. Discussion

Sources of uncertainty in the measurement include random error proportional to the resolution of the camera and it's distance from the wall. Another uncertainty is characteristic of the orientation of the camera and the sun, and occurs when the side face of the frame is in view and not in a shadow; in which case, the detected centreline is slightly offset. A source of larger errors is false

Table 2: Performance of the CWM frame segmentation methodology, as compared to the segmentation masks produced by GDNNet and TransLab. Averaged over the 60 image sub-dataset.

	IoU	Precision	Recall	F_β	BA	MCC
This study	0.44	0.61	0.68	0.59	0.80	0.56
GDNNet ¹	0.39	0.42	0.91	0.46	0.83	0.51
TransLab ²	0.27	0.36	0.64	0.37	0.70	0.33

¹ GDNNet is introduced in [45].

² TransLab is introduced in [46].

detections, however, this generally effects the slope of the centreline and the detected aspect ratio of the boundary. Hence, these error cases are detected by the algorithm.

The algorithm is designed to be conservative in labelling a measurement as successful to reduce the risk of accident due a false detection. Verification of the detection scenario through the expected aspect ratio was found to be critical in this. Before the check was implemented, there was a large error spike in the results distribution where the algorithm tried to use a non-CWM-boundary line as a CWM-boundary line. Using the check both completely eliminated this error case and enabled obtaining a good measurement from the bad detection.

Another cause of unsuccessful measurement occurred when the image did not contain an entire CWM. The algorithm requires seeing all four boundaries of a CWM; hence, the scenario was left unmeasured in lieu of potentially obtaining a false measurement. For the system to function, the camera should be far enough from the wall that an entire CWM can be viewed in one image-frame. This is dependent on the camera. For example, a camera with a wide-angle lens (100° field of view) can operate up to 1.5m away from a 3.5m tall CWM.

When the measurement system is not in operational range, dead reckoning with an IMU may be used to localise with respect to the most recent measurement. Dead reckoning is appropriate because it is only needed for a short duration, in which the effect of error accumulation is insignificant.

The following subsection proposes a practical implementation of the algorithm which considers these conditions.

4.1. A Practical Implementation of the Measurement System

The proposed implementation places the camera on a below-the-hook-lifting-device (BTHLD); a device that attaches between the crane hook and the CWM. Use of spreader bars, a type of BTHLD, is already common in CWM installation. A BTHLD can be fit to any crane, and the connection/disconnection procedure is fast and simple. Therefore, this makes the system versatile and compatible with existing cranes. By placing the camera on the BTHLD, the camera never needs manual repositioning, the view is never occluded, and the camera is sufficiently close to the building to image it in high resolution.

The proposed BTHLD has three main features. Firstly, it acts as a spreader bar; the ends of the CWM are attached to the ends of the bar. This functions both to bear bending stress, and to ensure that the relative pose between the CWM and the bar remains fixed. The second feature is the measurement camera attached to the bar. Because the relative pose between the bar and CWM is fixed, the value of $\mathbf{T}_{\text{payload}}^{\text{camera}}$ is static and can be derived from its design. Hence, the device only needs to be calibrated once during manufacturing, and can then be operated with few setup requirements.

The camera is fixed to the bar with orientation facing towards the building with respect to the CWMs aligned pose. Hence, the wall is in view of the camera when the skew orientation (angle of rotation of the payload about the hoist rope) is aligned. Therefore, the third feature of the BTHLD is to ensure that the skew orientation is always aligned; the BTHLD implements an active rotary crane hook (also known as a ‘Rotator’ or ‘Power Swivel’ [20, 50, 51, 52, 53, 54]). If the CWM is roughly oriented by the workers on the ground at the moment when the CWM is attached to the device, then the measurement algorithm can be used to measure the skew error. This measurement can then be used by the rotator to actively maintain alignment throughout the whole lift operation. Thus, less manipulation work is required, improving both the safety and speed of the operation [20, 54, 55].

The proposed CWM installation procedure to use this device follows:

1. The device is attached to the crane instead of a conventional spreader bar.
2. A CWM is attached to the device at the ground level, and roughly rotated to face towards the building.
3. The rotator and measurement system are activated to automatically align skew orientation of the CWM to the face of the building and maintain the alignment.
4. The CWM is vertically transported by the crane while held a few metres away from the building.
5. When the CWM is at the target x and y coordinates (Fig. 2), as indicated by the measurement system, it is gently moved towards the building.
6. When within reach, the workers at the installation location take hold of the CWM, manipulate it into alignment, fix it to the attachment brackets, and then release the CWM from the device.

The final step for workers to manually manipulate the CWM into alignment is still required because cranes are unable to apply forces required to push the CWMs together. The benefits of the new method to these workers are improved safety and speed.

The system increases worker safety: In the conventional method the workers must lean out over the edge of the building to manipulate the orientation while the large rotational inertia of the CWM makes their task challenging. The method which uses a rotator improves safety by enabling the pre-alignment of the payload to the installation location mid-lift; thereby reducing the need for the workers to lean out from the building to take hold of the CWM [20, 54, 55]. The method which we propose further increases safety by measuring the alignment, so that the rotator may be driven more accurately and/or autonomously. Enabling pre-alignment also increases the speed of the operation because the adjustments are performed simultaneously to the vertical transportation, instead of after [54, 55].

Safety is additionally increased due to the measurement system providing the crane operator with precise information of the pose of the payload and side face of the building. In the conventional method, the crane operator may be entirely dependent on signalling by the dogman, which is imprecise and susceptible to communication delay [4]. The methodology to place a downward-facing camera at the top of the hoist provides vision to the crane operator, however, the view angle is sharp and distant [9] (Fig. 1d). The method which we propose automatically obtains a precise numeric measurement, which can be communicated to the crane operator.

The measurements should be presented to the crane operator in a clear, intuitive way. The following subsection discusses how the measurement may be presented to the operator.

4.2. Presentation of the measurement to the crane operator

The measurement (1) should be decomposed into information that is directly actionable by the crane operator, without need for further interpretation. The control of the payload position is separate from the control of twist orientation, and swing orientation is not directly controllable. Hence, the measurement is decomposed into the set of position, twist, and swing.

The z component of the position is the distance between the payload and the building, which should be monitored to prevent collision. The x and y components describe the alignment of the payload with the grid of previously installed CWMs. A potentially useful representation of the y measurement is the vertical distance of the payload from alignment with the nearest row of CWMs.

$$y_n := \text{mod}_H\left(y + \frac{H}{2}\right) - \frac{H}{2} \quad (5)$$

This equation finds the residue after rounding to the nearest multiple of H . The modulo operation is analogous to the residue after rounding down, while the addition and subtraction of $\frac{H}{2}$ converts this to the residue from the nearest multiple, with a signed result. Likewise, the x measurement can be represented as the horizontal distance, along the plane of the wall, from the nearest column of CWMs.

$$x_n := \text{mod}_W\left(x + \frac{W}{2}\right) - \frac{W}{2} \quad (6)$$

The orientation can be interpreted through a swing-twist decomposition. The swing-twist decomposition is described by [56, 57]. Given a twist axis, it finds a pair of rotations to first swing towards the twist axis, and then to twist about it, or vice versa. Using the vertical axis as the twist axis, the twist angle describes the skew orientation misalignment, for which the rotator can be used to correct. The swing angle describes the sway angle of the payload, which is applicable to the crane anti-sway control system. The sway angle should be monitored to prevent collision between the payload and the building.

Each of x_n , y_n , z_n , swing, and twist, are labelled in Fig. 2. For simplicity, we define $z_n := z$. However, an alternative representation for z_n could be as the minimum distance between the CWM and the building. This is more directly related to the margin of safety from collision, in case the swing or twist is large.

The measurement may additionally be converted into a homography, which can be applied to the original image to produce a stabilised view for the crane operator. This concept is explored in [21]. In this usage scenario, our measurement system would replace the marker-based system used in [21].

5. Conclusions and Future Work

Measurement of the relative pose between a crane borne CWM and its installation location on the side face of a high-rise building has never before been successfully automated. The large size and unstructured nature of the workspace, combined with the imprecision of construction cranes makes precise global localisation challenging. The strong glare of the sun off the glass wall defeats most markerless proximity sensing techniques. This article introduces an algorithm and a practical implementation of a system to perform this measurement, as well as a dataset to validate the performance in the most challenging lighting conditions.

Markerless computer vision is applied with a forward-facing infrared camera attached to the crane spreader bar. The boundaries of the previously installed CWMs are identified by exploiting the properties of aluminium and architectural glass as viewed in infrared. The known aspect ratio of the CWMs is used to validate the detection. Correspondence between the detected boundary and the known CWM dimensions then results in the measurement.

This algorithm is experimentally validated to function in the presence of strong glare from the sun reflecting off the CWM, and when the sun is directly viewed in the reflection off the glass. For the cases where the algorithm failed to perform a measurement, it successfully recognised this and raised an error instead of returning malformed measurements. The algorithm was designed to fail safely, an important feature in the safety critical task of CWM installation.

In future work, the algorithm and implementation should be trialled at full scale on a construction site. A possible extension to the algorithm may be to fuse the measurements from the algorithm with IMU data to improve pose estimation accuracy. This may also be used to produce an initial pose estimate to feed into the algorithm, against which the boundary detection may be verified (e.g. if the image is preprocessed with a homography, then the detected boundary lines should be near-vertical / near-horizontal).

We also recommend that glass detection algorithms for outdoor use should be evaluated in high-glare lighting conditions. Use of the known CWM aspect ratio to verify measurements is recommended for CWM segmentation systems, as it was found to be an effective method to filter out malformed detections.

Appendix A. The Algorithm

Pseudocode of the measurement algorithm described in Section 2 is Algorithm [A.1](#).

Algorithm A.1: Algorithm to measure the relative pose between a camera and a partially constructed curtain wall.

Type Definitions

Image : 2D array of values

Lines : set of (slope, intercept, value) triads per the definition of the Radon transform

iPoints : set of pixel indices to values in an instance of **Image**

wPoints: set of coordinates as measured in $\mathcal{F}_{\text{wall}}$

Pose : position and orientation of $\mathcal{F}_{\text{camera}}$, as measured in $\mathcal{F}_{\text{wall}}$

1 **Function Measure**

Input

 | C : Camera calibration (intrinsic parameters and distortion coefficients)

 | I : [**Image**] An image taken by the camera

 | W : [**Float**] CWM width in world units

 | H : [**Float**] CWM height in world units

 | H_C : [**Float**] Height from top of CWM to the floor slab above it, in world units

end

2 Use C to undistort I

3 Downsample the result

4 Calculate the entropy local to each pixel

5 Threshold the entropy array into a binary image

6 Perform morphological skeletonization on the result

7 Calculate the Radon transform of the result

8 Find the of local maxima of the Radon transform

9 **Lines** $L_v \leftarrow$ Find the 2 most vertical maxima

10 **Lines** $L_h \leftarrow$ Find the 2 most horizontal maxima

11 Find the 4 coordinates that intersect the lines L_v with the lines L_h

12 Upscale the resulting coordinates to reverse the downsampling

13 **iPoints** $P_i \leftarrow$ Sort the result into {bottom-left, top-left, bottom-right, top-right}

14 **Float** $AR \leftarrow$ Calculate the aspect ratio of the undeformed rectangle

15 **if** $AR \approx W/H$

16 | **Float** $H_R \leftarrow H$

17 **else if** $AR \approx W/H_C$

18 | **Float** $H_R \leftarrow H_C$

19 **else if** $AR \approx W/(H + H_C)$

20 | **Float** $H_R \leftarrow (H + H_C)$

21 **else**

22 | **return** *The camera pose can not be determined*

end

23 **wPoints** $P_w \leftarrow \{(0,0,0), (0,-H_R,0), (W,0,0), (W,-H_R,0)\}$

24 **Pose** $P_c \leftarrow$ Use C to estimate the camera pose, P_c , such that P_i corresponds to P_w

25 **return** P_c , *The camera pose estimate, as measured in $\mathcal{F}_{\text{wall}}$*

end

Appendix B. Supplementary Results

Fig. B.7 depicts the experimental setup as viewed by the red channel of the camera used in the experiments, as compared to a true NIR camera. The reflections in the NIR image are sharper than in the red image, otherwise, the images are very similar. We use this comparison to justify that the experimental procedure produced a close approximation of an NIR image.

Fig. B.8 presents a visualisation of the results Table 1.



Figure B.7: Comparison of the experimental model as viewed by the red channel of an RGB camera (left), and by a NIR camera (right), with equivalent exposure settings.

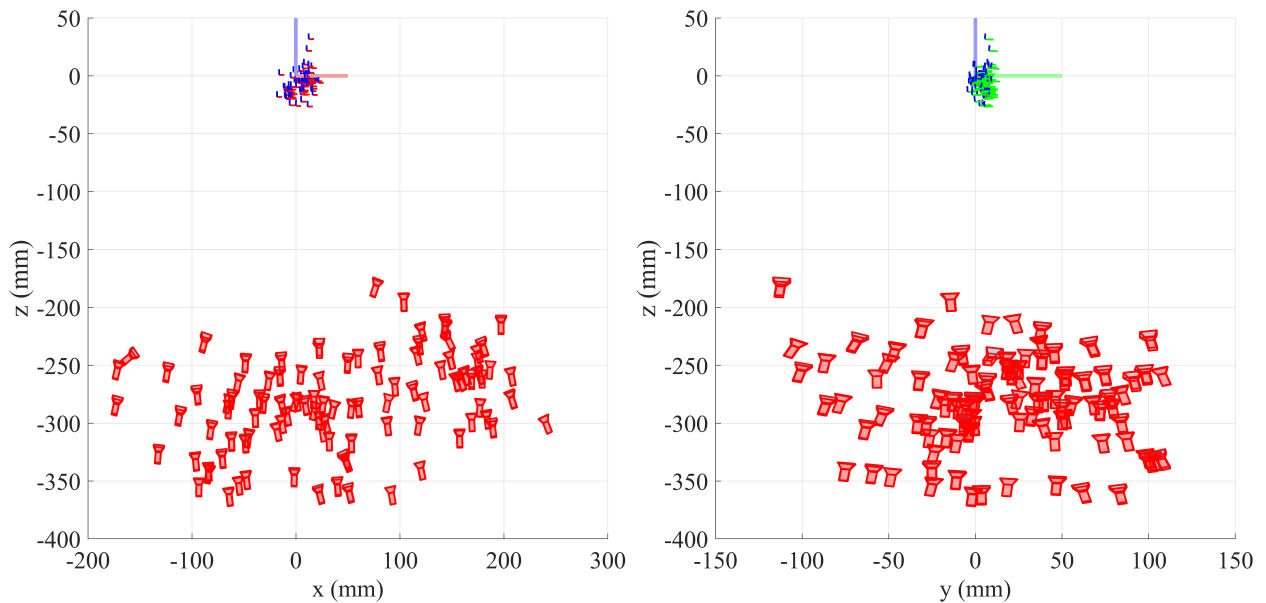


Figure B.8: Visualisation of the experimental results using the coordinate systems in Fig. 2. The large axis at $(0,0,0)$ is the installation location according to the motion capture. The camera symbols are the camera locations. The small axes are the measurements of the installation location.

References

- [1] S. Xu, J. Wang, W. Shou, T. Ngo, A.-M. Sadick, X. Wang, Computer vision techniques in construction: A critical review, *Archives of Computational Methods in Engineering* 28 (5) (2021) 3383–3397. doi:10.1007/s11831-020-09504-3.
- [2] Y. Zhang, W. Qiu, Q. Chen, X. Hu, A. Yuille, Unrealstereo: Controlling hazardous factors to analyze stereo vision, in: *2018 International Conference on 3D Vision (3DV)*, 2018, pp. 228–237. doi:10.1109/3DV.2018.00035.
- [3] M. Taghavi, K. Iturralde, T. Bock, Cable-driven parallel robot for curtain wall modules automatic installation, in: *Proceedings of the 35th International Symposium on Automation and Robotics in Construction (ISARC2018)*, 2018, pp. 396–403. doi:10.22260/ISARC2018/0056.
- [4] Details omitted for double-anonymized reviewing (a). (2023).
- [5] S. N. Yu, S. Y. Lee, C. S. Han, K. Y. Lee, S. H. Lee, Development of the curtain wall installation robot: Performance and efficiency tests at a construction site, *Autonomous Robots* 22 (3) (2007) 281–291. doi:10.1007/s10514-006-9019-2.
- [6] F. Friblick, I. D. Tommelein, E. Mueller, J. H. Falk, Development of an integrated facade system to improve the high-rise building process, in: *17th Annual Conference of the International Group for Lean Construction*, 2009, pp. 359–370.
- [7] S. D. Choi, L. Guo, J. Kim, S. Xiong, Comparison of fatal occupational injuries in construction industry in the united states, south korea, and china, *International Journal of Industrial Ergonomics* 71 (2019) 64–74. doi:10.1016/j.ergon.2019.02.011.
- [8] E. Gharaie, H. Lingard, T. Cooke, Causes of fatal accidents involving cranes in the australian construction industry, *Construction Economics and Building* 15 (2) (2015) 1–12. doi:10.5130/AJCEB.v15i2.4244.
- [9] A. Shapira, Y. Rosenfeld, I. Mizrahi, Vision system for tower cranes, *Journal of Construction Engineering and Management* 134 (5) (2008) 320–332. doi:10.1061/(ASCE)0733-9364(2008)134:5(320).
- [10] *Workplace Health and Safety Queensland, A guide for doggers* (2010).
- [11] Y. Fang, Y. K. Cho, F. Durso, J. Seo, Assessment of operator’s situation awareness for smart operation of mobile cranes, *Automation in Construction* 85 (2018) 65–75. doi:10.1016/j.autcon.2017.10.007.
- [12] G. Lee, J. Cho, S. Ham, T. Lee, G. Lee, S.-H. Yun, H.-J. Yang, A bim- and sensor-based tower crane navigation system for blind lifts, *Automation in Construction* 26 (2012) 1–10. doi:10.1016/j.autcon.2012.05.002.
- [13] M. Chatzimichailidou, Y. Ma, Using bim in the safety risk management of modular construction, *Safety Science* 154 (2022) 105852. doi:10.1016/j.ssci.2022.105852.
- [14] Y. Fang, J. Chen, Y. K. Cho, K. Kim, S. Zhang, E. Perez, Vision-based load sway monitoring to improve crane safety in blind lifts, *Journal of Structural Integrity and Maintenance* 3 (4) (2018) 233–242. doi:10.1080/24705314.2018.1531348.
- [15] G. Lee, H.-H. Kim, C.-J. Lee, S.-I. Ham, S.-H. Yun, H. Cho, B. K. Kim, G. T. Kim, K. Kim, A laser-technology-based lifting-path tracking system for a robotic tower crane, *Automation in Construction* 18 (7) (2009) 865–874. doi:10.1016/j.autcon.2009.03.011.
- [16] M. Zhang, S. Ge, Vision and trajectory-based dynamic collision prewarning mechanism for tower cranes, *Journal of Construction Engineering and Management* 148 (7) (2022) 04022057. doi:10.1061/(ASCE)CE.1943-7862.0002309.
- [17] L. C. Price, J. Chen, J. Park, Y. K. Cho, Multisensor-driven real-time crane monitoring system for blind lift operations: Lessons learned from a case study, *Automation in Construction* 124 (2021) 103552. doi:10.1016/j.autcon.2021.103552.
- [18] L. Ramli, Z. Mohamed, A. M. Abdullahi, H. I. Jaafar, I. M. Lazim, Control strategies for crane systems: A comprehensive review, *Mechanical Systems and Signal Processing* 95 (2017) 1–23. doi:10.1016/j.ymsp.2017.03.015.
- [19] J. Ye, J. Huang, Analytical analysis and oscillation control of payload twisting dynamics in a tower crane carrying a slender payload, *Mechanical Systems and Signal Processing* 158 (2021) 107763. doi:10.1016/j.ymsp.2021.107763.
- [20] C.-J. Liang, S.-C. Kang, M.-H. Lee, Ras: a robotic assembly system for steel structure erection and assembly, *International Journal of Intelligent Robotics and Applications* 1 (4) (2017) 459–476. doi:10.1007/s41315-017-0030-x.
- [21] Details omitted for double-anonymized reviewing (b). (2023).
- [22] K. Iturralde, M. Feucht, D. Illner, R. Hu, W. Pan, T. Linner, T. Bock, I. Eskudero, M. Rodriguez, J. Gorrotxategi, J. Izard, J. Astudillo, J. Cavalcanti Santos, M. Gouttefarde, M. Fabritius, C. Martin, T. Henninge, S. Nornes, Y. Jacobsen, A. Pracucci, J. Cañada, J. Jimenez-Vicaria, R. Alonso, L. Elia, Cable-

- driven parallel robot for curtain wall module installation, *Automation in Construction* 138 (2022) 104235. doi:10.1016/j.autcon.2022.104235.
- [23] P. Hyla, Night vision applicability in anti-sway vision-based solutions, in: 2015 20th International Conference on Methods and Models in Automation and Robotics (MMAR), 2015, pp. 358–363. doi:10.1109/MMAR.2015.7283902.
- [24] G. O. Tysse, A. Cibicik, O. Egeland, Vision-based control of a knuckle boom crane with online cable length estimation, *IEEE/ASME Transactions on Mechatronics* 26 (1) (2021) 416–426. doi:10.1109/TMECH.2020.3024637.
- [25] R. Gutiérrez, M. Magallón, D. C. Hernández, Vision-based system for 3d tower crane monitoring, *IEEE Sensors Journal* 21 (10) (2021) 11935–11945. doi:10.1109/JSEN.2020.3042532.
- [26] Q. Wu, X. Wang, L. Hua, G. Wei, The real-time vision measurement of multi-information of the bridge crane’s workspace and its application, *Measurement* 151 (2020) 107207. doi:10.1016/j.measurement.2019.107207.
- [27] Y. Diao, W. Cheng, R. Du, Y. Wang, J. Zhang, Vision-based detection of container lock holes using a modified local sliding window method, *EURASIP Journal on Image and Video Processing* 2019 (1) (2019) 69. doi:10.1186/s13640-019-0472-1.
- [28] L. C. Price, J. Chen, Y. K. Cho, Dynamic crane workspace update for collision avoidance during blind lift operations, in: E. Toledo Santos, S. Scheer (Eds.), *Proceedings of the 18th International Conference on Computing in Civil and Building Engineering*, Springer International Publishing, 2021, pp. 959–970. doi:10.1007/978-3-030-51295-8_66.
- [29] H. Zhang, Y. Jin, Q. Liu, Y. Zhao, Q. Gao, Intelligent monitoring method for tamping times during dynamic compaction construction using machine vision and pattern recognition, *Measurement* 193 (2022) 110835. doi:10.1016/j.measurement.2022.110835.
- [30] M. Vega-Heredia, I. Muhammad, S. Ghanta, V. Ayyalusami, S. Aisyah, M. R. Elara, Multi-sensor orientation tracking for a façade-cleaning robot, *Sensors* 20 (5) (2020) 1483. doi:10.3390/s20051483.
- [31] H. Li, X. Duan, Y. Zhan, L. Gao, A handle inspection device for curtain wall installation based on structured laser, in: 2016 IEEE International Conference on Mechatronics and Automation, 2016, pp. 1623–1628. doi:10.1109/ICMA.2016.7558807.
- [32] S. Sasaki, S. Hatakeyama, M. Iwase, S. Nansai, Construction of SLAM algorithm for window cleaning robot moving along window frame, *Journal of Physics: Conference Series* 1487 (2020) 012023. doi:10.1088/1742-6596/1487/1/012023.
- [33] E. Yamaguchi, H. Higuchi, A. Yamashita, H. Asama, Glass detection using polarization camera and lrf for slam in environment with glass, in: 2020 21st International Conference on Research and Education in Mechatronics (REM), 2020, pp. 1–6. doi:10.1109/REM49740.2020.9313933.
- [34] X. Zhao, Z. Yang, S. Schwertfeger, Mapping with reflection - detection and utilization of reflection in 3d lidar scans, in: 2020 IEEE International Symposium on Safety, Security, and Rescue Robotics (SSRR), 2020, pp. 27–33. doi:10.1109/SSRR50563.2020.9292595.
- [35] H. Wei, X. Li, Y. Shi, B. You, Y. Xu, Multi-sensor fusion glass detection for robot navigation and mapping, in: 2018 WRC Symposium on Advanced Robotics and Automation (WRC SARA), 2018, pp. 184–188. doi:10.1109/WRC-SARA.2018.8584213.
- [36] X. Wang, J. Wang, Detecting glass in simultaneous localisation and mapping, *Robotics and Autonomous Systems* 88 (2017) 97–103. doi:10.1016/j.robot.2016.11.003.
- [37] I. Jeong, J. Hwang, J. Kim, S. Chi, B.-G. Hwang, J. Kim, Vision-based productivity monitoring of tower crane operations during curtain wall installation using a database-free approach, *Journal of Computing in Civil Engineering* 37 (4) (2023) 04023015. doi:10.1061/JCCEE5.CPENG-5105.
- [38] L. Shen, H. Tao, Y. Ni, Y. Wang, V. Stojanovic, Improved yolov3 model with feature map cropping for multi-scale road object detection, *Measurement Science and Technology* 34 (4) (2023) 045406. doi:10.1088/1361-6501/acb075.
- [39] G. Zhang, Y. Pan, L. Zhang, Deep learning for detecting building façade elements from images considering prior knowledge, *Automation in Construction* 133 (2022) 104016. doi:10.1016/j.autcon.2021.104016.
- [40] Z. Mao, X. Huang, Y. Gong, H. Xiang, F. Zhang, A dataset and ensemble model for glass façade segmentation in oblique aerial images, *IEEE Geoscience and Remote Sensing Letters* 19 (2022) 1–5. doi:10.1109/LGRS.2022.3187760.
- [41] R. Gadde, V. Jampani, R. Marlet, P. V. Gehler, Efficient 2d and 3d facade segmentation using auto-context, *IEEE Transactions on Pattern Analysis and Machine Intelligence* 40 (5) (2018) 1273–1280. doi:10.1109/TPAMI.2017.2696526.
- [42] Y. Sun, S. Malihi, H. Li, M. Maboudi, Deepwindows: Windows instance segmentation through an improved

- mask r-cnn using spatial attention and relation modules, *ISPRS International Journal of Geo-Information* 11 (3) (2022). doi:10.3390/ijgi11030162.
- [43] J. Qu, J. Song, J. Qin, Z. Song, W. Zhang, Y. Shi, T. Zhang, H. Zhang, R. Zhang, Z. He, X. Xue, Transparent thermal insulation coatings for energy efficient glass windows and curtain walls, *Energy and Buildings* 77 (2014) 1–10. doi:10.1016/j.enbuild.2014.03.032.
- [44] Details omitted for double-anonymized reviewing (c). (2023).
- [45] H. Mei, X. Yang, Y. Wang, Y. Liu, S. He, Q. Zhang, X. Wei, R. W. Lau, Don't hit me! glass detection in real-world scenes, in: 2020 IEEE/CVF Conference on Computer Vision and Pattern Recognition (CVPR), 2020, pp. 3684–3693. doi:10.1109/CVPR42600.2020.00374.
- [46] E. Xie, W. Wang, W. Wang, M. Ding, C. Shen, P. Luo, Segmenting transparent objects in the wild, in: *Computer Vision – ECCV 2020*, Springer International Publishing, 2020, pp. 696–711. doi:10.1007/978-3-030-58601-0_41.
- [47] Z. Zhang, L.-W. He, Whiteboard scanning and image enhancement, *Digital Signal Processing* 17 (2) (2007) 414–432. doi:10.1016/j.dsp.2006.05.006.
- [48] F. L. Markley, Y. Cheng, J. L. Crassidis, Y. Oshman, Averaging quaternions, *Journal of Guidance, Control, and Dynamics* 30 (4) (2007) 1193–1197. doi:10.2514/1.28949.
- [49] D. Chicco, Ten quick tips for machine learning in computational biology, *BioData Mining* 10 (1) (2017) 35. doi:10.1186/s13040-017-0155-3.
- [50] T. Ho, K. Suzuki, M. Tsume, R. Tasaki, T. Miyoshi, K. Terashima, A switched optimal control approach to reduce transferring time, energy consumption, and residual vibration of payload's skew rotation in crane systems, *Control Engineering Practice* 84 (2019) 247–260. doi:10.1016/j.conengprac.2018.11.018.
- [51] U. Schaper, C. Dittrich, E. Arnold, K. Schneider, O. Sawodny, 2-dof skew control of boom cranes including state estimation and reference trajectory generation, *Control Engineering Practice* 33 (2014) 63–75. doi:10.1016/j.conengprac.2014.09.009.
- [52] Liebherr, Liebherr port cranes fcc and tcc (2011).
- [53] A. Cibicik, T. A. Myhre, O. Egeland, Modeling and control of a bifilar crane payload, in: 2018 Annual American Control Conference (ACC), 2018, pp. 1305–1312. doi:10.23919/ACC.2018.8431375.
- [54] F. Inoue, K. Wiuanabe, Y. Ikeda, T. Wakisaka, A. Wakabayashi, Y. Nekomoto, A practical development of the suspender device that controls load rotation by gyroscopic moments, in: *Proceedings of the 14th International Symposium on Automation and Robotics in Construction (ISARC)*, 1997, pp. 486–495. doi:10.22260/ISARC1998/0036.
- [55] C. Lee, G. Lee, S. Park, J. Cho, Analysis of field applicability of the rotation-controllable tower-crane hook block, *Automation in Construction* 21 (2012) 81–88. doi:10.1016/j.autcon.2011.05.015.
- [56] B. Huyghe, Design and implementation of a mobile sensor system for human posture tracking, Ph.D. thesis, Ghent University (2011).
- [57] P. Dobrowolski, Swing-twist decomposition in clifford algebra, *CoRR* abs/1506.05481 (2015). doi:10.48550/arXiv.1506.05481.

4.2 Outlook

The outcomes of this work are directly applicable to the CWM mid-air alignment task. The proposed implementation follows the outcomes of Chapter 3, circumventing the limitations of global crane payload localisation by directly measuring the relative pose. The use of a BTHLD follows the recommendations in Chapter 2, and the crane borne CWM can be locked to the BTHLD as recommended in Chapter 3.

5 Conclusions and Outlook

Building with unitised curtain walls affords strict quality control and facilitates the integration of high precision and complex features into the building envelope. However, the on-site installation task to align CWMs to the outer face of the building is difficult. The conventional direct methodologies require workers to reach outwards past the open edge of the building to take hold of the free-swinging crane-borne CWM, so that they can manipulate it into alignment. The workers risk being struck, crushed, or falling from a height.

The safety and efficiency of this procedure can be improved with a system to align the crane borne CWM before workers have to physically interact with it. However, the location and orientation of the crane payload is difficult to monitor and control. Improved crane payload localisation is required to make mechanised and automated mid-air alignment viable.

This thesis contributes to developing the core processes and technologies that are required to make automated localisation of the crane borne CWM viable. The key contributions are:

- Identification of the barriers and opportunities to increasing the level of automation in CWM installation. The opportunities include using a BTHLD for control, using a hook-mounted camera for sensing, and strengthening the communication between the crane operator and dogman by providing them with rich localisation information.
- A guideline for system designers to choose the optimal dynamical models to represent the boom tower cranes that are commonly deployed on construction sites. Use of an accurate model facilitates precise control and state estimation.
- An algorithm and methodology to measure the pose of a crane borne CWM, as relative to its installation location on the side face of a high-rise building. This localisation may be used by automated alignment systems, or presented to the crane operator and dogman.
- A practical framework for incorporating these advancements into the conventional direct CWM installation methodologies.

The outcomes of this work are directly applicable to the CWM mid-air alignment task:

- In Chapter 3, it is found that crane control systems alone can not feasibly achieve the required precision in payload localisation and control, that manual handling might be eliminated. It is also found that the system dynamics can be simplified through mechanically locking the CWM, BTHLD, and crane hook together. Thus, the system would become easier to precisely control.
- In Chapter 4, the algorithm makes use of the thermally insulative properties of CWM coatings to robustly localise the crane borne CWM to its installation location. The proposed implementation then follows the prior outcomes to ensure practicality and likelihood of adoption.

Future work is recommended to further develop, trial, and commercialise the proposed devices and user interfaces. Specific directions for future work are:

- To systematically review and compare the rotary boom crane dynamical models that include complex geometry, wind, frictional damping, and elasticity of the hoist rope, tower, and boom.
- To expand the investigation in Chapter 3 to more types of crane.
- To extend the algorithm (Chapter 4) with IMU data and use inter-frame correspondence to improve the pose estimation accuracy.
- To develop user interfaces to communicate the results of the algorithm (Chapter 4) to the crane operator and dogman.

Bibliography

- [1] Brandon Johns, Elahe Abdi and Mehrdad Arashpour. 'Dynamical modelling of boom tower crane rigging systems: model selection for construction'. In: *Archives of Civil and Mechanical Engineering* 23.3 (2023), p. 162. DOI: [10.1007/s43452-023-00702-x](https://doi.org/10.1007/s43452-023-00702-x).
- [2] Brandon Johns, Elahe Abdi and Mehrdad Arashpour. 'Crane payload localisation for curtain wall installation: A markerless computer vision approach'. In: *Measurement* (2023). (In press), p. 113459. DOI: [10.1016/j.measurement.2023.113459](https://doi.org/10.1016/j.measurement.2023.113459).
- [3] Brandon Johns, Mehrdad Arashpour and Elahe Abdi. 'Curtain Wall Installation for High-Rise Buildings: Critical Review of Current Automation Solutions and Opportunities'. In: *Proceedings of the 37th International Symposium on Automation and Robotics in Construction (ISARC)*. 2020, pp. 393–400. DOI: [10.22260/ISARC2020/0056](https://doi.org/10.22260/ISARC2020/0056).
- [4] Kerry He, Brandon Johns, Elahe Abdi and Mehrdad Arashpour. 'Camera View from Crane Payload: Video Stabilization'. In: *Australasian Conference on Robotics and Automation, ACRA*. 2021. URL: https://ssl.linklings.net/conferences/acra/acra2021_proceedings/views/includes/files/pap104s2-file1.pdf.
- [5] Brandon Johns, Elahe Abdi and Mehrdad Arashpour. *Glass Curtain Wall Installation Dataset*. 2023. DOI: [10.26180/23538198](https://doi.org/10.26180/23538198).
- [6] Trevor C. Pavitt. 'Managing construction interfaces within the building facade'. PhD thesis. Loughborough University, 2002. URL: https://repository.lboro.ac.uk/articles/thesis/Managing_construction_interfaces_within_the_building_facade/9455153.
- [7] Thomas Bock. 'The future of construction automation: Technological disruption and the upcoming ubiquity of robotics'. In: *Automation in Construction* 59 (2015), pp. 113–121. DOI: [10.1016/j.autcon.2015.07.022](https://doi.org/10.1016/j.autcon.2015.07.022).
- [8] Fredrik Friblick, Iris D. Tommelein, Edith Mueller and Jon Henrik Falk. 'Development of an Integrated Facade System to Improve the High-Rise Building Process'. In: *17th Annual Conference of the International Group for Lean Construction*. 2009, pp. 359–370. URL: <http://iglc.net/Papers/Details/636>.
- [9] Iris D Tommelein and Greg Beeche. 'De-Coupling Cladding Installation From Other High-Rise Building Trades: A Case Study'. In: *Proceedings of the 9th Annual Conference International Group for Lean Construction, Singapore*. 2001. URL: <https://iglc.net/Papers/Details/159>.

- [10] Henrik Falk, Henrik Andersson, Fredrik Friblick and M. J. Mul. 'A Novel Facade System to Improve the Whole High-Rise Building Process'. In: *CTBUH 2016*. 2016, pp. 1077–1086. URL: <http://www.brunkeberg.com/docs>.
- [11] Meysam Taghavi, Kepa Iturralde and Thomas Bock. 'Cable-driven parallel robot for curtain wall modules automatic installation'. In: *Proceedings of the 35th International Symposium on Automation and Robotics in Construction (ISARC2018)*. 2018, pp. 396–403. DOI: [10.22260/ISARC2018/0056](https://doi.org/10.22260/ISARC2018/0056).
- [12] Frans Van Gassel, Pascal Schrijver and Jos Lichtenberg. 'Assembling wall panels with robotic technologies'. In: *The 23rd International Symposium on Automation and Robotics in Construction Japan (ISARC)*. 2006, pp. 728–733. DOI: [10.22260/ISARC2006/0135](https://doi.org/10.22260/ISARC2006/0135).
- [13] Seung Nam Yu, Seung Yeol Lee, Chang Soo Han, Kye Young Lee and Sang Heon Lee. 'Development of the curtain wall installation robot: Performance and efficiency tests at a construction site'. In: *Autonomous Robots* 22.3 (2007), pp. 281–291. DOI: [10.1007/s10514-006-9019-2](https://doi.org/10.1007/s10514-006-9019-2).
- [14] Sang D. Choi, Liangjie Guo, Jaehoon Kim and Shuping Xiong. 'Comparison of fatal occupational injuries in construction industry in the United States, South Korea, and China'. In: *International Journal of Industrial Ergonomics* 71 (2019), pp. 64–74. DOI: [10.1016/j.ergon.2019.02.011](https://doi.org/10.1016/j.ergon.2019.02.011).
- [15] Ehsan Gharaie, Helen Lingard and Tracy Cooke. 'Causes of fatal accidents involving cranes in the Australian construction industry'. In: *Construction Economics and Building* 15.2 (2015), pp. 1–12. DOI: [10.5130/AJCEB.v15i2.4244](https://doi.org/10.5130/AJCEB.v15i2.4244).
- [16] M Taghavi, T Kinoshita and T Bock. 'Design, Modelling and Simulation of Novel Hexapod-Shaped Passive Damping System for Coupling Cable Robot and End Effector in Curtain Wall Module Installation Application'. In: *Proceedings of the 36th International Symposium on Automation and Robotics in Construction (ISARC)*. Vol. 36. IAARC Publications. 2019, pp. 665–671. DOI: [10.22260/ISARC2019/0089](https://doi.org/10.22260/ISARC2019/0089).
- [17] Fumihiko Inoue, Kouji Wiuanabe, Yuichi Ikeda, Tatuya Wakisaka, Akira Wakabayashi and Yoshitsugu Nekomoto. 'A Practical Development of the Suspender Device that Controls Load Rotation by Gyroscopic Moments'. In: *Proceedings of the 14th International Symposium on Automation and Robotics in Construction (ISARC)*. 1997, pp. 486–495. DOI: [10.22260/ISARC1998/0036](https://doi.org/10.22260/ISARC1998/0036).
- [18] Yihai Fang, Yong K. Cho, Frank Durso and Jongwon Seo. 'Assessment of operator's situation awareness for smart operation of mobile cranes'. In: *Automation in Construction* 85 (2018), pp. 65–75. DOI: [10.1016/j.autcon.2017.10.007](https://doi.org/10.1016/j.autcon.2017.10.007).
- [19] Liyana Ramli, Z. Mohamed, Auwalu M. Abdullahi, H. I. Jaafar and Izzuddin M. Lazim. 'Control strategies for crane systems: A comprehensive review'. In: *Mechanical Systems and Signal Processing* 95 (2017), pp. 1–23. DOI: [10.1016/j.ymsp.2017.03.015](https://doi.org/10.1016/j.ymsp.2017.03.015).

- [20] National Institute of Building Sciences. *Building Envelope Design Guide*. 2021. URL: <https://www.wbdg.org/guides-specifications/building-envelope-design-guide> (visited on 28/07/2023).
- [21] Wen Pan, Thomas Bock, Thomas Linner and Kepa Iturralde. 'Development of a fast and effective solution for on-site building envelope installation'. In: *Proceedings of the 33rd International Symposium on Automation and Robotics in Construction (ISARC2016)*. 2016. DOI: [10.22260/ISARC2016/0097](https://doi.org/10.22260/ISARC2016/0097).
- [22] Chang Soo Han, Seung Yeol Lee, Kye Young Lee and Bum Seok Park. 'A multidegree-of-freedom manipulator for curtain-wall installation'. In: *Journal of Field Robotics* 23.5 (2006), pp. 347–360. DOI: [10.1002/rob.20122](https://doi.org/10.1002/rob.20122).
- [23] Seungyeol Lee and Jeon Il Moon. 'Case studies on glazing robot technology on construction sites'. In: *Proceedings of the 32nd International Symposium on Automation and Robotics in Construction (ISARC)*. Vol. 32. IAARC Publications, 2015, p. 1. DOI: [10.22260/ISARC2015/0077](https://doi.org/10.22260/ISARC2015/0077).
- [24] Kepa Iturralde, Thomas Linner and Thomas Bock. 'Development and preliminary Evaluation of a concept for a Modular End-Effector for automated/robotic Facade Panel Installation in Building Renovation'. In: *Proceedings of the 10th Conference on Advanced Building Skins*. 2015. URL: <https://mediatum.ub.tum.de/1484214>.
- [25] Workplace Health and Safety Queensland. *A Guide for doggers*. Pamphlet. 2010. URL: <https://www.worksafeconnect.com/guide-for-doggers.pdf>.
- [26] Aviad Shapira, Yehiel Rosenfeld and Israel Mizrahi. 'Vision System for Tower Cranes'. In: *Journal of Construction Engineering and Management* 134.5 (2008), pp. 320–332. DOI: [10.1061/\(ASCE\)0733-9364\(2008\)134:5\(320\)](https://doi.org/10.1061/(ASCE)0733-9364(2008)134:5(320)).
- [27] K Iturralde, T Linner and T Bock. 'Comparison of Automated and Robotic Support Bodies for Building Facade Upgrading'. In: *Proceedings of the 32nd International Symposium on Automation and Robotics in Construction and Mining (ISARC2015)*. 2015. DOI: [10.22260/ISARC2015/0078](https://doi.org/10.22260/ISARC2015/0078).
- [28] Meysam Taghavi, Homero Heredia, Kepa Iturralde, Håvard Halvorsen and Thomas Bock. 'Development of a Modular End Effector for the installation of Curtain Walls with cable-robots'. In: *Journal of Facade Design and Engineering* 6.2 (2018), pp. 001–008. DOI: [10.7480/jfde.2018.2.2067](https://doi.org/10.7480/jfde.2018.2.2067).

- [29] Kepa Iturralde, Malte Feucht, Rongbo Hu, Wen Pan, Marcel Schlandt, Thomas Linner, Thomas Bock, Jean-Baptiste Izard, Ibon Eskudero, Mariola Rodriguez, Jose Gorrotxategi, Julen Astudillo, Joao Cavalcanti, Marc Gouttefarde, Marc Fabritius, Christoph Martin, Tomas Henninge, Stein Normes, Yngve Jacobsen, A. Pracucci, Jesús Cañada, José David Jimenez-Vicaria, Carlo Paulotto, Rubén Alonso and Lorenzo Elia. 'A Cable Driven Parallel Robot with a Modular End Effector for the Installation of Curtain Wall Modules'. In: *Proceedings of the 37th International Symposium on Automation and Robotics in Construction (ISARC)*. 2020, pp. 1472–1479. DOI: [10.22260/ISARC2020/0204](https://doi.org/10.22260/ISARC2020/0204).
- [30] K. Iturralde, M. Feucht, D. Illner, R. Hu, W. Pan, T. Linner, T. Bock, I. Eskudero, M. Rodriguez, J. Gorrotxategi, J.B. Izard, J. Astudillo, J. Cavalcanti Santos, M. Gouttefarde, M. Fabritius, C. Martin, T. Henninge, S.M. Nornes, Y. Jacobsen, A. Pracucci, J. Cañada, J.D. Jimenez-Vicaria, R. Alonso and L. Elia. 'Cable-driven parallel robot for curtain wall module installation'. In: *Automation in Construction* 138 (2022), p. 104235. DOI: [10.1016/j.autcon.2022.104235](https://doi.org/10.1016/j.autcon.2022.104235).
- [31] Kyoungmo Jung, Baeksuk Chu and Daehie Hong. 'Robot-based construction automation: An application to steel beam assembly (Part II)'. In: *Automation in Construction* 32 (2013), pp. 62–79. DOI: [10.1016/j.autcon.2012.12.011](https://doi.org/10.1016/j.autcon.2012.12.011).
- [32] Yong Liang, Zhiyan Che, Xinyou Chen and Cipei Liu. 'Total Assembly Construction Technology of Ultra-long Variable Cross-section Spiral Aluminum Plate Unit of Qingdao Citizen Fitness Center Sports Stadium'. In: *Engineering and Applied Sciences* 4.5 (2019), p. 98. DOI: [10.11648/j.eas.20190405.12](https://doi.org/10.11648/j.eas.20190405.12).
- [33] Shiyao Cai, Zhiliang Ma, Miroslaw J. Skibniewski and Song Bao. 'Construction automation and robotics for high-rise buildings over the past decades: A comprehensive review'. In: *Advanced Engineering Informatics* 42 (2019), p. 100989. DOI: [10.1016/j.aei.2019.100989](https://doi.org/10.1016/j.aei.2019.100989).
- [34] A. Arena, A. Casalotti, W. Lacarbonara and M. P. Cartmell. 'Dynamics of container cranes: three-dimensional modeling, full-scale experiments, and identification'. In: *International Journal of Mechanical Sciences* 93 (2015), pp. 8–21. DOI: [10.1016/j.ijmecsci.2014.11.024](https://doi.org/10.1016/j.ijmecsci.2014.11.024).
- [35] Tho Ho, Kensuke Suzuki, Mitsuo Tsume, Ryosuke Tasaki, Takanori Miyoshi and Kazuhiko Terashima. 'A switched optimal control approach to reduce transferring time, energy consumption, and residual vibration of payload's skew rotation in crane systems'. In: *Control Engineering Practice* 84 (2019), pp. 247–260. DOI: [10.1016/j.conengprac.2018.11.018](https://doi.org/10.1016/j.conengprac.2018.11.018).
- [36] Richard F Wehrli and Joseph Gallione. 'Method and Apparatus for Vertically Orienting Precast Concrete Wall Panels'. WO2011028879A1. 2011. URL: <https://patents.google.com/patent/WO2011028879A1/en>.

- [37] Ulf Schaper, Christina Dittrich, Eckhard Arnold, Klaus Schneider and Oliver Sawodny. '2-DOF skew control of boom cranes including state estimation and reference trajectory generation'. In: *Control Engineering Practice* 33 (2014), pp. 63–75. DOI: [10.1016/j.conengprac.2014.09.009](https://doi.org/10.1016/j.conengprac.2014.09.009).
- [38] Ci-Jyun Liang, Shih-Chung Kang and Meng-Hsueh Lee. 'RAS: a robotic assembly system for steel structure erection and assembly'. In: *International Journal of Intelligent Robotics and Applications* 1.4 (2017), pp. 459–476. DOI: [10.1007/s41315-017-0030-x](https://doi.org/10.1007/s41315-017-0030-x).
- [39] Masaomi WADA, Yoshihito MORI and Yasutaka TAGAWA. 'Development of a suspended-load rotation-control device for cranes with gyroscopic damper and control by wind force (concept, modeling and experiments)'. In: *Mechanical Engineering Journal* 7.5 (2020), p. 2000268. DOI: [10.1299/mej.20-00268](https://doi.org/10.1299/mej.20-00268).
- [40] Chijoo Lee, Ghang Lee, Suyeul Park and Joonbeom Cho. 'Analysis of field applicability of the rotation-controllable tower-crane hook block'. In: *Automation in Construction* 21 (2012), pp. 81–88. DOI: [10.1016/j.autcon.2011.05.015](https://doi.org/10.1016/j.autcon.2011.05.015).
- [41] Liebherr. *Liebherr Port Cranes FCC and TCC*. Pamphlet. 2011. URL: <https://www.liebherr.com/external/products/products-assets/240861/liebherr-sc-fcc-tcc-brochure-overview.pdf>.
- [42] A. Cibicik, T. A. Myhre and O. Egeland. 'Modeling and Control of a Bifilar Crane Payload'. In: *2018 Annual American Control Conference (ACC)*. 2018, pp. 1305–1312. DOI: [10.23919/ACC.2018.8431375](https://doi.org/10.23919/ACC.2018.8431375).
- [43] Jung Kyungmo, Kim Dongnam, Bae Kihyun, Hong Daehie, Park Shinsuk and Lim Myo-Taeg. 'Pre-acting manipulator for shock isolation in steel construction'. In: *2007 International Conference on Control, Automation and Systems*. 2007, pp. 1203–1208. DOI: [10.1109/ICCAS.2007.4406517](https://doi.org/10.1109/ICCAS.2007.4406517).
- [44] Il Gary Michael Hatton. 'Fly jib for a crane and method of use'. US8979148B1. 2015. URL: <https://patents.google.com/patent/US8979148B1/en>.
- [45] Ghang Lee, Joonbeom Cho, Sungil Ham, Taekwan Lee, Gaang Lee, Seok-Heon Yun and Hyung-Jun Yang. 'A BIM- and sensor-based tower crane navigation system for blind lifts'. In: *Automation in Construction* 26 (2012), pp. 1–10. DOI: [10.1016/j.autcon.2012.05.002](https://doi.org/10.1016/j.autcon.2012.05.002).
- [46] Yu Wang, Hiromasa Suzuki, Yutaka Ohtake, Takayuki Kosaka and Shinji Noguchi. 'Generating a visual map of the crane workspace using top-view cameras for assisting operation'. In: *Proceedings of the Creative Construction Conference (CCC2018)*. 2018. DOI: [10.20965/jrm.2020.p0409](https://doi.org/10.20965/jrm.2020.p0409).
- [47] Beau Domingue and Joshua Vaughan. 'Crane Workspace Mapping via a Scanning Laser Rangefinder'. In: *ASME 2015 International Mechanical Engineering Congress and Exposition*. Vol. 4A. 2015. DOI: [10.1115/imece2015-52194](https://doi.org/10.1115/imece2015-52194).

- [48] Yihai Fang, Jingdao Chen, Yong K Cho, Kinam Kim, Sijie Zhang and Esau Perez. 'Vision-based load sway monitoring to improve crane safety in blind lifts'. In: *Journal of Structural Integrity and Maintenance* 3.4 (2018), pp. 233–242. DOI: [10.1080/24705314.2018.1531348](https://doi.org/10.1080/24705314.2018.1531348).
- [49] Baeksuk Chu, Kyoungmo Jung, Myo-Taeg Lim and Daehie Hong. 'Robot-based construction automation: An application to steel beam assembly (Part I)'. In: *Automation in Construction* 32 (2013), pp. 46–61. DOI: [10.1016/j.autcon.2012.12.016](https://doi.org/10.1016/j.autcon.2012.12.016).
- [50] Mikela Chatzimichailidou and Yue Ma. 'Using BIM in the safety risk management of modular construction'. In: *Safety Science* 154 (2022), p. 105852. DOI: [10.1016/j.ssci.2022.105852](https://doi.org/10.1016/j.ssci.2022.105852).
- [51] Ghang Lee, Hong-Hyun Kim, Chi-Joo Lee, Sung-Il Ham, Seok-Heon Yun, Hunhee Cho, Bong Keun Kim, Gu Taek Kim and Kyunghwan Kim. 'A laser-technology-based lifting-path tracking system for a robotic tower crane'. In: *Automation in Construction* 18.7 (2009), pp. 865–874. DOI: [10.1016/j.autcon.2009.03.011](https://doi.org/10.1016/j.autcon.2009.03.011).
- [52] Mingyuan Zhang and Shoumeng Ge. 'Vision and Trajectory-Based Dynamic Collision Prewarning Mechanism for Tower Cranes'. In: *Journal of Construction Engineering and Management* 148.7 (2022), p. 04022057. DOI: [10.1061/\(ASCE\)CO.1943-7862.0002309](https://doi.org/10.1061/(ASCE)CO.1943-7862.0002309).
- [53] Leon C. Price, Jingdao Chen, Jisoo Park and Yong K. Cho. 'Multisensor-driven real-time crane monitoring system for blind lift operations: Lessons learned from a case study'. In: *Automation in Construction* 124 (2021), p. 103552. DOI: [10.1016/j.autcon.2021.103552](https://doi.org/10.1016/j.autcon.2021.103552).
- [54] Jiahui Ye and Jie Huang. 'Analytical analysis and oscillation control of payload twisting dynamics in a tower crane carrying a slender payload'. In: *Mechanical Systems and Signal Processing* 158 (2021), p. 107763. DOI: [10.1016/j.ymsp.2021.107763](https://doi.org/10.1016/j.ymsp.2021.107763).
- [55] Keum-Shik Hong and Umer Hameed Shah. *Dynamics and control of industrial cranes*. Springer, 2019. DOI: [10.1007/978-981-13-5770-1](https://doi.org/10.1007/978-981-13-5770-1).
- [56] Florentin Rauscher and Oliver Sawodny. 'Modeling and Control of Tower Cranes With Elastic Structure'. In: *IEEE Transactions on Control Systems Technology* 29.1 (2021), pp. 64–79. DOI: [10.1109/TCST.2019.2961639](https://doi.org/10.1109/TCST.2019.2961639).
- [57] Dawid Cekus, Renata Gnatowska and Paweł Kwiatkoń. 'Impact of Wind on the Movement of the Load Carried by Rotary Crane'. In: *Applied Sciences* 9.18 (2019), p. 3842. DOI: [10.3390/app9183842](https://doi.org/10.3390/app9183842).
- [58] Lianghai Jin, Han Liu, Xiazhong Zheng and Shu Chen. 'Exploring the Impact of Wind Loads on Tower Crane Operation'. English. In: *Mathematical Problems in Engineering* 2020 (2020). DOI: [10.1155/2020/2807438](https://doi.org/10.1155/2020/2807438).

- [59] J. Yoon, S. Nation, W. Singhose and J. E. Vaughan. 'Control of Crane Payloads That Bounce During Hoisting'. In: *IEEE Transactions on Control Systems Technology* 22.3 (2014), pp. 1233–1238. DOI: [10.1109/TCST.2013.2264288](https://doi.org/10.1109/TCST.2013.2264288).
- [60] Jingdao Chen, Yihai Fang and Yong K. Cho. 'Real-Time 3D Crane Workspace Update Using a Hybrid Visualization Approach'. In: *Journal of Computing in Civil Engineering* 31.5 (2017), p. 04017049. DOI: [10.1061/\(ASCE\)CP.1943-5487.0000698](https://doi.org/10.1061/(ASCE)CP.1943-5487.0000698).
- [61] Yunfeng Diao, Wenming Cheng, Run Du, Yaqing Wang and Jun Zhang. 'Vision-based detection of container lock holes using a modified local sliding window method'. In: *EURASIP Journal on Image and Video Processing* 2019.1 (2019), p. 69. DOI: [10.1186/s13640-019-0472-1](https://doi.org/10.1186/s13640-019-0472-1).
- [62] Alan M. Lytle and Kamel S. Saidi. 'NIST research in autonomous construction'. In: *Autonomous Robots* 22.3 (2007), pp. 211–221. DOI: [10.1007/s10514-006-9003-x](https://doi.org/10.1007/s10514-006-9003-x).
- [63] Joshua Vaughan, Ajeya Karajgikar and William Singhose. 'A study of crane operator performance comparing PD-control and input shaping'. In: *Proceedings of the 2011 American Control Conference*. IEEE. 2011, pp. 545–550. DOI: [10.1109/ACC.2011.5991506](https://doi.org/10.1109/ACC.2011.5991506).